RESOURCE ALLOCATION IN ENERGY SUSTAINABALE WIRELESS MESH NETWORKS

Resource Allocation In Energy Sustainable Wireless Mesh Networks

By
Amir Antoun Renne Sayegh, M.Sc.

A Thesis
Submitted to the School of Graduate Studies
in partial fulfilment of the requirements for the degree of

Ph.D.

Department of Electrical and Computer Engineering
McMaster University

© Copyright by Amir Antoun Renne Sayegh, August 2008

DOCTOR OF PHILOSOPHY (2008) McMaster University
(ELECTRICAL AND COMPUTER ENGINEERING) Hamilton, Ontario

TITLE:
Resource Allocation In Energy Sustainable Wireless Mesh Networks

AUTHOR: Amir Antoun Renne Sayegh, M.Sc.
(Cairo University, Egypt)

SUPERVISOR: Dr. Terence D. Todd

NUMBER OF PAGES: xix, 211

Abstract

Wireless LAN (WLAN) mesh networks are now being used to deploy Wi-Fi coverage in a wide variety of outdoor applications. In these types of networks, conventional WLAN mesh nodes must be operated using continuous electrical power connections. This requirement may often be very expensive, especially when the network includes expansive outdoor wireless coverage areas. An alternative is to operate some of the WLAN mesh nodes using an energy sustainable source such as solar or wind power. This eliminates the need for a fixed power connection, making the node truly tether-less and allowing for more flexibility in node positioning. The cost of the battery and the solar panel or wind turbine can be a significant fraction of the total node cost, therefore the resource allocation must be performed optimally.

In this thesis we investigate this problem. First, we present geographic provisioning results for solar and wind powered WLAN mesh nodes. The results suggest that in certain geographic locations a hybrid wind/solar powered WLAN mesh node is the optimum minimum cost configuration. The results also provide strong motivation for introducing power saving to the IEEE 802.11 standard. We then consider the problem of cost-optimal node placement in a hybrid network containing traditional and energy sustainable nodes. Our results show that there is a significant improvement in cost that can be obtained

using the proposed methodology. Finally, we consider the problem of energy management in these networks. A control algorithm is proposed that uses access to publicly available meteorological databases. We show that the proposed algorithm minimizes node outage and performs favorably compared to the analytic performance bounds. Overall, the work in this thesis develops analytical and simulation models which investigate the key aspects pertaining to resource allocation in energy sustainable WLAN mesh networks.

Acknowledgements

First of all I would like to thank God who gave me the patience and perseverance needed in order to complete this work. I would like to thank my supervisor, Professor Terence D. Todd, for his continuous mentoring and support throughout the past few years. I would like to thank the members of my Ph.D. supervisory committee and the members of the examining committee for reading this thesis and providing valuable feedback. I would like to thank my parents for always encouraging me to be the best I can be. I would also like to thank them for their love and support and for investing in my education throughout the years. Finally, I would like to dedicate this work and thesis to my wife and best friend Mirette and my son Joseph. Mirette, you stood by me through all these difficult years with your love and encouragement, and you made several sacrifices in order for me to achieve this life-long dream, for that I am truly thankful. Joseph, I hope that one day you will know more than I ever know!

Finally, this thesis is dedicated to you the reader, I sincerely hope you enjoy reading this thesis as much as I enjoyed writing it.

Amir Sayegh

Hamilton, Ontario, 2008.

Contents

List of Figures

List of Tables

Chapter 1

Introduction

1.1 Overview

Wireless LAN (WLAN) mesh networks are currently being deployed for outdoor wireless coverage in many metro-area Wi-Fi hotzones. One of the major costs of certain WLAN mesh network deployments is that of providing the nodes with electrical power and wired network connections. This is especially true in Wi-Fi hot-zones, where WLAN coverage is provided over extended outdoor areas. Although power can sometimes be supplied through power over Ethernet (PoE), such a solution requires a wired network connection, which may not exist. An alternative to continuous power connections is to operate some of the mesh nodes using a sustainable energy source such as solar or wind power. A sustainable energy source as defined in this thesis is an energy source that can power the node at a given power consumption level indefinitely with

some statistical confidence. These kinds of nodes can be quickly installed and have additional node positioning advantages compared with conventional mesh nodes.

In either solar or wind powered options, node resource allocation involves assigning solar panel or wind turbine size, and battery capacity to each mesh node. This assignment must use "geographic provisioning" to account for the solar insolation or wind power capability of the node location. Resource assignment is done using a target load profile for the node, which specifies the power consumption workload for which it is being configured. Depending on the geographic location of the node and the expected workload, the cost of the battery and the solar panel or wind turbine can be a significant fraction of the total node cost.

The design, operation, and deployment of these networks represents some challenges that must be taken into account. The dependence of the renewable energy powered node cost on the expected workload and geographic location motivates careful selection of the allocated resources. In addition, the choice of the routing methodology and node placement will strongly influence the overall cost of the network. Once the node is deployed, its performance could become unreliable in cases of workload surges if no energy management is in place, meaning that a node could experience outage events during which it could deny all traffic requests.

1.2 Motivation

The main motivation for this thesis is to focus on some of the most important issues related to deploying and operating renewable energy powered wireless mesh nodes. This thesis aims to formulate these problems with enough mathematical rigor that allows for the proposal of optimal solutions and best practices.

In traditional wireless mesh networks two of the main objectives are minimizing cost in the planning phase and maximizing node reliability in the operational phase. Designing networks that include renewable energy powered nodes is a challenging task when compared to traditional network design.

The node costs are highly sensitive to the geographic location and workload meaning that the network designer must take this into account or else the network costs will be too high. There are extreme cases where the deployment of these nodes is not justified economically, and it is one the main goals of this thesis to identify these cases. Since the node costs are dependent on the workload, the choice of routing algorithms that are proposed at design time must also take this into account or else the designer could face rising network costs and unacceptable performance.

Finally, the nodes are more prone to failure than traditionally powered nodes if left without an energy management scheme. Since users have come to expect ubiquitous presence of wireless services, this is no longer acceptable, and hence an energy management framework must be set in place in order to provide statistical guarantees on the node performance.

1.3 Scope of Thesis

The wireless mesh nodes under consideration in this thesis are assumed to adhere to the IEEE 802.11 and 802.11s standards. We also assume that it is possible to practically modify the operation of the access points in order to introduce forced power saving (FPS). This is necessary in order to evaluate the cost savings made possible by the proposed resource allocation methodology. In addition, we assume that the access points can be easily modified in order to collect local meteorological information and communicate with an external server.

The cost models described in this work are based on available market data. These models can be extended to include other factors such as economies of scale. Our results suggest that these models will not affect the proposed methodologies. The lack of availability of realistic cost models for wind turbines has been one of the major obstacles that we faced while extending the work in Chapter 3 into Chapters 4 and 5. Therefore, the results shown in these chapters are for solar-only powered nodes to simplify the presentation of the material.

In renewable energy powered wireless mesh networks, resource allocation will greatly affect the overall cost of the node. The focus of this thesis is on the different factors that influence this resource allocation. These factors include the workload required of the node and the meteorological conditions at the geographic location where it will be installed. The results shown will provide a strong motivation for implementing power saving at the access points. In addition, the work in this thesis will show that combining more than one

energy source at a given location significantly reduces the overall node cost for some geographic locations.

This thesis then deals with the case when these nodes are deployed in networks that contain a mixture of traditional and renewable energy nodes. Since the cost of the node is a function of the forecasted traffic flow through it, then the location of these nodes and the traffic routed through them should carefully be chosen in order to minimize overall netwok cost. We present a mathematical formulation of the mathematical problem and present a formal proof of hardness. We then evaluate heuristic algorithms that successfully minimize the overall cost of these hybrid networks.

Once the node has been properly commissioned and installed, the power consumption of the node is affected by the traffic requests that the node receives. When the requests exceed the available energy, the node must implement an energy management algorithm in order to decide the admissible requests at the beginning of every time interval. If an energy management algorithm is not implemented, the node could go into outage until its energy supplies are sufficiently replenished. This behavior of the node leads to temporal unfairness in handling traffic requests. This motivates an energy management algorithm which will rely on Forced Power Saving (FPS) in order to avoid outages by shedding excess load. However, this leads to a capacity deficit which must also be minimized. In this thesis we present a mathematical formulation of this problem and propose an online algorithm that takes into account forecasted weather data in order to minimize this capacity deficit and re-distribute it in a more fair manner. This algorithm was found to achieve the theoretical

lower bounds on capacity deficit and to redistribute the admitted loads fairly while eliminating the node outage events completely.

1.4 Organization of Thesis

Chapter 2 introduces the background information related to the work in this thesis. Background information on Wireless Local Area Networks (WLANs) and Wireless Mesh Networks (WMNs) is presented. A survey of previous work that deals with power saving for wireless infrastructure networks is then presented. Finally, simulation methodologies for solar and wind powered systems are presented.

In Chapter 3 we present geographic provisioning results for solar and wind powered WLAN mesh nodes. A cost model is introduced which is used to optimize the hybrid provisioning of the nodes. The results suggest that in certain geographic locations a hybrid wind/solar powered WLAN mesh node is the optimum cost configuration. Cases will be included using existing IEEE 802.11 standard assumptions and will also consider the case where modifications are made to the standard so that mesh AP power saving is possible. Several North American locations have been chosen for these results. These locations have been chosen to illustrate a variety of differing meteorological situations.

In Chapter 4 we consider cost-optimal placement of solar powered sustainable nodes in a hybrid WLAN mesh network which is defined as a network containing nodes powered using traditional AC sources and renewable energy. A complicating factor is that the cost of renewable energy powered nodes is depen-

dent on the amount of traffic for which a given node is provisioned, and therefore the node placement and traffic routing must be considered jointly. The design problem is formulated as a Mixed Integer Quadratic Problem (MIQP) and a branch and bound approach is used to obtain node positioning solutions. This is compared with a proposed algorithm that uses optimum shortest path routes for this purpose. The proposed algorithms result in significant improvements in cost and the branch and bound approach achieves the optimum assignment for small network examples which can be computed exhaustively.

In Chapter 5 we consider the problem of energy management in solar powered WLAN mesh networks. The problem is first formulated as a non-linear optimal control problem. A Linear Programming (LP) approximation is then given and solved based on an offline optimization where future solar insolation is known. This result gives a bound on the performance of any real control algorithm. We show that the LP solution is accurate in that it achieves results which are very close to a known no-control capacity deficit lower bound. A control algorithm is then proposed that uses access to publicly available meteorological databases. This approach uses on-line data but could also use data from weather forecasts. We show that the proposed algorithm minimizes node outage and performs favorably compared to the offline and no-control bounds.

We then conclude the thesis in Chapter 6.

1.5 List of Acronyms

In the following, we present a summary of the most commonly used acronyms throughout this thesis.

AC	Access Category
AC	Alternating Current
ADHDP	Action Dependent Heuristic Dynamic Programming
AP	Access Point
APSD	Automatic Power Save Delivery
ATIM	Ad-hoc Traffic Indication Message
BE	Best Effort
BSP	Base Station Positioning
BSS	Basic Service Set
CAC	Call Admission Control
CAP	Controlled Access Phase
CD	Capacity Deficit
CFP	Contention Free Period
CO	Connection Oriented

CP	Contention Period
CRM	Cloud Cover Radiation Model
CSMA/CA	Carrier Sense Multiple Access with Collision Avoidance
DCF	Distributed Coordination Function
DS	Distribution System
DTIM	Delivery Traffic Indication Message
EDCA	Enhanced Distributed Channel Access
EOF	Empirical Orthogonal Functions
EOSP	End of Service Period
ESS	Extended Service Set
EWMA	Exponentially Weighted Moving Average
FPS	Forced Power Saving
GPS	Global Positioning System
HC	Hybrid Coordinator
HCCA	HCF Controlled Channel Access
HCF	Hybrid Coordination Function
IBSS	Independent Basic Service Set
IEEE	Institute of Electrical and Electronics Engineers
IP	Internet Protocol

ISO/OSI	International Organization for Standardization/Open System Interconnect
L2	Layer 2
L3	Layer 3
LAN	Local Area Network
LPDP	Linear Programming/ Dynamic Programming
MAC	Medium Access Control
MAP	Mesh Access Point
MIMO	Multiple Input Multiple Output
MIQP	Mixed Integer Quadratic Program
MINLP	Mixed Integer Non-Linear Programming
MMSE	Minimum Mean Square Error
MP	Mesh Point
MPC	Model Predictive Control
MRM	Meteorological Radiation Model
MS	Mobile Station
MSC	Meteorological Service of Canada
MSDU	MAC Service Data Unit
NAM	Network Allocation Map
NAV	Network Allocation Vector

NCLB	No Control Lower Bound
NIC	Network Interface Card
NIST	National Institute of Standards and Technology
NREL	National Renewable Energy Laboratory
NSRDB	National Solar Radiation DataBase
OFDM	Orthogonal Frequency Division Multiplexing
OFP	Optimal Flow Placement
ONU	Optical Network Unit
OOC	Optimal Offline Controller
PBEMC	Prediction Based Energy Management Controller
PCF	Point Coordination Function
PHY	Physical Layer
PoE	Power over Ethernet
PRM	Page Radiation Model
PS	Power Saving
PSMP	Power Save Multi-Poll
PV	Photo-Voltaic
QoS	Quality of Service
RTS/CTS	Request to Send/ Clear to Send
S-APSD	Scheduled Automatic Power Save Delivery

SIFM	Solar Insolation Forecasting Model
SMAP	Solar Powered MAP
SMP	Solar Powered MP
SM	Spatial Multiplexing
SP	Service Period
S-PSMP	Scheduled PSMP
STA	Station
TBTT	Target Beacon Transmission Time
TC	Traffic Class
TIM	Traffic Indication Message
TOA	Top of Atmosphere
TS	Traffic Stream
U-APSD	Unscheduled APSD
UMTS	Universal Mobile Telecommunication System
U-PSMP	Unscheduled PSMP
VBS	Virtual Base Station
VoIP	Voice over IP
WDS	Wireless Distribution System
WLAN	Wireless Local Area Network
WMN	Wireless Mesh Network

Chapter 2

Background

2.1 Introduction

This chapter presents an overview of the background information and concepts relevant to our analysis of renewable energy powered WLAN mesh networks. The chapter starts by presenting background information on Wireless Local Area Networks (WLANs) and Wireless Mesh Networks (WMNs). We then survey previous work that deals with power saving for wireless infrastructure networks. Finally, we present methodologies used to simulate solar and wind powered systems based on available meteorological records.

2.2 WLAN Networks

The past few years have witnessed a phenomenal growth in the sales of Wireless Local Area Network (WLAN) equipment. While several standards for WLANs exist, equipment compliant with the IEEE 802.11 standard for WLANs has by far exceeded all expectations in terms of revenue and sales growth. Equipment complying with this standard is commonly referred to as Wi-Fi equipment. The brand "Wi-Fi" was introduced by the Wi-Fi Alliance to describe interoperable WLAN products that are based on the IEEE 802.11 standards. The Wi-Fi Alliance is a consortium of separate and independent companies, which agrees on a set of common interoperable products based on the family of IEEE 802.11 standards.

Forecasts for 2008 are predicting overall sales of 2.1 Billion USD for WLAN chipsets. In addition, the WLAN chipset market is projected to soar from just over 140 million annual chipset unit shipments in 2005 to 430 million in 2009. The number of Wi-Fi enabled cellphones is expected to exceed 100 million by 2010. Finally, ninety per cent of notebook PCs sold worldwide will contain embedded WLAN in 2008 [2].

The IEEE 802.11 standard [65] was first approved in 1997 and specifies the protocol details of the Physical (PHY) layer and Medium Access Control (MAC) sublayer for wireless networking for outdoor and indoor situations. The typical range of a WLAN network based on the standard is 100-200 meters. The standard also defines different network architectures while specifying the roles of the access point (AP) and mobile stations (MS). More details will be presented in the next section.

The standard has significantly evolved since the first version was published in 1997 with several amendments introduced since then. These are summarized in Tables 2.1 and 2.2 which are reproduced from [11] and [19] and [31]. The first table presents the amendments that have been ratified while the latter presents the amendments that are still under discussion.

Amendment Name	Description
802.11	The original WLAN Standard. Supports 1 Mbps to 2 Mbps.
802.11a (9/1999)	High speed WLAN standard for 5 GHz band. Supports 54 Mbps.
802.11b (9/1999)	WLAN standard for 2.4 GHz band. Supports 11 Mbps.
802.11c (2001)	Bridge operation procedures included in the IEEE 802.1D standard.
802.11d (6/2001)	International roaming automatically configures devices to meet local RF regulations.
802.11e (9/2005)	Addresses quality of service requirements for all IEEE WLAN radio interfaces.
802.11f (2003)	Defines inter-access point communications to facilitate multiple vendor-distributed WLAN networks.
802.11g (6/2003)	Establishes an additional modulation technique for 2.4 GHz band. Supports speeds up to 54 Mbps.
802.11h (12/2003)	Transmit power control, dynamic channel selection. Defines the spectrum management of the 5 GHz band.
802.11i (6/2004)	Addresses the current security weaknesses for both authentication and encryption protocols. The standard encompasses 802.1X, TKIP, and AES protocols.
IEEE 802.11j (2004)	Extensions for Japan.
IEEE 802.11 (7/2007)	A new release of the standard that includes amendments a, b, d, e, g, h, i & j.

Table 2.1: Ratified IEEE 802.11 Amendments

2.2.1 System Description

The IEEE 802.11 architecture is comprised of several components and services that interact to provide station mobility transparent to the higher layers of the network stack.

Amendments Under Development	Description
802.11k	Radio resource management
IEEE 802.11l	Reserved and will not be used.
802.11m	Standard maintenance. Recent edits became 802.11-2007.
802.11n (Expected 9/2008)	Provides higher throughput improvements. Intended to provide speeds up to 500 Mbps.
IEEE 802.11o	Reserved and will not be used.
IEEE 802.11p	WAVE - Wireless Access for the Vehicular Environment.
IEEE 802.11q	Reserved and will not be used.
802.11r	Fast roaming.
802.11s	WLAN mesh networks.
IEEE 802.11t	Wireless Performance Prediction (WPP) - test methods and metrics.
802.11u	Interworking with external networks.
802.11v	Wireless network management.
802.11w	Protected management frames.
IEEE 802.11x	Reserved and will not be used.
IEEE 802.11y	3650-3700 MHz Operation in the USA.
IEEE 802.11z	Extensions to Direct Link Setup (DLS).

Table 2.2: IEEE 802.11 Amendments Under Development

The standard [1] defines the station (STA) as the most basic component of the IEEE 802.11 WLAN network. By definition, a station is a device that contains the functionality of the IEEE 802.11 protocol. This includes the MAC and PHY layers and access to the wireless medium. In practice, the IEEE 802.11 functions are embedded in the hardware and software of a network interface card (NIC) of a computer such as a laptop. In addition, a station could be a regular client device or an Access Point (AP). The definition of stations does not distinguish between mobile or stationary devices. Within the IEEE 802.11 standard, Access Points (APs) are defined as ISO/OSI layer two (L2) internetworking devices. In contrast to Routers which work at the third layer

[1]The description presented here is mostly based on [12] and [49].

(L3), APs examine the MAC layer header in packets in a fashion similar to Bridges. APs can also bridge wireless and wired networks. When a STA has setup and established a connection to an AP, this is referred to as "association".

The IEEE 802.11 standard defines the Basic Service Set (BSS) as the building block of an IEEE 802.11 WLAN. It is made up of a group of stations that communicate with each other directly or through an AP. Consequently, there are two types of BSS networks defined within the standard, the Independent Basic Service Set (IBSS) and the Infrastructure Basic Service Set which is usually referred to as a BSS.

An Independent Basic Service Set (IBSS) is a set of at least two stations which have discovered each other and are connected in a peer-to-peer fashion. This network topology is also commonly referred to as an ad-hoc network since there is no need for a central controller to organize communications. An example of an IBSS is shown in Figure 2.1. The figure shows an IBSS consisting of three stations within communication range of each other. In this network setup the stations communicate directly with each other.

The case where an AP relays packets for the stations is referred to as an Infrastructure Basic Service Set (BSS). All stations in the BSS communicate with the access point and can no longer communicate directly. The access point may also provide connection to a *Distribution System* (DS). A typical setup is shown in Figure 2.2. As seen in the figure, three stations are associated with an AP and are communicating with each other through it. In addition, the AP is connected to a distribution system and can relay traffic to and from the distribution system and the stations. BSS is considered the most common net-

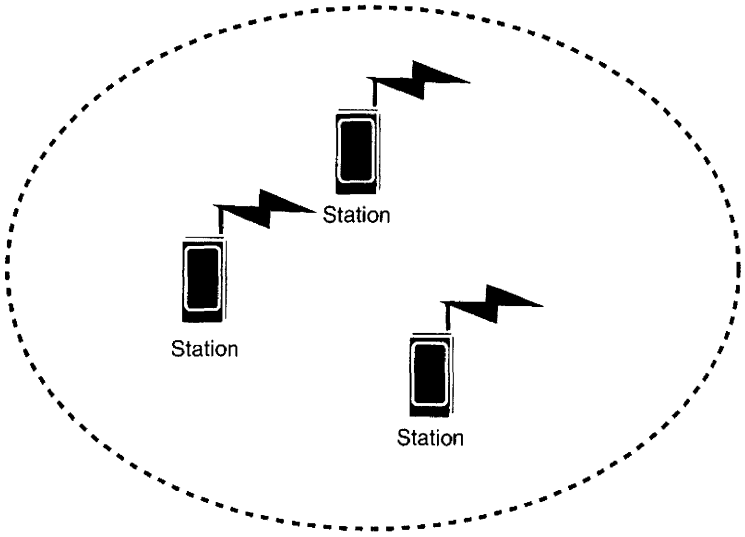

Figure 2.1: Independent Basic Service Set (IBSS)

work configuration, where the AP is connected to the wired network and acts as a gateway to the external network for its associated mobile stations (MSs).

Access points communicate with each other via the DS. The access points can exchange frames for stations in their respective BSSs, forward frames to follow mobile stations as they move from one BSS to another, and exchange frames with a wired network. The DS uses a four-address scheme defined under IEEE 802.11 for exchanging the frames between APs. If wireless links are used in the distribution system, it is called a *Wireless Distribution System* (WDS). The standard does not place any restrictions on how the distribution system is implemented, only on the services it must provide.

The IEEE 802.11 standard defines how to extend the range of mobility to an arbitrary range through the Extended Service Set (ESS). An extended service set is a set of infrastructure BSSs, where the access points communicate

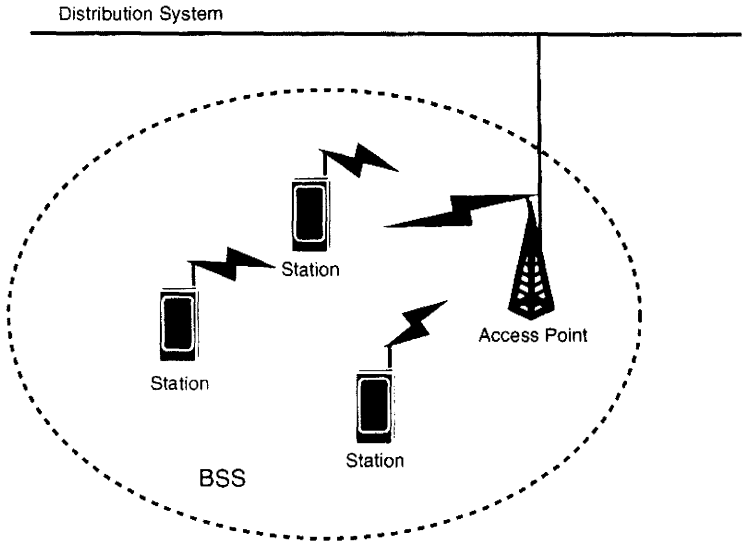

Figure 2.2: Basic Service Set (BSS)

amongst themselves to forward traffic from one BSS to another to facilitate movement of stations between BSSs. Therefore, when several BSSs are interconnected at layer two, the whole set is referred to as an ESS.

The distribution system determines how traffic should be relayed, whether back to a destination in the same BSS, or to another access point, or sent into the wired network to a destination not in the ESS. Frames received by an access point from the distribution system are transmitted to the destination mobile station in the BSS. On the other hand, devices outside of the ESS view the ESS and all of its mobile stations as a single MAC-layer network where all stations are physically stationary. Therefore, the ESS shields the outside world from the mobility of the mobile stations. This is shown in Figure 2.3 which shows an ESS made up of two identical BSS networks. Both APs can communicate through the distribution system and the stations from both BSS

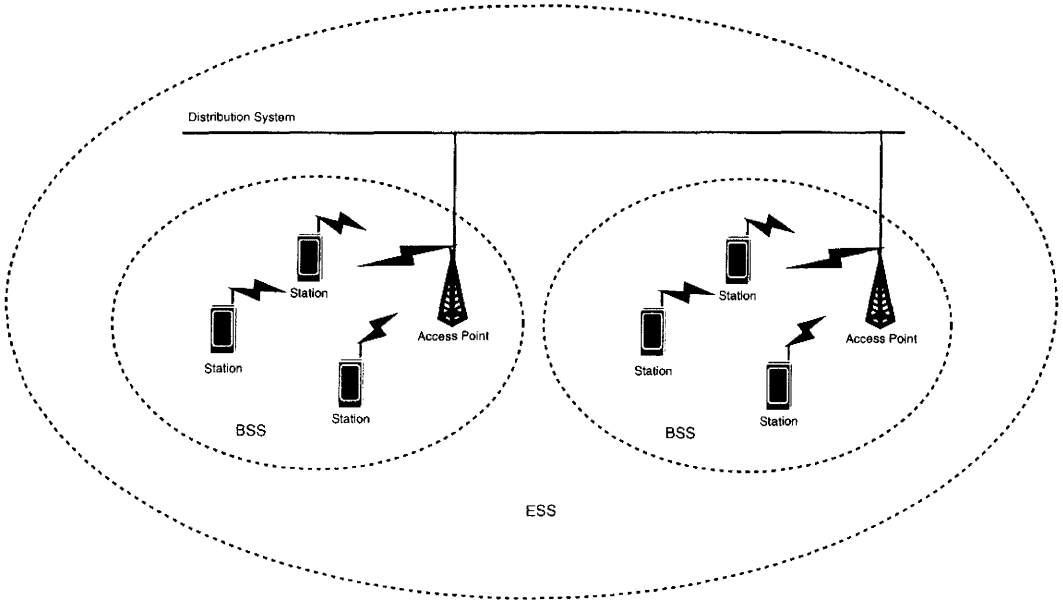

Figure 2.3: Extended Service Set (ESS)

networks can communicate with each other through their respective APs and the distribution system.

Since IEEE 802.11 devices that are within range of each other share the wireless medium which could lead to interference, the standard has specified two types of channel control algorithms at the MAC sublayer, Distributed Coordination Function (DCF) and Point Coordination Function (PCF). The standard defines the periodic broadcasting of beacons by the AP, these beacons represent service advertisements to the STAs. DCF is the basic access mechanism mandated by the standard and allows multiple wireless clients to access the wireless medium. It is a distributed scheme where the arbitration is decided using collision avoidance, where the stations use a distributed random algorithm in order to avoid collisions. The DCF mechanism is based on

Carrier Sense Multiple Access with Collision Avoidance (CSMA/CA). In wired LANs (e.g. Ethernet) collision detection is implemented, this is not possible in wireless networks for several reasons and hence a collision avoidance strategy is necessary.

PCF is a centralized MAC approach. The scheme is based on the AP polling stations and then granting them transmission opportunities. Therefore, the approach adopted by PCF resolves contention by not allowing it to happen since the AP has full control over the stations' timeline and transmission opportunities. Within the standard, PCF implementation is viewed as optional and thus in practice PCF is not supported by some devices.

The timeline of a PCF-enabled AP is divided into two parts, a contention-free period (CFP) and a contention period (CP). Together, these two periods make up a superframe. The start and end of a superframe are usually defined by the transmission of two successive beacons. However, the superframe can span more than one beacon transmission interval to allow more flexibility. For contention-free operation, the stations that have packets to transmit are polled by the AP and are granted a transmission opportunity. Once the CFP period is over, it is followed by a CP period during which all stations revert to the DCF access mechanism. The support of this CP is mandatory for all devices working in PCF mode to make the simultaneous co-existence of the DCF and PCF schemes in the same service area possible.

The IEEE 802.11e [67] standard introduced QoS enhancements. The standard introduces a new coordination function which is the Hybrid Coordination Function (HCF). HCF introduced modified versions of DCF and PCF which

have been renamed Enhanced Distributed Channel Access (EDCA) and HCF Controlled Channel Access (HCCA) respectively. Both EDCA and HCCA define Traffic Classes (TC) with different QoS requirements and priorities. EDCA contention access is an extension of the legacy CSMA/CA DCF mechanism to include priorities. The contention window and backoff times are adjusted to change the probability of gaining medium access to favor higher priority classes. A total of eight user priority levels are available. Each priority is mapped to an access category (AC) which has different parameters defined for it. The HCCA (HCF (Hybrid Coordinator Function) Controlled Channel Access) operation resembles that of PCF. The HCCA allows for CFPs to be initiated anytime during the CP as opposed to the PCF operation. This kind of CFP is referred to as Controlled Access Phase (CAP) in IEEE 802.11e. The other difference is that Traffic Class (TC) and Traffic Streams (TS) are defined. This means that the Hybrid Controller (HC) is not limited to per-station queuing and can provide per-session service. HCCA is the most complex coordination function. With HCCA, QoS can be configured with great precision. QoS-enabled stations have the ability to request specific transmission parameters. Similar to PCF, HCCA support is not mandatory for IEEE 802.11e APs.

2.3 WLAN Mesh Networks

A wireless mesh network is made up of wireless nodes that have one or more radios. These nodes create a so-called *mesh cloud* within a given coverage area where there may be several routes of communication to each node. Due to

the existence of route diversity, a mesh network offers redundancy and therefore offers enhanced reliability. When one node can no longer operate, all the rest can still communicate with each other, directly or through one or more intermediate nodes. For a comprehensive survey of wireless mesh networks the reader is referred to [20] and [25].

For WMNs that operate using IEEE 802.11 devices, a WLAN mesh network can be viewed as an ESS network. These mesh networks are currently being standardized under the IEEE 802.11s WLAN standard [66]. WLAN mesh networks provide IEEE 802.11 coverage for mobile stations (MSs) and also perform wireless distribution using multihop relaying between mesh APs (MAPs) and mesh points (MPs). In WLAN mesh networks, a mesh point (MP) performs traffic relaying functions only to other mesh nodes, including the relay of backhaul station traffic. However, an MP does not communicate directly with stations. A mesh AP (MAP) is a mesh point that also provides WLAN coverage for mobile stations [66]. Figure 2.4 [49] shows a sample WLAN mesh network. In the figure, 4 MAPs providing coverage for the MSs associated with them are shown. We can see that the MAPs can communicate with each other through the wired infrastructure, or through the MP or directly with each other. The figure shows how the MP relays frames between two MAPs while no MSs are associated with it. It is worth noting that the figure does not show all the possible paths of communication between MAPs and hence not all of the network redundancy is shown.

The unique architecture of WMNs allows the service provider to provide reliable high-bandwidth service over a specific coverage area. The architecture

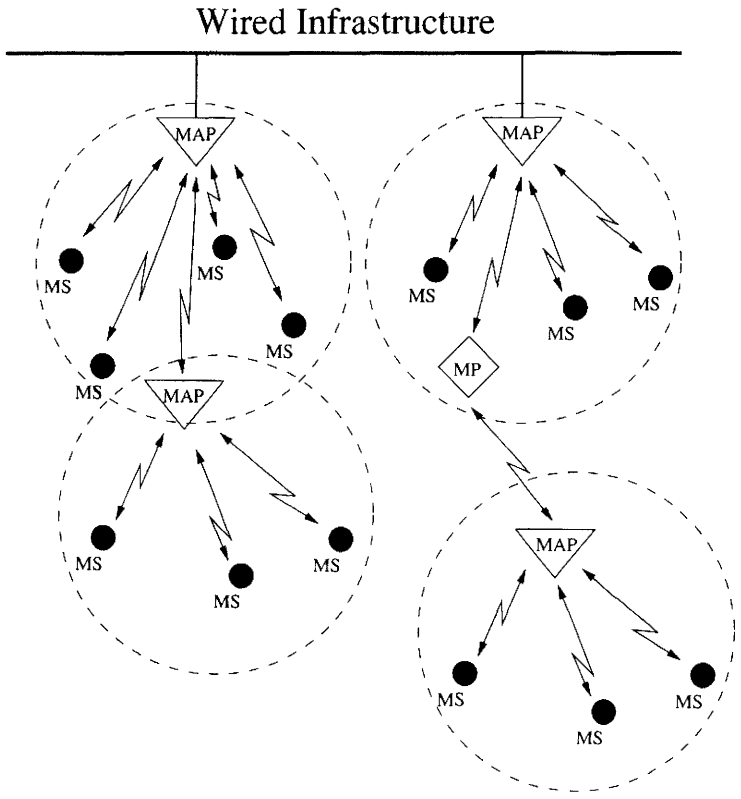

Figure 2.4: Example of an WLAN Mesh Network [49]

can be viewed as being similar to a traditional router network. The WMN architecture maintains the radio signal strength by breaking long distances into a series of shorter hops. Therefore, intermediate WMN nodes act as signal repeaters in addition to cooperatively making forwarding decisions based on their knowledge of the network. Thus, the main advantages of the WMN architecture can be summarized as providing high bandwidth, spectral efficiency, and economic advantage for a given coverage area.

Three types of mesh architectures have been identified according to [25]. In infrastructure wireless mesh networks the mesh routers form an infrastructure

for stations and in client wireless mesh networks station nodes constitute the actual network to perform routing and configuration functionalities and finally hybrid wireless mesh networks where the mesh clients can perform mesh functions with other mesh stations as well as accessing the network through mesh routers. Throughout this thesis, we focus on an infrastructure type wireless mesh network since it is currently the most prevalent network architecture. One example of a campus deployment of a mesh network is shown in Figure 2.5. The figure depicts the suggested deployment of a wireless mesh network at McMaster University. The pentagons represent MAP deployment sites on the rooftops of the buildings on campus while each line connecting the circles represents a radio link that must be commissioned. The circles around each MAP deployment site represent the radio coverage area for STAs. The example shown represents a typical usage scenario for a WMN, it is obvious that not all node sites will have unhindered access to traditional power sources due to the fact that node locations are usually chosen to maximize radio coverage or capacity. Therefore, there is a need to explore the feasibility of utilizing alternative sources of energy such as solar power for these nodes. In the following section, we present a survey of previous efforts related to the deployment of solar powered wireless networks in general.

2.4 Solar Powered Wireless Networks

Solar power is starting to appear in many Wi-Fi infrastructure scenarios. For example, a solar powered Wi-Fi network has recently been deployed in Min-

Figure 2.5: Example of an WMN Deployment at McMaster University

neapolis as part of the ParkWiFi project which consists of more than 400 APs [18]. The city of Boulder, Colorado, has also deployed solar powered wireless Internet access at the Pearl Street mall, in co-operation with Lumin Innovative products which have launched a commercial line of solar powered wireless communications networks [15]. Meraki have announced plans for a solar powered outdoor Wi-Fi mesh node (Meraki Outdoor) [16], and IR Data Corporation provides a solar powered Wi-Fi AP, which includes a 900 MHz radio mesh router [14]. Inveneo, a non-profit organization, currently offers information and communications technologies in the developing world, which includes solar-powered wireless Wi-Fi networks [13]. An example of this is the Battery Operated Systems for Community Outreach (BOSCO) initiative, which is expected to provide Internet services for displaced people in north-

ern Uganda [8]. In a similar way, the One Laptop Per Child (OLPC) project includes the use of an IEEE 802.11 WLAN mesh repeater powered using solar power. These repeaters can then be easily mounted to provide ubiquitous WLAN mesh coverage for OLPC users. The Green Wi-Fi initiative also provides solar powered access for developing countries [10].

The use of sustainable energy in WLAN mesh networks is fairly recent. For the past several years, the SolarMESH network has been under development and has been undergoing deployment trials at McMaster University [114]. This network has been carrying live traffic since 2003 and has helped to validate the use of solar power for this type of application. Recently, many WLAN mesh network operators have realized the commercial potential of solar powered solutions. For example, DropZone Networks [9] have developed solar powered wireless routers for use at the network edge. Nodes are equipped with GPS units and other air interface options (such as cellular) to create a location-aware network that can be placed in remote locations. Another interesting initiative at the University of Abertay in Scotland, involves embedding WLAN APs in solar powered lampposts. These "smart lampposts" are being proposed as revenue generators for cities with existing lighting infrastructure.

The level of research in this area has also increased significantly in recent years. Node power consumption has always been an important consideration in battery powered communication networks but very little deals specifically with renewable energy sources. In [80] a power-aware routing algorithm is presented for wireless networks under this assumption. The proposed routing algorithm uses a composite cost metric that includes power for transmission and reception,

replenishment rate, and residual energy. In [119] improved communication energy efficiency is considered for networks powered by renewable energy sources. The work analyzes the energy consumption in the one transmitter, multiple receiver, case. Optimal scheduling algorithms are presented for data transmission at different rates such that the throughput is maximized under given time limits and energy constraints. Reference [70] presents an analysis of environmentally powered sensor networks. A model is presented for characterizing energy sources and includes a harvesting theory that governs storage and power consumption requirements. This is expanded in [69] to develop a characterization model for energy sources and traffic loads. The authors also develop an optimization for duty cycle adjustment and present a simple algorithm solution. In [92], solar powered OFDM wireless mesh networks with sleep management and connection admission control were described. An analytic queuing model was formulated to evaluate the performance at the mesh nodes, and an optimization problem is formulated to determine the sleep/wakeup parameters or the connection admission control threshold in order to meet the desired QoS constraints.

Finally, the design of solar-powered WLAN mesh networks has been considered from a resource allocation and outage control viewpoint [49]. This work includes a solar panel/battery configuration methodology based on a proposed power-aware version of IEEE 802.11. This activity coincided with the development of the previously mentioned SolarMESH network.

Since this thesis assumes that an appropriate power saving scheme is in place, the following section presents an overview of power saving in different

wireless networks.

2.5 Power Saving

2.5.1 Power Saving in IEEE 802.11 Networks

The original IEEE 802.11 standard defines a power management scheme for IEEE 802.11 stations since it is expected that for most applications they will be battery-operated. However, the standard assumes that APs are always available and do not perform power saving. The standard specifies power management for both infrastructure and IBSS networks.

The standard defines two power states for a (non-AP) station, namely, *Awake* and *Doze*. The Awake state is an active mode where the station radio interface is sufficiently powered so that it is capable of sensing activity on the radio channel and transmitting/receiving packets. Conversely, the Doze state is associated with Power Saving (PS) mode, where various parts of the radio circuitry are powered off, and a station is unable to perform any of the above functions. In current IEEE 802.11 chipsets, stations in PS mode can typically reduce their radio interface power consumption by over two orders of magnitude compared with that in the Awake state. During the time that a station is in PS mode, the access point must buffer incoming traffic that is destined for that station. These packets are then held until the station in question reverts to the awake state and arranges for them to be delivered [65].

For the infrastructure mode case, a STA changing power management

modes informs the AP of this fact using a specific set of power management bits within the frame control field of transmitted frames. The AP will maintain a power management status for each associated STA. The AP will then buffer packets for power saving STAs.

An IEEE 802.11 AP transmits periodically scheduled beacon packets. These are used (among other things) to announce the presence and configuration of the access point. This includes a traffic indication map (TIM) which informs a PS-mode station if one or more packets are being held for that station. The TIM also lists the STAs operating in PS mode. Using this mechanism, a PS mode station can transition to the Awake mode just prior to the beacon transmission and listen to learn if there are awaiting packets. The beacon listening interval is a parameter that is controlled by the STA.

In a BSS operating under the DCF, or during the CP of a BSS using the PCF, upon learning that it has buffered packets, a station with buffered packets sends a PS-Poll frame to the AP to retrieve each packet. The AP can either respond with the requested packets immediately or acknowledge the PS-Poll frame and send the requested frames at a later time.

The original standard also provides for power saving in stations which use PCF (the AP-polled point coordination function) channel access. The procedures are similar to that described above except that frame transmission is done in accordance with the rules governing PCF channel access. If the TIM indicating the buffered packets is sent during a CFP, then the CF-pollable STA in PS mode does not send a PS-Poll frame, rather it remains awake until the buffered frames are received or the CFP period ends.

The standard distinguishes between two different TIM types: TIM and DTIM (Delivery Traffic Indication Message). After a DTIM, the AP sends out the buffered broadcast/multicast MAC Service Data Units (MSDUs) before transmitting any unicast frames. A TIM is transmitted by the AP with every Beacon frame. A TIM of type DTIM is transmitted within a Beacon frame every DTIM period. Figure 2.6 illustrates the AP and STA activity. The figure assumes no PCF and that a DTIM is transmitted once every three TIMs. The top line in Figure 2.6 represents the time axis, with the beacon interval shown together with a DTIM Interval of three beacon intervals. The second line depicts AP activity. The AP schedules Beacon frames for transmission every beacon interval, but the Beacon frames may be delayed if there is traffic at the Target Beacon Transmission Time (TBTT). This is shown as busy medium on the second line. We notice that the second STA with ReceiveDTIMs set to false does not power-on its receiver for all DTIMs. The third and fourth lines in Figure 2.6 depict the activity of two STAs operating with different power management requirements. Both STAs power-on their receivers when they need to listen for a TIM. This is indicated as a ramp-up of the receiver power prior to the TBTT. For example,the first STA powers up its receiver and receives a TIM in the first Beacon frame. In this case, the TIM indicates the presence of a buffered MSDU for the receiving STA. The receiving STA then generates a PS-Poll frame, which triggers the transmission of the buffered data MSDU from the AP. Broadcast and multicast MSDUs are sent by the AP subsequent to the transmission of a Beacon frame containing a DTIM [65].

In the IBSS case, the approach is similar to the one in the infrastructure

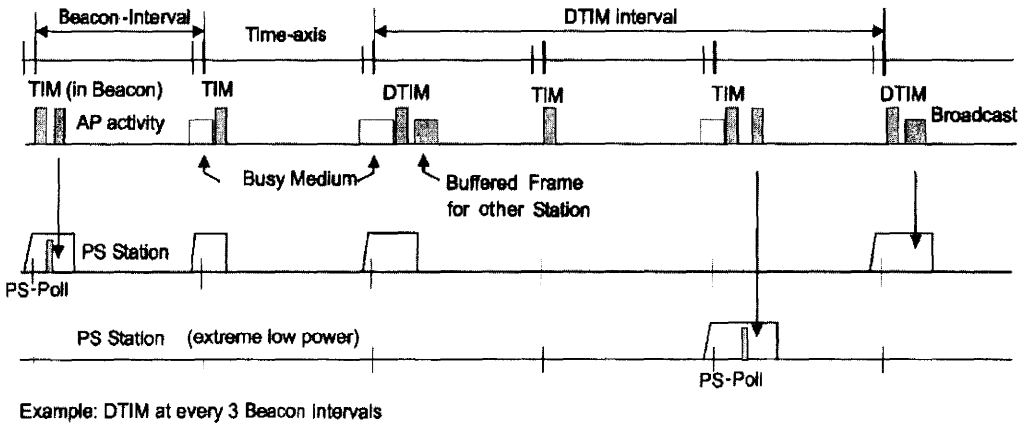

Figure 2.6: Infrastructure Power Management Operations (No PCF Operating) [65]

case. Announcements for buffered packets are done via an ad-hoc TIM (ATIM).

Various enhancements to the above scheme have been included in some of the follow-on standards. For example, IEEE 802.11e defines Automatic Power Save Delivery (APSD). This includes both contention-based operation (referred to as EDCA) and a polling-based option (called HCCA). In the latter case the AP functions as a hybrid coordinator (HC), and defines periodic service intervals which allow the synchronous delivery of traffic using Scheduled Automatic Power Save Delivery (S-APSD). In the former case, the unscheduled APSD (U-APSD) mechanism permits the station to initiate communication activity by transmitting trigger frames on the uplink in EDCA contention mode [67]. These mechanisms provide for improved flexibility and power saving compared with the original procedures.

APSD is slightly different from the power management method defined

in the 802.11 standard. A station is awake during a Service Period (SP) as opposed to being awake from the beginning of the awake state for Beacon reception until the return to doze state after acknowledging the receipt of the last frame buffered at the AP. When an AP receives a trigger frame from a station this signals the start of an unscheduled SP. It ends when the station receives a QoS Data or QoS Null frame indicating the end of the service period (EOSP). The station uses QoS Null frames instead of PS-Polls. Therefore frame delivery can be requested from the AP even if a station has no data frame to transmit in the uplink. This enables the usage of U-APSD by applications which do not generate uplink traffic often enough to meet the QoS application requirements. Each AC at the stations can be configured separately to be delivery/trigger-enabled respectively. When a station has an AC configured as delivery-enabled, the AP is allowed to use EDCA to deliver traffic from the AC to a STA during an unscheduled SP triggered by a station. When a station AC is trigger-enabled, frames of subtype QoS Data and QoS Null from the station, that map to the AC, trigger an unscheduled SP if one is not in progress. [98]

The IEEE 802.11n standard [68] adopts a MIMO approach in order to increase data rates. However, operating several radios increases the power demands. To address this situation, 802.11n has extended the power management capability of IEEE 802.11. There are two extensions beyond the existing mechanisms established in the original standard and the automatic power save delivery added in 802.11e. The two new mechanisms provided by 802.11n are Spatial Multiplexing Power Save and Power Save Multi-Poll as described in [45].

The spatial multiplexing (SM) power save mode allows an 802.11n client to power down all its radios except for one. The SM power save mode has two submodes of operation, static operation and dynamic operation. The static SM power save mode allows the client to turn off all its radios except for one. Therefore, it becomes equivalent to an 802.11a or 802.11g client. In addition, the AP is also notified that the client is operating in the static single-radio mode. This implies that the AP will only send a single spatial stream to this client. The dynamic SM power save mode also turns off all of the client's radios except for one. However, this mode of operation allows the client to turn on its additional radios rapidly when it receives a frame that is addressed to it. The Power Save Multi-Poll (PSMP) mode is an extension of the Automatic Power Save Delivery (APSD) mechanism defined in 802.11e. PSMP again provides the same delivery-enable and trigger concepts for delivery of downlink frames. This mechanism reduces the contention between clients and between the client and the AP. This reduced contention improves power conservation in the clients because it reduces the time the client spends in backoff and reduces the number of times a frame must be transmitted before it is delivered successfully. PSMP also adjusts dynamically to changes in traffic demand by the clients using it. As in the case of IEEE 802.11e, PSMP has scheduled (i.e., S-PSMP) and unscheduled (i.e., U-PSMP) versions. Tighter control over the AP/station timeline is established using S-PSMP. In this case, the AP defines a PSMP sequence which includes scheduled times for downlink and uplink transmissions. This allows (non-AP) stations to remain in Doze mode during the times when other stations are scheduled to be using the channel and

reduces AP/station interaction overheads. U-PSMP is similar to U-APSD in that it supports both triggered and delivery enabled modes. [45]

2.5.2 Technical Challenges of WLAN Mesh AP Power Saving

Currently, IEEE 802.11 does not provide a mechanism for placing APs into a power saving mode. As discussed, the standard does define extensive provisions for (non-AP) client node power saving. We now discuss some of the key issues relating to the implementation of power saving at the AP and a discussion of recent work that has started to address them.

Station QoS: In conventional IEEE 802.11, the access point always remains available to process mobile station traffic. When power saving is introduced into the AP, a mechanism must be used to prevent stations from transmitting packets during the periods when the AP is unavailable. In a polling-based system such as Bluetooth, this type of control is straightforward since the polling station (e.g., piconet master) can control slave transmission activity, however, care must be taken so that master power saving is not at the expense of increased power consumption at the slave nodes [48]. It is also important that the power saving behavior is consistent with the QoS requirements of the associated stations. This latter issue is a topic which has not as yet been very well addressed.

Two variations of IEEE 802.11 have recently been proposed for access point power saving in [120] and [79]. In [120], the AP uses "NAV blocking" to pre-

vent channel access to the AP when it is in Doze mode. In conventional IEEE 802.11, a network allocation vector (NAV) is used at each station to implement a virtual carrier sense mechanism [65]. The NAV is used to block stations from transmitting in cases where the channel has been reserved for some other purpose. This occurs for example, when an RTS/CTS exchange reserves the channel for the duration of the expected station/AP packet interaction. Another example is when contention free periods (CFPs) are advertised by an AP functioning as a point coordinator. During a CFP, the point coordinator polls stations one at a time, rather than allowing contention based access. When this mode is used, all stations set their network allocation vectors (NAVs) for the nominal duration of the advertised CFP, which prevents them from accessing the channel during that part of the superframe.

Rather than its intended use, in this case the NAV blocking mechanism is used to prevent stations from transmitting to the AP during the time that the AP is in Doze mode. An example of this is shown in Figure 2.7. In this system the AP advertises itself as a point coordinator (PC) and defines a contention free period (CFP) shown as "NAV Blocking" in the figure. During this part of the superframe, the mesh AP is free to sleep by entering Doze mode as shown in the figure. Following the sleep period the AP reverts to the Awake mode and functions as a normal AP during the contention period. Other minor changes would be required on the MS end in order to ensure full compatibility with IEEE 802.11.

Unfortunately, the proposed NAV-blocking mechanisms are too coarse-grained to permit reasonable QoS for many types of real-time traffic. The

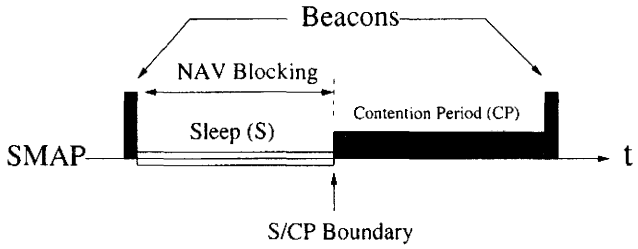

Figure 2.7: Best Effort Power Saving with Sleep/Contention Period Boundary

proposal in [79] is more complex but allows greater flexibility for this purpose. The IEEE 802.11 Network Allocation Vector (NAV) mechanism is generalized, and a power saving AP includes a Network Allocation Map (NAM) in its beacon broadcasts. The NAM specifies periods of time within the superframe when the AP is unavailable, and during these periods the AP is assumed to be inactive and conserving power. Figure 2.8 shows an example of this type of activity for a single inter-beacon period. The channel activity is shown in the upper timeline, and the NAMs are shown on the lower timeline. In this example, three access periods (labeled HCCA/EDCA) have been defined and separated by 40ms. This arrangement could be used, for example, when servicing VoIP connections with a 40ms packetization interval. During each of the access periods, both HCCA (which supports the VoIP connections) and EDCA access would be provided. This type of mechanism is consistent with the evolving trend towards allowing the AP more granular control over its timeline [67], except that explicit AP power saving periods should be defined.

When the traffic supported by the AP is connection oriented and is allocated fixed access periods per superframe (such as when carrying conventional VoIP traffic), then the allocation of the NAMs and the Doze periods is very

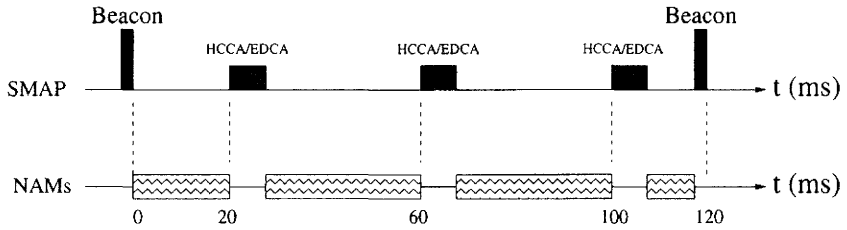

Figure 2.8: NAM Power Saving with HCCA Service Periods

straightforward. This is the case shown in Figure 2.8. However, in general more dynamic mechanisms are needed for updating NAM durations when supporting non-synchronous QoS and for best effort traffic. An algorithm was proposed for this latter case in [79] which updates the next availability period based on the utilization observed in the current interval.

Station Power Saving: It is very important that power saving at the access point does not significantly affect power saving on the mobile stations. This is sometimes a difficult problem to overcome, and various tradeoffs exist between station and AP power saving. For example, obviously a station in power save mode which generates a packet for transmission on the uplink should defer its transition to Awake mode until some future AP availability period. Otherwise the station will incur unnecessary power consumption.

When using the NAM scheme discussed previously, the above procedure raises questions of consistency in cases where stations enter PS mode for long (multi-superframe) time periods. To address this issue, the start and end of each NAM period is defined with one of two boundary types, either fixed (i.e., an `F-Boundary`.) or movable (i.e., an `M-Boundary`.) An `F-Boundary` type is one where the transition to the new subframe type is guaranteed to occur at

that point in the superframe. `F-Boundary`'s can be used so that end stations which have not seen the most recent AP beacon can know the times of AP availability. A need for this is for stations in a deep power save state which awaken to transmit uplink packets. In the absence of `F-Boundary`'s the station would have to sample a beacon first to determine the AP's future availability. Instead, the station can choose to delay its awakening in accordance with an appropriate `F-Boundary` location.

An `M-Boundary` is different in that it can be changed on a dynamic basis by the AP from one superframe beacon interval to the next, and is advertised in the most recent beacon. Instead, the AP may dynamically move that boundary to the left or right, to accommodate traffic conditions. If a station has successfully seen the most recent beacon, then the current `F-Boundary`'s and `M-Boundary`'s are known. Clearly there is a tradeoff between the flexibility with which the AP can dynamically allocate its timeline, and the power consumption of stations that wish to do deep power saving.

AP Discovery and Station Mobility: In WLAN mesh networks with power saving mesh APs, station procedures that deal with AP discovery and station mobility need to be improved. AP discovery is done in IEEE 802.11 using standard scanning procedures [65]. Scanning can be either passive or active. In passive scanning the station listens on a given channel for a time period which is sufficient to hear AP beacon transmissions with a reasonable degree of certainty. However, since beacons are typically transmitted every 100 ms, basic passive scanning can incur long delays compared with active scanning especially when a large number of channels need to be scanned.

Rather than passively listening, in active scanning a mobile station transmits a Probe Request packet on the channel that is being scanned. When this packet is received by one or more appropriate APs, they respond with a Probe Response packet. Under ideal conditions an active scan can be done very quickly since the turnaround time is very low. The issue of improving scan latency performance has been addressed in a number of studies [116] and clearly the actions of a power saving mesh AP can have a negative affect on scan latency. The initial discovery of the AP is not a significant issue from a power and latency viewpoint, and conventional passive scanning will clearly find power saving APs.

A much more serious issue is the scanning latency associated with mesh AP handoff. Mobile stations which move through the WLAN mesh network coverage area will use standard IEEE 802.11 handoff procedures. As an MS passes out of its mesh AP coverage area, it must find a more suitable AP, so that a layer 2 handoff can be executed. Each handoff imposes a temporary disconnection from the network referred to as handoff latency. For real-time applications such as VoIP, it is very important to minimize this interruption. Power saving APs may spend a considerable percentage of time in a power saving sleep mode. For this reason, the AP scanning latency for a mobile station may be increased substantially beyond levels which are suitable for real-time applications. This issue has been studied in detail in [50] and various mechanisms have been suggested for reducing latency. The proposed techniques are based on "infrastructure activation" (IA). In IA the mesh APs use the quality of their current AP-to-MS links to determine which of several power saving

modes they should assume. Using this mechanism the nodes increase their level of availability when handoff is imminent, so that scanning and handoff latency is acceptable.

The Mobile Station Legacy Issue: Perhaps the single issue which would impede the development of power saving IEEE 802.11 infrastructure is that of dealing with legacy client devices. In many cases simple changes would be required, and these would have to be phased in as new IEEE 802.11 chipset products are developed. But even today, there are many emerging applications which would benefit immediately from the availability of power saving infrastructure. In many applications, the developer also has control over both ends of the link, and could readily exploit mesh AP power saving.

2.5.3 Power Saving in Infrastructure Wireless Networks

Various research and commercial activities have motivated and have contributed to the techniques needed for WLAN infrastructure power saving. In "infrastructure-based" wireless networks such as those found in cellular networks and wireless LANs, the infrastructure nodes (such as basestations and access points) are normally powered from a continuous energy source. For this reason, power saving in these types of systems has focused on the client devices, so that handset battery lifetime can be extended as much as possible [43]. Only recently has this focus included power saving on the infrastructure side of the link.

Power saving has also been a major topic in the study of both ad-hoc and sensor networks. In ad-hoc networks, nodes are often mobile, and the system

tries to continually provide full network connectivity. Reference [115] describes different power saving protocols for ad-hoc networks that use IEEE 802.11. Although these types of networks are different than in typical infrastructure network deployments, there are often interesting similarities. For example, some designs attempt to explicitly mimic the operation of their fixed infrastructure counterparts, by forming a node hierarchy. For example, in [107] a virtual basestation (VBS) architecture is considered for ad-hoc networks. The proposal emulates the operation of fixed cellular network infrastructure by electing a mobile station as a VBS which then functions as a temporary basestation. In [108] a power-aware version of this mechanism is described, where virtual base stations are chosen based on their residual energy reserves. In another example of this approach [88], mechanisms for forming and exchanging "cluster heads" is proposed for sensor networks, which shares the power consumption overhead due to packet forwarding. Reference [48] describes an example whereby Bluetooth slave nodes communicate directly (rather than through the piconet master, as is normally the case), for the purpose of reducing the Bluetooth master's energy consumption. This is yet another example where fixed infrastructure power saving is the objective.

Having surveyed different power saving techniques, it is important to gain a thorough understanding of how renewable energy systems are modeled in practice. In the following section, we provide a detailed description of how energy sources are modeled in practice using available meteorological data in order to be able to simulate renewable energy powered systems.

2.6 Energy Source Conversion

The work in [60] provides a step-by-step analysis of both wind and solar energy starting from the underlying physical laws that govern them. The reader is referred to this reference for more details. In the following, we focus on the necessary background in order to simulate a system powered using solar or wind energy as described in the following chapter.

2.6.1 Solar Conversion

In this section we describe how solar radiation is typically modeled in practice. In general, the solar radiation received at a geographical location is a random variable. This is due to several factors, some of which can be assumed to be cyclostationary such as the position of the sun in the sky. However, there are also strong random components introduced by such factors such as cloud cover, shading, and sky clearness. In the following subsection we provide an overview of the definitions commonly used in solar modeling.

In most photovoltaic (PV) applications, fixed panels are pointed directly south (for the northern hemisphere) and sloped slightly greater than the geographic latitude so that solar absorption is highest during winter months. Meteorological data however, is only available for horizontal and fully-tracking (direct normal) components and cannot be used directly for a fixed planar solar panel. For this reason a conversion model is used to compute the energy incident on the panel using horizontal and fully-tracking irradiance records. The total energy received by a solar panel consists of three components as follows.

1. Direct radiation, I_c. This is the radiation beams coming on direct paths from the sun.

2. Diffuse radiation, D_c. This component is caused by diffraction through the sky and consists of non-direct radiation components.

3. Ground-Reflected radiation, R_c. This is the result of solar insolation components that reflect from the ground plane and impinge on the solar panel.

The total solar irradiation on the panel is therefore the sum of the above components, i.e.,

$$G_c = I_c + D_c + R_c. \tag{2.1}$$

The direct component calculation is a straightforward geometric problem. The diffuse component estimation requires a more complex model, and several have appeared in the literature. The ground-reflected component is typically a small fraction of the total and does not significantly contribute to total solar insolation. However, when it is not considered the results obtained by the simulator can be considered to be a worst-case underestimation. This is a reasonable practical design approach.

In US and Canadian weather records, at least five different solar radiation data fields are commonly available. They are briefly described below.

1. Extraterrestrial Horizontal Radiation. This is the amount of solar radiation received on a horizontal surface at the top of the atmosphere. It is also known as "top-of-atmosphere" (TOA) irradiance, and is the amount of global horizontal radiation that a location on Earth would receive if

there was no atmosphere. This number is used as the reference amount against which actual solar energy measurements are compared.

2. Extraterrestrial Direct Normal Radiation. This reading is the level of solar radiation received on a surface normal to the sun at the top of the atmosphere.

3. Global Horizontal Radiation. The total amount of direct and diffuse solar radiation received on a horizontal surface at ground level where the measurements are taken.

4. Direct Normal Radiation. This is the amount of solar radiation received directly from the sun at the measurement point within a field of view centered on the sun.

5. Diffuse Horizontal Radiation, (D_h). This is the level of solar radiation received from the sky (excluding the solar disk) on a horizontal surface.

The first two fields are deterministic and can be calculated using the sun-earth distance and position equations, but the rest of the fields are random processes. In general, due to the motion of the earth around the sun and its rotation, solar insolation experiences cyclic changes over a year and these variations are deterministic to a large extent. However, some complex weather processes such as humidity, temperature, air pressure and cloud type affect the received insolation. The conversion models attempt to translate the above readings into the actual total solar energy impinging on a tilted plane solar panel. This is done by defining various solar angles which are used in the conversion. In addition to the solar radiation intensity, the angle of incidence

determines the energy received by the panel, which is a function of the time of day and day of the year.

The angle at which the solar radiation strikes the panel is called the incidence angle, θ. This is a function of the position of the sun in the sky and the slope and orientation of the panel. These two factors are specified using several parameters which are briefly described below. These parameters are shown in Figure 2.9. A list of notation is also given in Table 2.3.

1. Solar Declination Angle, δ. This is the angle between a plane perpendicular to incoming solar radiation and the rotational axis of the earth. It can be calculated as follows [75]

$$\delta = 23.45^\circ \cdot \sin[360(284 + n)/365], \tag{2.2}$$

where n is the Julian day.

2. Hour Angle. The Hour Angle is the angular distance that the earth has rotated in a day. It is equal to 15 degrees multiplied by the number of hours from local solar noon and can be expressed as,

$$h = 15 \cdot (t_s - 12). \tag{2.3}$$

3. Zenith Angle. This is the angle which is formed between the solar radiation beam and a vertical line at the panel location. It can also be computed as follows,

$$\cos(\theta_z) = \sin(\phi)\sin(\delta) + \cos(\phi)\cos(\delta)\cos(h). \tag{2.4}$$

Parameter	Definition
ϕ	Location's Latitude
β	Plane Slope
θ	Incidence Angle
γ	Plane Azimuth Angle
h	Hour Angle
t_s	Solar Time
n	Julian Day $(1 \ldots 365)$
ϵ	Sky's Clearness
Δ	Sky's Brightness
θ_z	Zenith Angle
m	Relative Optical Airmass
D_h	Horizontal Diffuse Irradiance
I	Direct Normal Irradiance
I_0	Extraterrestrial Irradiance
I_c	Direct Irradiance on Tilted Plane
D_c	Diffuse Irradiance on Tilted Plane
G_c	Total Irradiance on Tilted Plane

Table 2.3: Solar Conversion Definitions

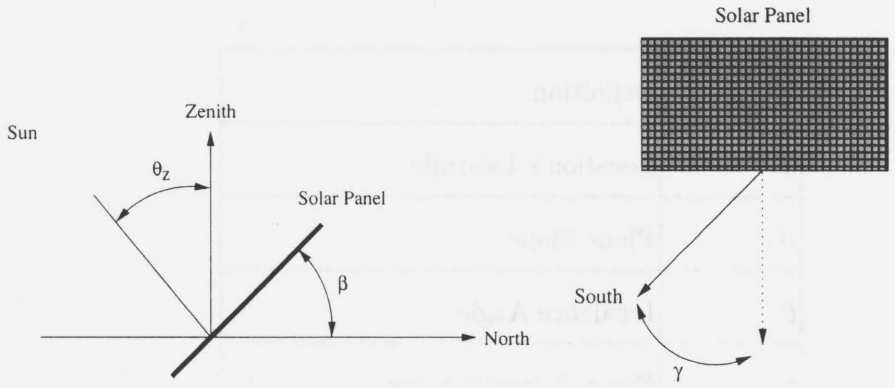

(a) Side View (b) Front View

Figure 2.9: Solar Angles

Solar Radiation Conversion Methodology

There are several methodologies available for performing the conversion. Some are based on the assumptions that the diffuse radiation is measured by the weather station, while others assume that it is not. References [49] and [82] provide methodologies that a designer can use when developing a simulator. In the following is a brief summary of the methodology.

In the first step, the direct component is estimated based on the zenith angle, the tilt angle of the plane, the hour angle and the solar declination angle. The sky clearness is then estimated and discretized which depends on the zenith angle, the direct component and the horizontal diffuse radiation. Next, the sky brightness is estimated using the procedure in [95]. Finally the diffuse component on a tilted plane is calculated [95].

The direct component of solar radiation on a tilted plane is a function of the direct normal solar radiation and the incidence angle. In [21], for an inclined

plane facing towards the equator the incidence angle is given as

$$\cos(\theta) = \cos(\phi - \beta)\cos(h)\cos(\delta) + \sin(\phi - \beta)\sin(\delta). \tag{2.5}$$

This can be simplified further for the case where the tilt angle is equal to the value of the latitude, i.e.,

$$\cos(\theta) = \cos(h)\cos(\delta). \tag{2.6}$$

This means that the solar incidence angle for an equator-facing plane is only a function of the hour angle and the declination angle. Now, the direct component of solar radiation can be written as

$$I_c = I \cdot \max[0, \cos(\theta)]. \tag{2.7}$$

The reason that we are taking the maximum of zero and $\cos(\theta)$ is to account for the fact that the sun is below the horizon at night.

We now describe the widely accepted Perez model for estimation of the diffuse component of solar irradiance on tilted planes [97]. This model has been extensively verified and yields accurate results. In simplistic models, a simple isotropic distribution of radiance throughout the sky dome has been assumed. Further refinements have incorporated the observed directionality of diffuse radiation [97]. In [95], estimations were improved by introducing a simple representation of the sky dome, and circumsolar and horizon anisotropy factors, F_1 and F_2. In this model the diffuse radiation is described by an isotropic background, similar to previous models, but it also includes two regions of enhanced radiation, i.e., a disk of variable size around the sun, represented by F_1 which is a multiplier for circumsolar region (See Figure 2.10), and, a

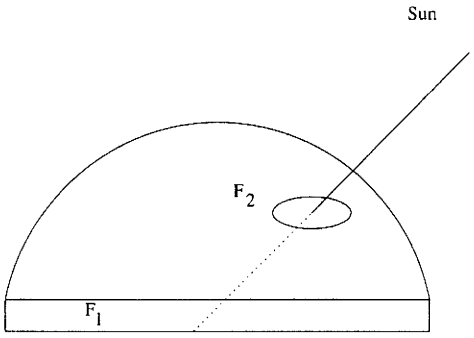

Figure 2.10: Representation of the Sky Dome Model Used in [96]

horizontal band of variable height at the horizon, represented by F_2 which is a multiplier for the horizon region (i.e., see Figure 2.10).

F_1 and F_2 are a function of the sky condition and have been reported to be consistent from site to site [95]. In this model, two parameters, ϵ (sky clearness), and, Δ (sky brightness), are used to characterize the condition of the sky. ϵ is given in [95] as follows,

$$\epsilon = [(D_h + I)/D_h + \kappa\theta_z^3]/[1 + \kappa\theta_z^3], \tag{2.8}$$

where κ is assumed to be 1.041 for θ_z in radians. Furthermore, ϵ values are discretized [95] to eight different levels ranging from 1 (overcast) to 8 (clear sky). The mapping table is given in table 1 [95]. In Equation 2 of [95], Δ is given as a measure of the sky's brightness, i.e.,

$$\Delta = D_h \cdot m/I_0, \tag{2.9}$$

where m can be obtained from Reference 11 in [95]. The F_1 and F_2 values can be obtained by looking up Table 6 in [95] where a set of coefficients are chosen based on the category into which the current sky's clearness index, ϵ,

falls. This table of coefficients is the result of experimental work in which it has been attempted to adjust coefficients so that RMS and mean bias error for all sites studied are minimized.

Finally, the diffuse component on tilted plane ([95], Equation 9) is given as follows,

$$D_c = D_h[(1 - F_1)(1 + \cos\beta)/2 + F_1 a/b + F_2 \sin\beta], \tag{2.10}$$

where $a = \max(0, \cos\theta)$ and $b = \max(0.087, \cos(\theta_z))$. As described, the three different parts of the above equation are specifying the the isotropic diffuse radiation from the sky dome, the radiations originated from the circumsolar region and those originated from the horizon region. The conversion algorithm is summarized below.

1. Estimation of the direct component

$$I_c = I \cdot \max(0, \cos\theta), \tag{2.11}$$

where θ is computed using the Equation (4a) from [21],

$$\cos\theta = \cos(\phi - \theta_s)\cos(h)\cos(\delta) + \sin(\phi - \theta_s)\sin(\delta) \tag{2.12}$$

2. δ is calculated using Equation 4 from [75],

$$\delta = 23.45^\circ \cdot \sin[360(284 + n)/365], \tag{2.13}$$

3. h, or hour angle is estimated according to the formula:

$$h = 15 \cdot (t_s - 12) \tag{2.14}$$

4. Zenith Angle Calculation

$$\cos(Z) = \sin(\phi)\sin(\delta) + \cos(\phi)\cos(\delta)\cos(h) \tag{2.15}$$

5. Calculation of ϵ

$$\epsilon = [(D_h + I)/D_h + \kappa Z^3]/[1 + \kappa Z^3] \tag{2.16}$$

and κ is assumed to be 1.041 for Z in radians.

6. Calculation of Δ

$$\Delta = D_h * m/I_0, \tag{2.17}$$

where m can be obtained using Reference 11 in [95], $m = (\cos(Z) + a(b - z)^{-c})^{-1}$ and we have $a = 0.50572, b = 6.07995, c = 1.6364$.

7. ϵ category

ϵ values are discretized to 8 different categories ranging from 1 (overcast) to 6.5 (clear sky)

Epsilon Categories = (1, 1.065 , 1.230 , 1.500 , 1.950 , 2.800 , 4.500 , 6.200);

8. Diffuse component on tilted plane ([95], Equation 9)

$$D_c = D_h[(1 - F_1)(1 - cos\theta_s)/2 + F_1 a/b + F_2 Sin\theta_s, \quad (2.18)$$

where $a = \max(0, cos\theta)$ and $b = \max(0.087, cosZ)$.

9. Estimation of F_1 and F_2. F_1 and F_2 are calculated based on the coefficients given in Table 6 in [95].

10. The total irradiance on a tilted plane would be the sum of the results of step 1 and 8

    $G_c = I_c + D_c$

Solar Model Refinements

In addition to the solar aspects, it is important to perform some adjustments for temperature effects, inaccuracies in measurements and losses in the electrical control circuitry. In [46] a model is used to predict the efficiency decrease of a solar panel that occurs with increased temperature. A set of temperature coefficients is provided that can be used for this purpose. In [81] the measured versus predicted performance of a PV system was evaluated based on a testbed implementation of different PV panel technologies, and compared to the model in [46]. They also created a model based on the Sandia Labs model [46] and the NIST cell temperature model and reported mixed results. The maximum error was found to be 7% for all modules tried. The study in [40] reported on experiences with solar-powered systems at the south pole with temperature variations of -20 to -70 degrees Celsius. Their experiences over 410 days showed

the survivability of the system. They reported that when the sun angle approaches its highest value and under high visibility conditions, the panel output approached peak rated power. Their work shows that solar panels perform well under extremely cold weather conditions.

In [87] a description is given of the instruments necessary to measure solar radiation and the potential sources of inaccuracies. Several solar models are described and divided into 3 categories: Solar radiation models (MRM, CRM, PRM), a diffuse ratio model to estimate diffuse irradiation when global irradiation is provided as the input parameter, and luminous efficacy models that enable estimation of diffuse and global illuminance once the respective irradiation components have been obtained. The work is based on weather measurements in the UK, but the paper discusses how it can be applied to other locations. Reference [34] constructs a solar model based on actual measurements in Australia for hourly and 15 minute increments. It is shown that both yield the same results. The model aims to predict the diffuse component based on the clearness index and time of day.

2.6.2 Wind Conversion

The calculation of available energy based on wind speed data is simpler than the case of solar energy since all that needs to be taken into account is the actual wind speed at a given location. Typically wind data is modelled using statistical models such as the Weibull distribution or using historical data directly.

In wind-powered systems designed using publicly available meteorological data, data collection and modeling is done in discrete time, using 1 hour Δ

increments. $\mathcal{E}_{turbine}(k)$ is the energy produced by the wind turbine and it is a function of wind speed W, i.e.,

$$\mathcal{E}_{turbine}(k) = \frac{1}{2}\xi\rho\pi R^2 W^3 \Delta, \tag{2.19}$$

where ξ is the efficiency of the turbine, which cannot exceed the theoretical limit of 59.26 %. This restriction was discovered by Betz in 1919. In practice, the achievable wind turbine output power is much lower than this limit due to losses in the alternator and due to the non-ideal aerodynamic properties of the turbine blades. Typical values for commercial wind turbines are in the 30% range. In Equation 2.19, ρ represents the air density which is roughly 1.23 kg per cubic meter at sea level. Wind turbines have two additional key parameters, namely, the *cut-in speed* which is the minimum wind speed at which the turbine starts generating power, and the *cut-out speed* where the turbine must be turned away from the wind to protect the blades.

2.7 Resource Allocation in Renewable Energy Systems

Different solar panel and battery sizing methods and their accuracy are studied in [89] along with discussions of how various PV components result in different system configurations. Three probabilistic methods for sizing PV systems are compared in [84]. The first method sizes the battery so that it can support a fixed load for a set number of days. Similarly, the panel is sized so that a full battery re-charge can be done within a specified time period. The second

scheme is based on detailed computer simulations. The last approach is based on Markov chain modeling of the battery state-of-charge. It has been shown that generally the second method yields the most accurate results [84].

In [39] a Markov chain model was used for battery state of charge in PV systems. To use this approach however, the variance and mean of the daily solar insolation must be known. This model was refined in [38] and includes the effects of inter-daily correlation in solar irradiation. Another performance evaluation of PV systems based on Markov chain modeling is presented in [106]. A closed form solution for PV system sizing is studied in [22]. In [22] and [58] the sky clearance index is used for simulation of solar irradiance. Reference [35] considers the optimum PV array sizing for a stand-alone hybrid wind/PV system. In [105] variable loading is taken into account in the sizing of PV systems. A fuzzy decision-making process is used in [83] to evaluate subjective factors in the PV system sizing decision. Energy management issues in a space station have also been considered under limited energy constraints [36]. Much of the quoted work assumes idealized battery models which can lead to significant inaccuracies. In practical PV systems for example, battery capacity is a strong function of the ambient temperature. In [29, 109] and [99] some relevant models for the battery behavior are studied.

In [49] a study is presented of the resource allocation problem in solar powered WLAN mesh nodes. This work also shows the potential of mesh node power saving on the resource assignment. It was shown that there can be a significant reduction in node cost when AP power saving is used. In addition, several outage control strategies are presented that can be used to prevent mesh

node outage.

A variety of previous work investigates the use of hybrid powered systems [35],[28],[71] [77]. In [35], long-term hourly weather data for 30 years is used in order to calculate the optimum size of a PV array for a stand-alone hybrid wind/PV system. This was done by generating probability density functions of the wind speed and solar insolation for each hour in any given month. A least squares method is then used in order to find the best fit of the PV array and wind turbine for a given load. In [28] a similar approach is used, except that a more refined method is introduced for calculating the probability density function. This is then used to compute the number of required storage batteries and PV panels. The reader who is interested in the theoretical background of wind and solar power characteristics should refer to [60], which provides a step-by-step analysis of both energy sources.

In [71] a simple numerical algorithm is used to compute the optimum generation capacity and storage needed for three scenarios in a remote area in Montana, with a typical residential load. These options are stand-alone wind, PV, and hybrid wind/PV. The paper then performs an economic analysis in order to measure the cost effectiveness of the three scenarios. Finally, in [77] the output power of wind turbines in cold weather is discussed. The conclusions are based on experiments performed in Tiverton, Canada, and show that wind turbines are practical in cold regions.

Many of the above studies deal with the tradeoffs between node resource requirements and the power consumption of the node. The ability for WLAN mesh infrastructure to conserve power is a highly desirable capability and can

lead to significantly reduced node cost. This issue is discussed in detail in the next chapter.

2.8 Conclusions

In this chapter we have presented an overview of the necessary background information in addition to previous work in this area. We began our discussion by presenting an overview of Wireless Local Area Networks (WLANs) and Wireless Mesh Networks (WMNs) including a summary of the most relevant features of the IEEE 802.11 standard. We then surveyed previous work that provides motivation for power saving in wireless infrastructure networks. This was followed by a survey of power saving techniques in different wireless networks. Finally, we presented current methodologies used to simulate solar and wind powered systems based on available meteorological records. In the following chapter, we present the resource allocation problem in wireless infrastructure networks that are powered using more than one energy source. We investigate the different cases where a hybrid approach is more cost-effective than a single-source approach based on the geographic location, power consumption profile, and the cost model. We conclude our analysis by highlighting the effect of power saving on the overall cost savings.

Chapter 3

Resource Allocation in Solar/Wind Powered WLAN Mesh Networks

3.1 Introduction

In this chapter, geographic provisioning results for solar and wind powered WLAN mesh nodes are presented. A cost model is introduced which is used to optimize the provisioning of nodes with potentially more than one energy source. The results suggest that in certain geographic locations a hybrid wind/solar powered WLAN mesh node provides the minimum cost configuration. Cases will be included using existing IEEE 802.11 standard assumptions

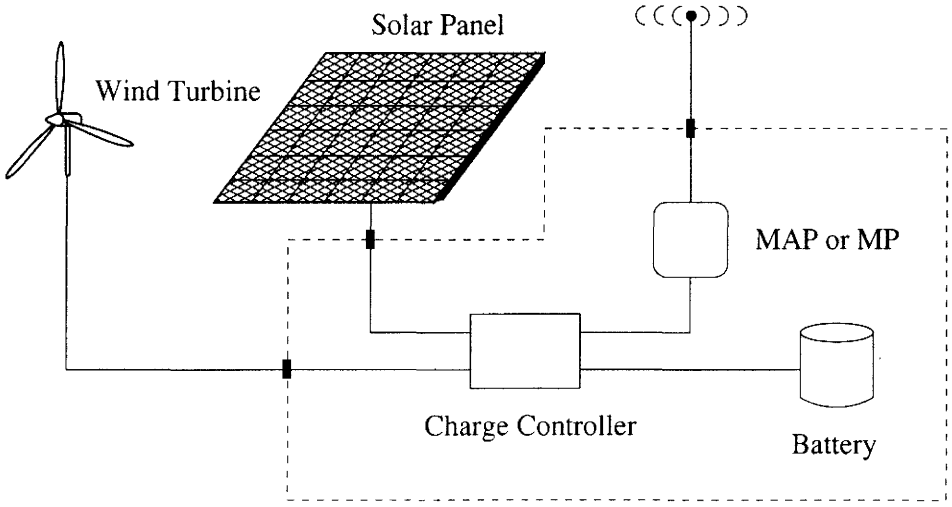

Figure 3.1: Solar/Wind Powered WLAN Mesh Node Components

and will also consider the case where modifications are made to the standard so that mesh AP power saving is possible. Several North American locations have been chosen for these results, i.e., Toronto and Yellowknife, Canada; Seattle, WA, and Phoenix, AZ. These locations have been chosen to illustrate a variety of differing meteorological situations. This is followed by a discussion of power saving effects on cost reduction. Specifically, we consider the case when the nodes are carrying connection-oriented traffic.

3.2 Introduction to the Energy Flow Model

In this section the basic configuration of a hybrid powered WLAN mesh AP (MAP) or mesh point (MP) node is discussed. A simplified block diagram is shown in Figure 3.1. The system includes a wind turbine and/or solar panel, and a battery. The solar panel and/or wind turbine are connected to the bat-

tery through a charge controller which disconnects the battery to protect it from under- and over-charging. For a comprehensive review of the underlying physical processes that govern wind and solar energy sources the reader is again referred to [60]. We can define an energy flow model for this configuration, where $\mathcal{E}_{panel}(k)$ is the energy produced in the solar panel over the time increment $[(k-1)\Delta, k\Delta]$, and Δ is the time-step length considered. In hybrid PV systems designed using publicly available meteorological data, data collection and modeling is done in discrete time, using 1 hour Δ increments. The solar panel size is given by S_{panel}, and is normally rated in watts at peak solar insolation. $\mathcal{E}_{turbine}(k)$ is the energy produced by the wind turbine.

We also define $\mathcal{B}(k)$ to be the residual battery energy stored at time $k\Delta$, and $\mathbf{B}_{max}$ is defined to be the total battery capacity. If we assume that $\mathcal{L}(k)$ is the load energy demand over the time duration $[(k-1)\Delta, k\Delta]$, then we can write that [106],

$$\mathcal{B}(k) = \min\{\max[\mathcal{B}(k-1)+\mathcal{E}_{panel}(k)+\mathcal{E}_{turbine}(k)-\mathcal{L}(k), \mathbf{B}_{outage}], \mathbf{B}_{max}\}. \quad (3.1)$$

In this equation $\mathbf{B}_{outage}$ is the maximum allowed depth of discharge, based on safety and battery life considerations [89]. When $\mathcal{B}(k) < \mathbf{B}_{outage}$, the charge controller will disconnect the MAP/MP load and the node will experience a radio outage. It is also important to consider temperature effects because any reduction in temperature leads to a reduced charge storage capability in the battery. This effect has been taken into account in the results that will be presented later.

In the remainder of this thesis, we assume that the solar data has been properly converted based on the methodology shown in [49] and in Chapter

2 to match the installed panel. The value of the solar insolation is rated in watts, and it is normalized to the panel's peak power. For example, when the insolation is 0.1 and it is incident on a 60 W solar panel, the overall power generated is 6 W.

3.3 Energy Flow Simulation Methodology

Our simulator, which is an extension of the simulator developed using MATLAB in [49] implements the energy balance equation shown in Equation 3.1 for a given geographic location. It also accepts as input the publicly available meteorological information for a given geographic location. Throughout this thesis we focus on North American records that are maintained in the USA and Canada. For the USA the records are kept at the National Solar Radiation Data Base (NSRDB), National Renewable Energy Laboratory (NREL), U.S. Department of Energy [91]. For Canada, the data may be obtained from the National Climate Data and Information Archive, The Meteorological Service of Canada (MSC) [90]. The data is usually presented on an hourly basis, i.e., $\Delta = 1$ hour.

The simulator incorporates the algorithm mentioned in [49] to convert the available solar data based on the different solar angles. The simulator provides the outage events and the battery charge at every hour during the simulation. As shown in the following section, it will be used to quantify the temporal behavior of the energy sources at a given geographic location.

3.3.1 Resource Allocation Example

Solar Example

In the following, we assume an all-solar powered node. If we assume that the traffic load can be translated into a mean power consumption profile, we can use the simulator developed in [49] to show the contour plots associated with each outage probability for a continuum of battery and panel sizes. We define the outage probability as the fraction of times the node is in outage over the time period of interest.

First consider several simple examples. Using data for the city of Toronto and 10 years of weather data (1981-1990), we can obtain the outage contours shown in Figure 3.2. In this case a fixed 4 W average load is assumed. We notice that the curves for all outage probabilities have the same shape, i.e., if the battery level is too low, then increasing the panel size has no perceptible effect on improving the outage probability. This can be explained by observing that if the battery is too small, it does not matter what the panel size is since there is no place to store the surplus energy. On the other hand, if the panel size is too small, there is a cap on the maximum solar energy that can be converted into energy for the system and increasing the battery size will not improve the performance. By observing the regions where the curves flatten out and the required panel size is constant for any battery size (let us assume 100Ah) we see that for $P_{Out} = 0.1$ the panel size is slightly less than 30 W while for the 0.01 case the value is slightly less than 50 W. For the 0.001 case the value is slightly above 60 W and for the 0.0001 case the value approaches 70 W. From this we can conclude that increasing the panel size by 66% will improve the 0.1

high outage case ten-fold. Going from 50 W to 60 W only represents a 20% increase in panel size again yields a dramatic ten-fold improvement. Finally going from 0.001 to 0.0001 only requires less than a 17% increase in panel size. It is also worth considering that panel cost is roughly proportional to its area. An 0.0001 outage represents an almost negligible 0.876 hours of outage per year while a 0.001 outage represents about 8.76 hours per year.

Let us now examine the constant battery regions of the curves. In this case we go from about 5 Ah to less than 20 Ah to less than 40 Ah to almost 50 Ah in order to improve the outage probability from 0.01, 0.01, 0.001 and 0.0001. Again, for high outage probabilities large investments must be made to improve them, while incremental investments lead to significant improvements when the outage probability is low. The results from the simulator do not indicate when the outage will occur, since only the frequency of outage events is measured. However, if one inspects the charge distribution, most of the outages will occur during the night after a succession of gloomy days in winter months. This is especially true for the low outage probability cases since the panel and battery are significantly over-engineered.

Figure 3.3 also shows the effect on the required resources of different traffic load levels for a negligible outage probability of 0.0001. From the graph obviously the outage probability can be improved by increasing the resources allocated to the node, this will be at the expense of the overall node cost. Let us illustrate this by an example. The 1 W case has an approximate minimum panel size of 10 W, while the 4 W case requires an approximate minimum panel size of 70 W. This means that a 400% increase in load requires a 700% increase

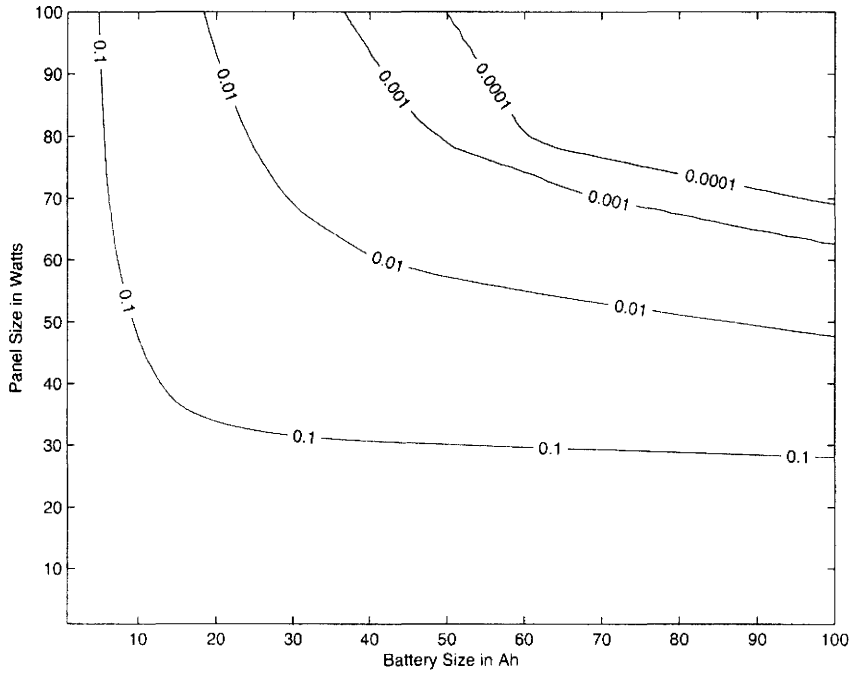

Figure 3.2: Solar Outage Contour Plots for Toronto

in investment for the panel. For the battery we need to increase the size from less than 5 Ah to 50 Ah.

For Phoenix, Arizona, similar results are shown in Figure 3.4. In this case, we see that when compared to Toronto, far less resources are required to significantly improve the outage probability. For example, again by examining the constant slope areas, we observe that to improve the performance from 0.1 outage to 0.0001 one needs to increase the battery size from less than 5 Ah to slightly less than 10 Ah. For the panel size one needs to increase the size of the panel from 15 to 25 W. Therefore, in Phoenix, protocol power saving will not be as valuable from a cost savings point of view. In addition, the overall size of the node will not increase significantly. In such situations the cost of the

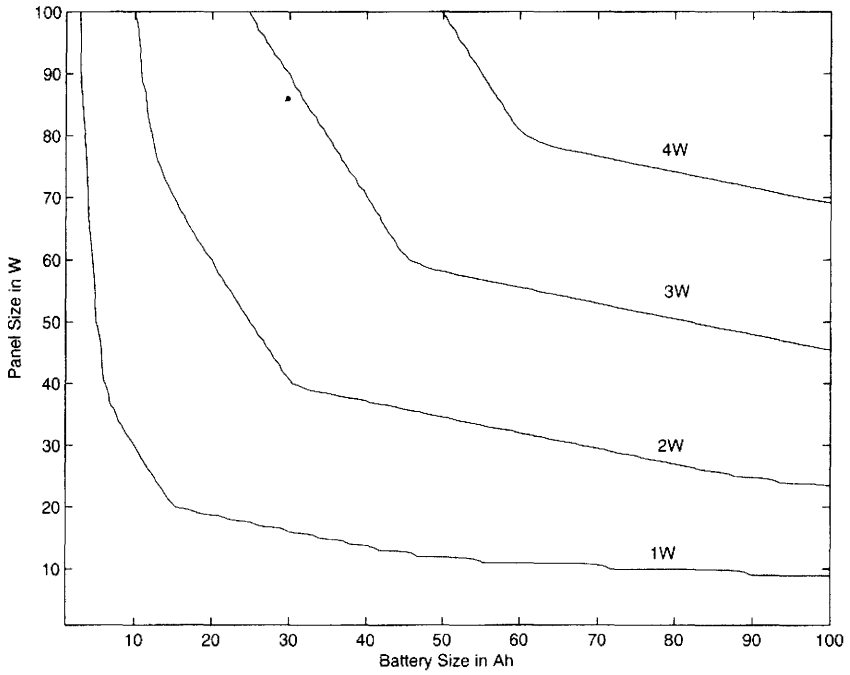

Figure 3.3: Solar Outage Contour Plots for different load levels for Toronto for $P_{Out} = 0.0001$

panel is likely to be a much smaller fraction of the total node cost compared with more temperate locations.

For Yellowknife, NWT, which represents a case of more extreme conditions, the results are shown in Figure 3.5. In this case, we need to increase the size of the battery from less than 10 Ah to around 125 Ah. Similarly for the panel we would need to go from 40 W to almost 130 W. We compare this to Toronto and Phoenix to deduce that the increase in investment is huge. We observe though that when the outage probability is low, only an incremental upgrade in resources leads to significant improvements in terms of outage performance. Therefore, in this geographic location, power saving may be very important

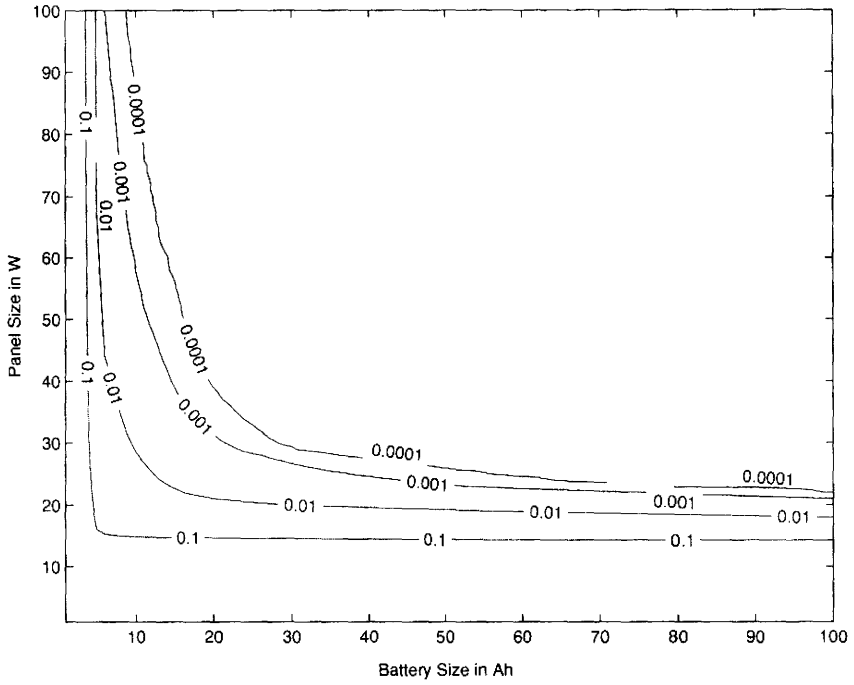

Figure 3.4: Solar Outage Contour Plots for Phoenix

and may lead to significant node cost savings.

In Figure 3.6 we show a comparison for a negligible outage probability (i.e., 0.0001) for several different cities at 1W loading for 10 years of solar insolation data. We see that Yellowknife represents the extreme case while Phoenix and Atlanta can be considered on the other end of the spectrum. This can be explained by 2 effects, one is the frequency of solar insolation received at each city, the other factor is the dips in temperature which negatively affect the battery capacity. We see that a node in Seattle would need more resources than Toronto, this can be attributed to the amount of cloudy days in Seattle.

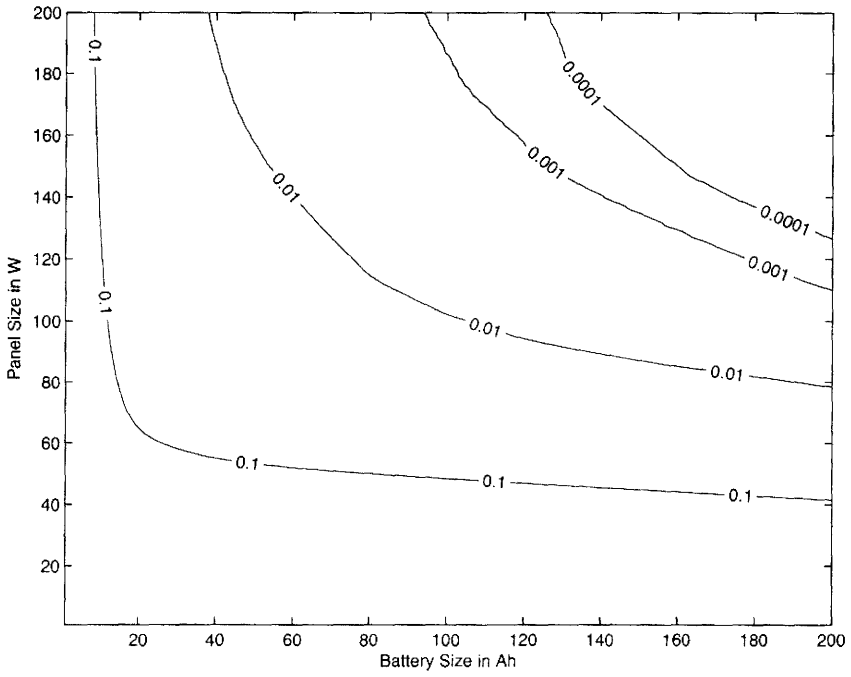

Figure 3.5: Solar Outage Contour Plots for Yellowknife

Wind Example

On the other hand, similar results can be shown for a wind turbine. The results can be seen in Figure 3.7 which shows the outage contour plots for different turbine and battery sizes for Toronto. The results are based on one year's data and assumes a turbine efficiency of 30 %. As seen, the wind turbine can also eliminate outages when deployed in the city of Toronto and the behaviour of the system is similar to the solar-powered case. We also observe that the increase in resources required is minimal in order to reduce outage. For example, for a battery size of 25 Ah, the turbine radius only needs to be increased from 12.5 cm to 13.75 cm to improve the outage level from 0.01 to 0.0001. In the

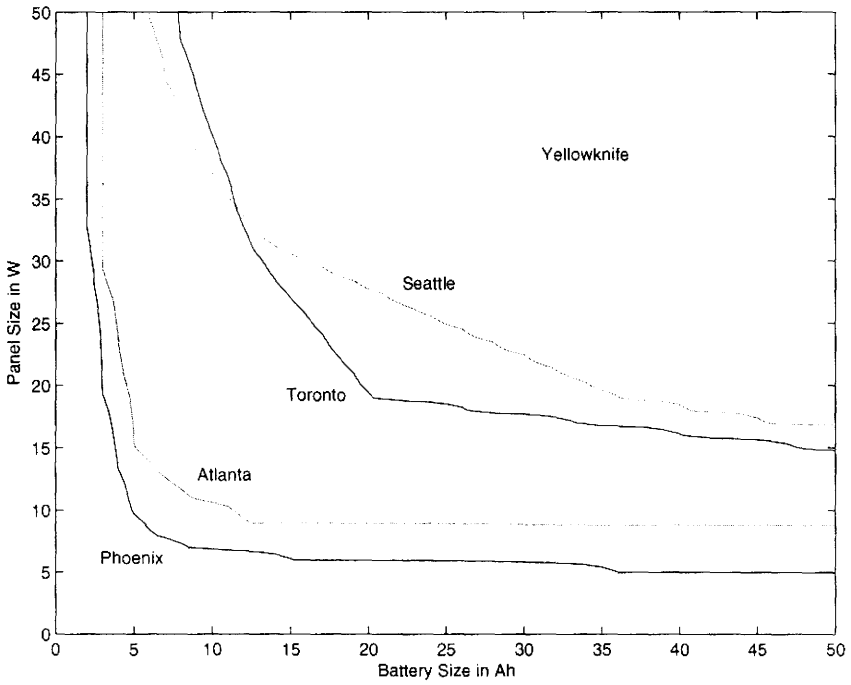

Figure 3.6: Solar Outage Contour Plots for Several Cities in North America for $P_{Out} = 0.0001$

following section we discuss a simulation-based characterization of different energy sources.

3.4 Characterizing Energy Sources

The designer of a renewable energy powered mesh network must take into account the nature of the energy source, especially its diurnal and seasonal cyclostationary properties. This section aims to provide a simulation-based quantification for the solar and wind energy in a few locations in North America.

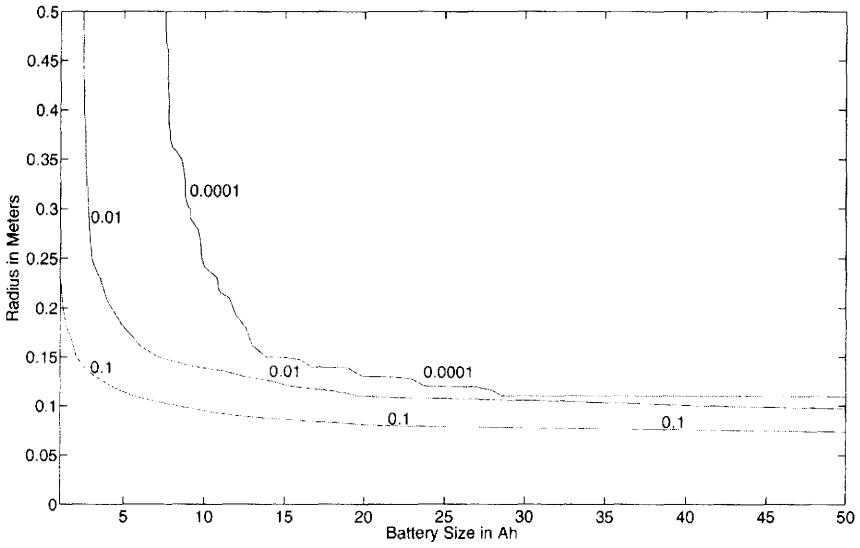

Figure 3.7: Wind Outage Contour Plots for Toronto

The methodology shown here is applicable to any other geographical location.

There have been previous attempts at quantifying energy sources as shown in [69, 70] which present an analysis of environmentally powered sensor networks. A model based on previously proposed leaky bucket Internet traffic models approach is proposed for characterizing energy sources and loads. The proposal also includes a harvesting theory that governs storage and power consumption requirements. The results shown by the authors are developed for constant and variable power operation.

3.4.1 Energy Source Examples

In this section we give some example configurations of renewable energy resource assignment using the above procedures for two diverse climatic locations,

i.e., Toronto, Canada, and Phoenix, AZ. For a given location it is important to quantify the joint statistical distribution of the wind and the solar energy. For example, if wind speed increases greatly during night-time hours and is almost zero during the day when there is bright sunlight, this would suggest that a hybrid wind/solar system might be cost effective. In this case a node could operate during the daytime hours from the solar panel and at night from the wind turbine thus minimizing the size of the battery needed for either case alone. The same argument applies to long term correlations between the energy sources.

Example of Short-Term Statistics

In this section, we investigate the short-term statistics of the different energy sources for two example locations, Toronto, Canada, and Phoenix, AZ. In the results, we assume that we use a small, commercially available wind turbine of fixed size, the Muartec Rutland 503 [85] which generates approximately 24 watts at a wind speed of 10 m/s. For the city of Toronto, we assume a 60 W solar panel which corresponds to the wind energy available at the maximum wind speed.

Figure 3.8 shows a time distribution example of solar power and wind power for the first 100 hours in January and July, 1990, for the city of Toronto. It can be seen that in January, the wind power is more dominant than solar power. We also observe that during some time instances, there is a strong positive correlation between the increase in solar insolation and the increase in wind speed, yet the power available from the wind is much greater. For example, if

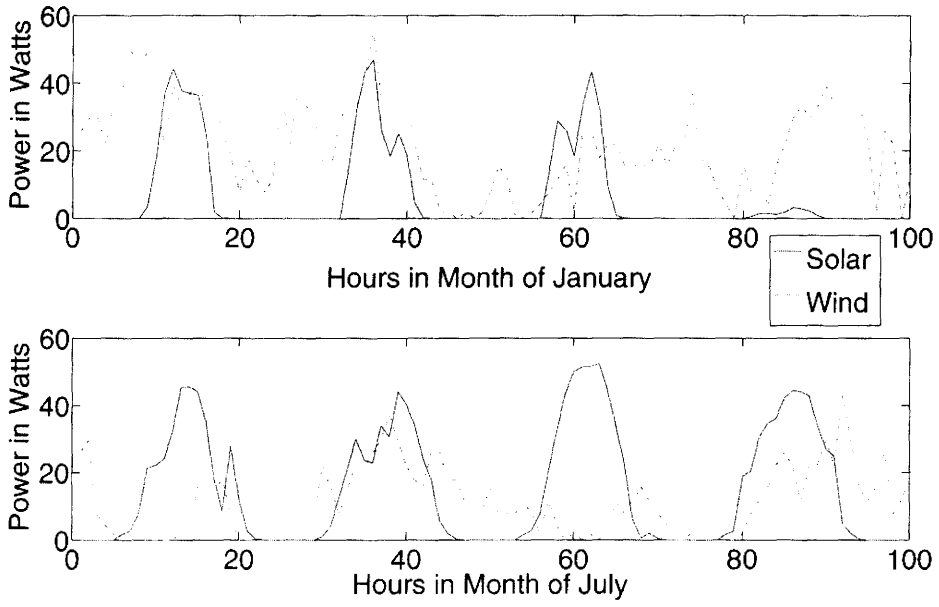

Figure 3.8: Comparison of Solar Power and Wind Power for Toronto in January and July

we examine the first 24 hours, we see that the wind power is always present and it peaks at almost 50 W while the solar insolation is not always available and peaks at 42 W.

The situation is reversed in July where we see that the solar insolation outperforms the wind power. For example, the solar insolation peaks during the day at slightly less than 45 W while at the same time the wind dies down to values less than 18 W during the day. During the night, we again see a very strong correlation, i.e, both sources produce negligible power.

The mostly positive solar/wind power correlation that is observed for Toronto would suggest that a hybrid solar/wind powered node may not be cost effective. When the sources are strongly correlated, it may be best to use

the one that is the most cost effective. However, this conclusion needs to be verified by incorporating a cost model which will influence the optimal mix of both energy sources. This will be treated in more detail in Section 3.5.

If we consider the city of Phoenix, the maximum wind power is 35 W. In this case we compare to a solar panel with peak power equal to 35 W. Figure 3.9 shows the power distribution over time for the first 100 hours of January and July, 1990. We can see that the solar power clearly dominates the wind power for January and July, indicating that it may always be more cost-effective. We can see that the collected solar power is almost always at its peak of 35 W (and zero at night), while the wind power rarely exceeds 10 W. In addition, we notice that even though the increase in wind speed is correlated to the decrease in solar insolation, the values are so low that it may not significantly reduce the required battery size. These traces suggest that in a location such as Phoenix, wind power alone or a hybrid wind/solar solution is probably not feasible.

Example of Long-Term Statistics

We now consider some examples of the long-term behavior of the wind and the solar energy sources. In the first set of results we present examples that compare the relative value of solar versus wind power, when the total average power from each source is the same. For comparison purposes we assume the source can generate a long term average power output of 2 W, which is roughly the minimum power consumption of a single radio WLAN mesh AP whose radio is always active [114].

For the city of Toronto (1990) the average wind speed is 7 m/s, and in order

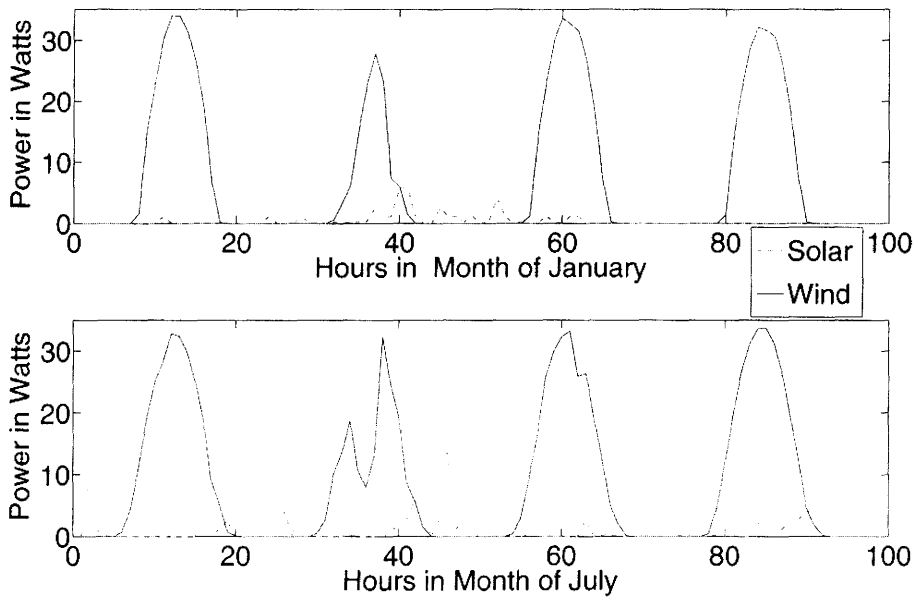

Figure 3.9: Comparison of Solar Power and Wind Power for Phoenix in January and July

to supply an average of 2 W, we would need a 7 cm wind turbine assuming a turbine efficiency of 30%. On the other hand, the average solar insolation is 0.1746, so the solar panel size would be approximately 11.5 W. The comparison is shown in Figure 3.10. We can see that for a city like Toronto with a temperate climate the solar powered node slightly outperforms the wind-powered node. For example, at a battery size of 10 Ah the wind outage is 0.28 while it is 0.2 for the solar-powered node. For Phoenix, the average wind speed is 2.6945 and therefore, the wind turbine radius would be 35 cm. The solar insolation is 0.2651, which yields a solar panel size of 7.5443 W. These results are also shown in Figure 3.10. We can see that the solar panel in Phoenix greatly outperforms the wind turbine. For example, at a battery size of 50 Ah, the solar panel

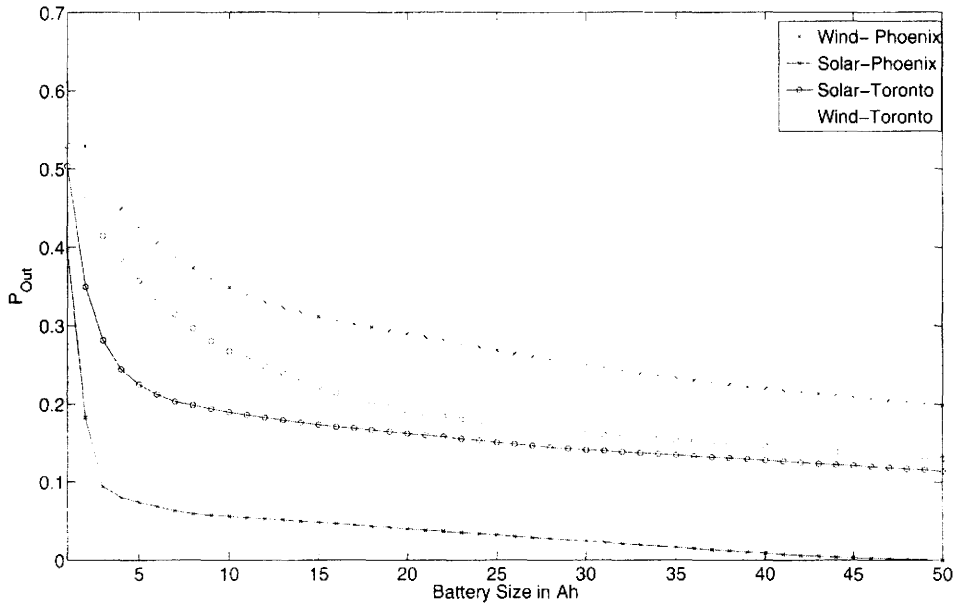

Figure 3.10: Comparison of Sources for Toronto and Phoenix for a 2 W load with the same average power.

outage is almost zero while it is still 0.2 for the wind turbine case.

The behavior seen in Figure 3.10 is somewhat counter-intuitive. If the long-term average output power from solar and wind power is the same, and if both processes were stationary over short time periods (on the order of days), then one might expect that wind power would achieve better outage performance than solar. This is because solar insolation is always absent at night time, whereas the same is not true for wind power. On this basis one could argue that solar insolation is more "bursty" than wind power (for the same long term average), and thus requires a higher battery capacity to achieve the same outage probability.

The above behavior is explained by considering the seasonal correlation

between solar and wind power. In Figure 3.11 we show the state of charge of an initially full battery when it is powered only by a wind turbine and then only by solar power. Again both sources produce an average of 2 W. Examining the curves carefully, we can see that the wind and solar energy have a strong negative seasonal correlation. For example, in the summer the battery is always full when powered by the sun while it is almost empty when powered by the wind. The situation is reversed to a lesser degree in late fall and winter when the wind energy increases while the solar energy is greatly reduced. These results strongly suggest that a node placed in Toronto would benefit from a hybrid design with more emphasis on solar energy, however, the ratios of the contributions of the sources will be dictated by cost considerations. The short-term statistics would have suggested that wind power is more perpetual on an hourly basis especially at night when the solar panel generates zero energy. However, after examining these results it is clear that the wind and solar energy for Toronto have the potential for augmenting each other on a seasonal basis. These observations cannot be generalized, i.e., if we examine Figure 3.12 we can see a similar comparison of sources for Phoenix. It is clear that the node almost never runs into an outage when powered by solar energy. On the other hand, we can see that the wind energy fluctuates seasonally, leading to outage. In this case it seems that without considering the relative costs involved, solar energy is the clear winner as the node's energy supply.

In Figure 3.13 for Seattle, the results are similar to Toronto, though both the wind and solar energy are slightly less. Finally, for Yellowknife, as shown in Figure 3.14, we can see that the solar energy is very weak and almost nonexis-

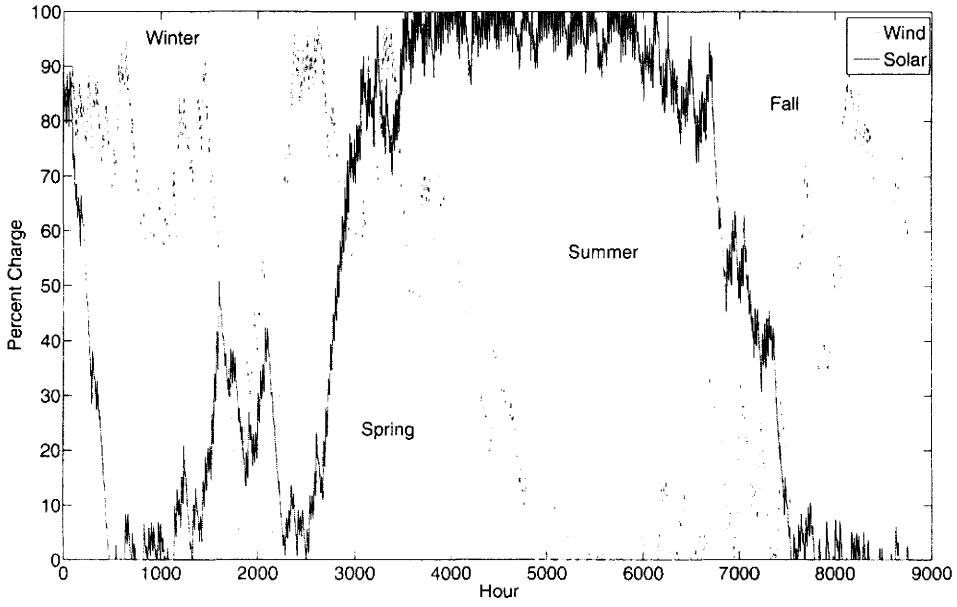

Figure 3.11: Percentage Charge versus Time for Different Sources for Toronto with a 50 Ah Battery

tent in the fall and winter. The wind power during this period is better, which suggests that the wind source would be useful in supplementing the node during the darker months. Again, the results suggest a hybrid approach.

3.4.2 Node Sustainability

In this section we consider the sustainability of a given hybrid system for the different geographical locations. By the term "sustainable" we refer to the continuous operation of the node without going into outage or what is referred to in the literature as a node death event. More details will be provided in Chapter 5. We consider two possible scenarios. In the first case, we assume a small

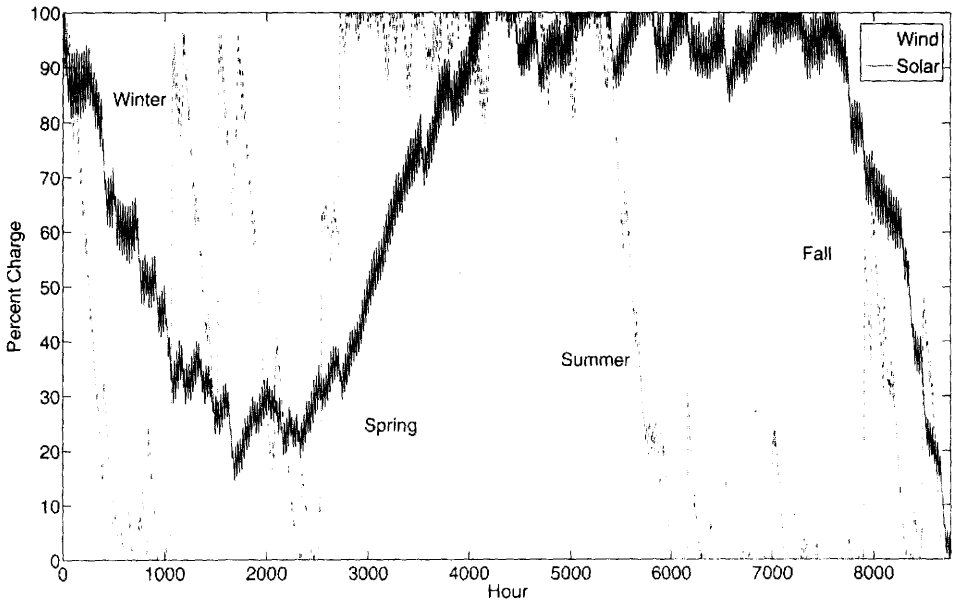

Figure 3.12: Percentage Charge versus Time for Different Sources for Phoenix with a 50 Ah Battery

commercial wind turbine (Muartec Rutland 503) that is used to supplement the system. The other scenario to be considered is when the turbine size may be arbitrarily chosen. It is important to point out that the performance of the Muartec Rutland 503 is less than the theoretical value of a corresponding wind turbine. This effect is shown in Figure 3.15. However, it should be noted that at the most common wind speeds the values of the power for both cases are almost identical. In all of the following simulations we assume a typical value for the wind density of 1.23 kg/m^3 and that the cut-in and cut-out speeds are cut_{in} = 3.75 m/s, cut_{out} = 20 m/s respectively. We also assume that the load to be powered is a constant 2 W.

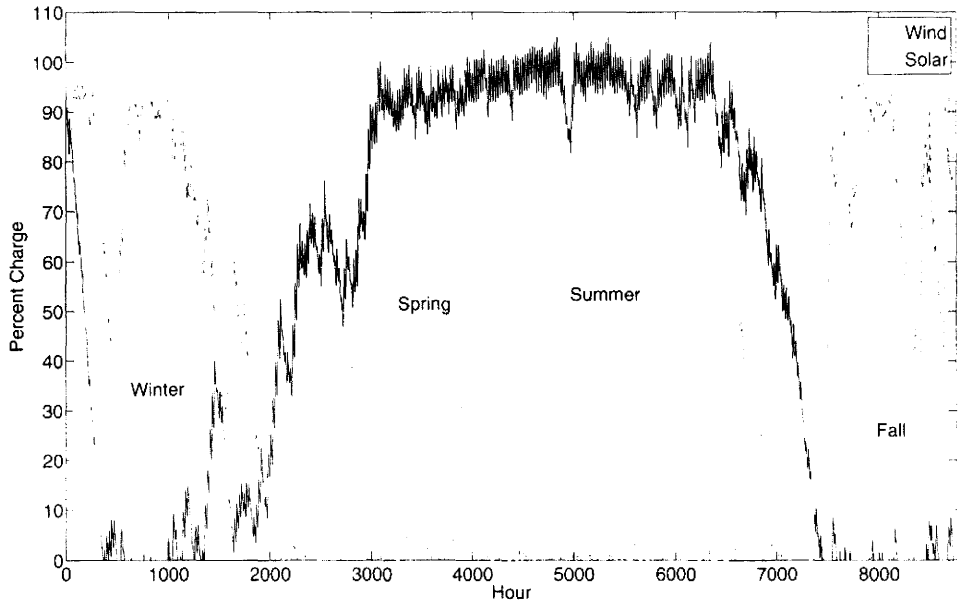

Figure 3.13: Percentage Charge versus Time for Different Sources for Seattle with a 50 Ah Battery

Fixed Wind Turbine Source

In this section we assume a specific wind turbine configuration (the Muartec Rutland 503) with no solar panel, and simulate the system to find the battery sizes needed to eliminate outage. This wind turbine is one of the few that are commercially available at about the size needed for WLAN mesh AP applications. Figure 3.16 shows the outage probability versus the battery size for the 4 different geographical locations. We can see that a battery size of 12.5 Ah will completely eliminate outages for Toronto, and for the other cities a much larger battery is needed and even then it may not eliminate outages completely. By comparison, the same turbine installed at Phoenix will never eliminate outages

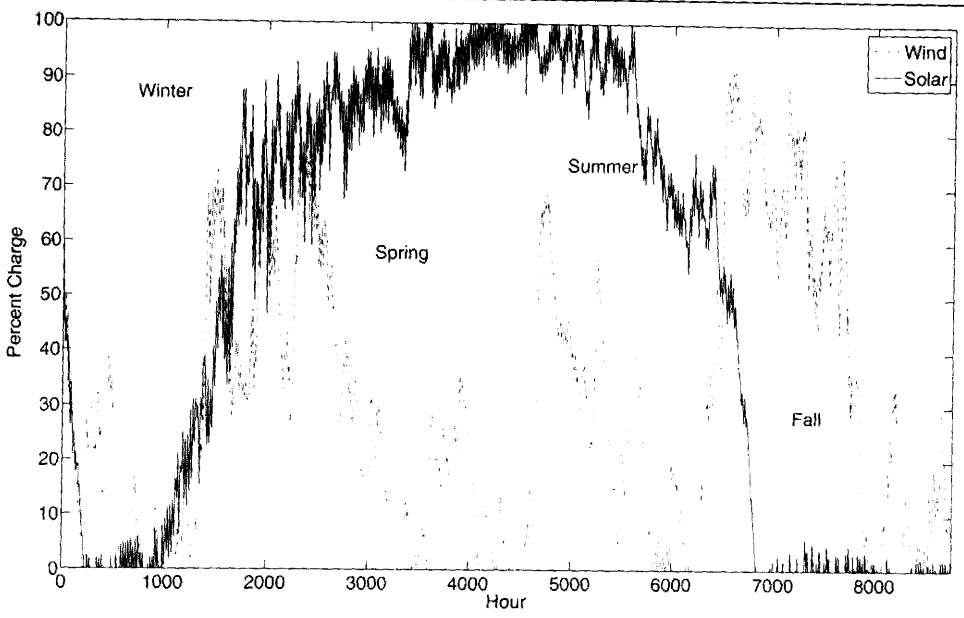

Figure 3.14: Percentage Charge versus Time for Different Sources for Yellowknife with a 50 Ah Battery

even for a very large battery due to the scarcity of wind power as previously discussed. We also see that the results for Yellowknife and Seattle are between those for Toronto and Phoenix. We notice that Yellowknife greatly outperforms Seattle which indicates that the wind energy is more abundant in that region even though the storage capabilities of the battery are greatly impaired due to cold temperature effects.

It can be seen that the option of simply installing a commercially available wind turbine will not eliminate outages in some cases even for very large battery sizes. In the following section, we examine the case when we can choose the size of the turbine freely without the restriction of current commercial availability.

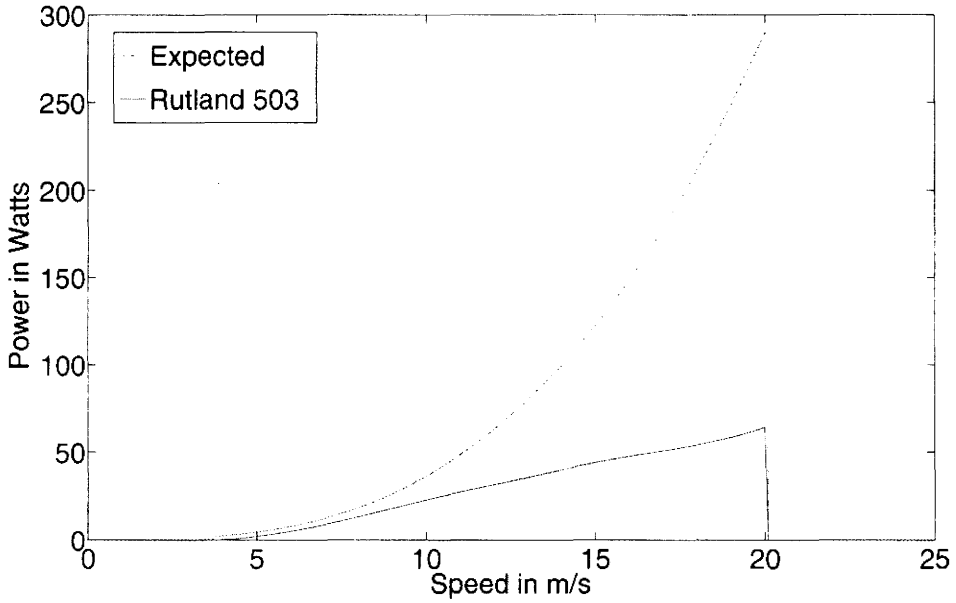

Figure 3.15: Theoretical vs. Real Performance of Turbine

Variable Wind Turbine Size

In this section we assume that we can select the wind turbine size for a given location. Figure 3.17 shows the contour plots of the outage probability for different turbine radii and battery sizes for Toronto. For example, if an outage probability of 0.0001 is required, the battery size will be 15 Ah with a turbine radius of 15 cm. From this we can conclude that wind power in Toronto can successfully eliminate outage. However, as we will see in the next section, it is important to take into account the cost of the turbine. In addition, examining the seasonal correlation with solar power will dictate the optimal mix of both sources.

On the other hand, Figure 3.18 shows the corresponding contour plots for Phoenix. Clearly the resources needed at Phoenix are much higher than

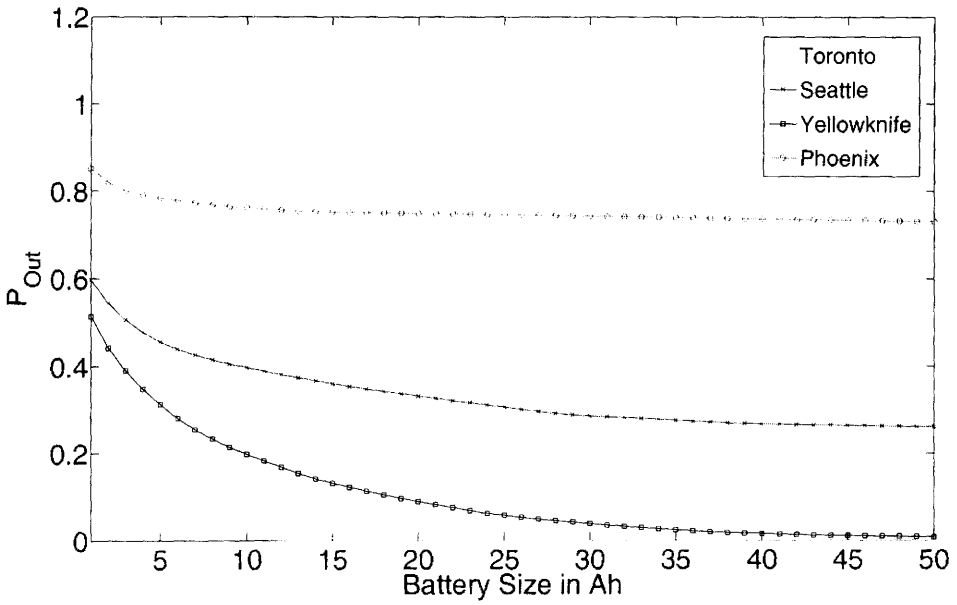

Figure 3.16: P_{Out} vs. Battery Size for the Muartec Rutland 503 Wind Turbine

Toronto. By following the same example, the battery size would be 45 Ah which is a threefold increase. The wind turbine radius is 70 cm which is an increase of 4.5 times over that of Toronto. We can conclude that installing a wind turbine at Phoenix is likely to be prohibitively expensive and will never successfully eliminate outages.

Figure 3.19 shows the results for Seattle, and we can see that the battery size is 25 Ah and the turbine radius is 30 cm. Finally, Figure 3.20 shows the results for Yellowknife, the required battery size is 70 Ah and the turbine radius is 35 cm. We can conclude that in most locations, wind energy will be sufficient to meet an acceptable outage probability criterion, however this will be at the expense of the costs associated with the size of the wind turbine and battery needed.

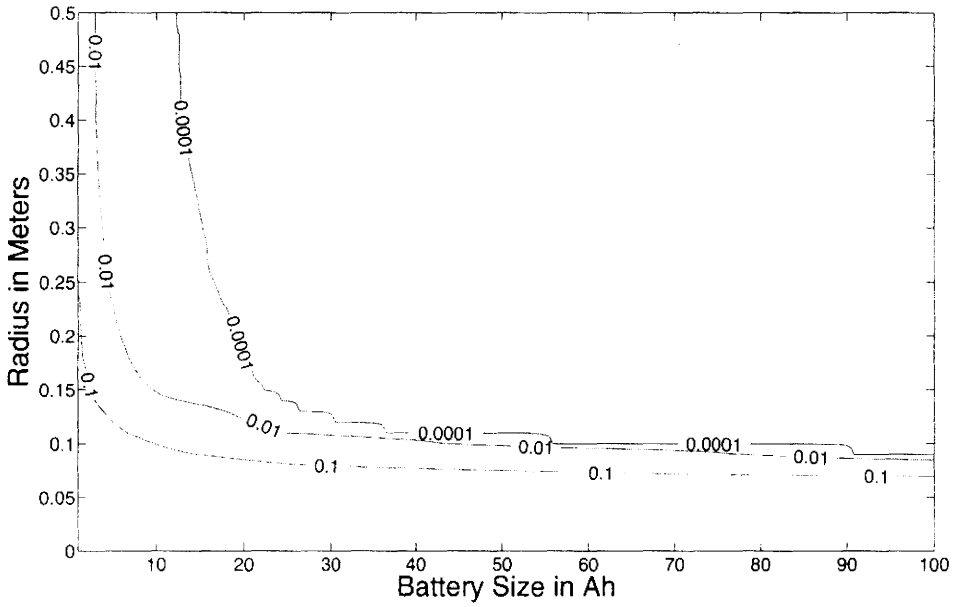

Figure 3.17: Contour Plot of P_{Out} for Different Wind Turbine and Battery Sizes for Toronto

In the following section, we examine the effect of integrating the cost model with the energy model for each city in order to obtain the optimal mix of energy sources and to find out when it would be best to deploy a hybrid node versus a node powered by a single energy source.

3.5 Cost-Based Optimal Resource Allocation

From the previous discussion, we can conclude that in most cases the addition of a wind turbine will greatly improve the performance of a WLAN mesh node. However, the addition of the turbine must justify its added cost to the system. In this section we provide a cost optimization for a hybrid solar/wind node.

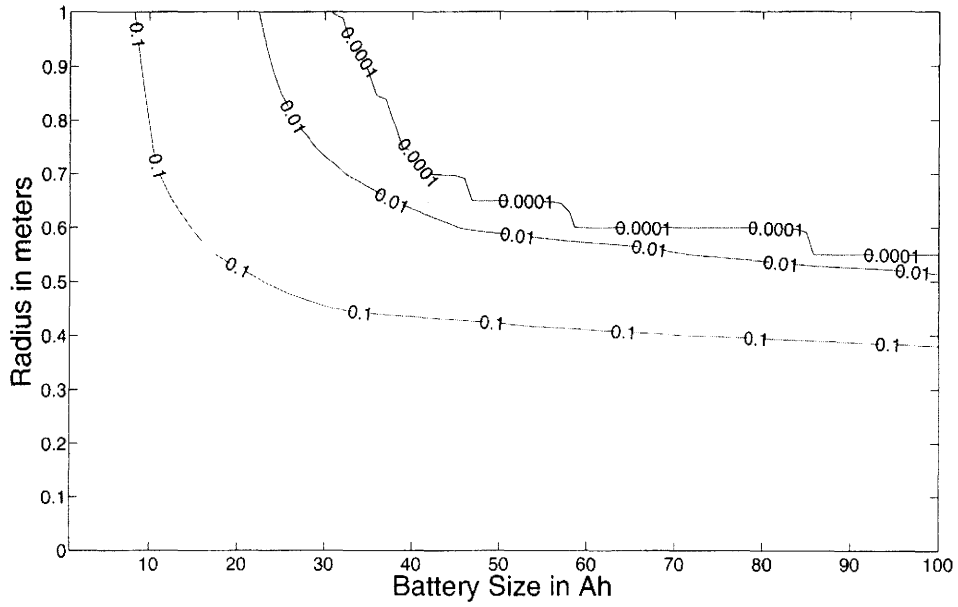

Figure 3.18: Contour Plot of P_{Out} for Different Wind Turbine and Battery Sizes for Phoenix

The optimization must incorporate a realistic model in order to determine the cost-optimal resource allocation. In the following we develop a cost model which aims to be as realistic as possible. We assume current (2008 year) retail values. We assume that the costs include the installation costs but do not account for differences in the ongoing maintenance of the solar or wind powered components. Also, the fixed cost of the node electronics is not included.

Currently, there are no commercially available wind turbines that generate power in the same range as that suitable for IEEE 802.11 APs. In the following is a survey of current academic and industrial efforts. We follow this discussion by showing results for two different wind turbine cost models. The first is based on extrapolation while the second employs a parametrized cost model.

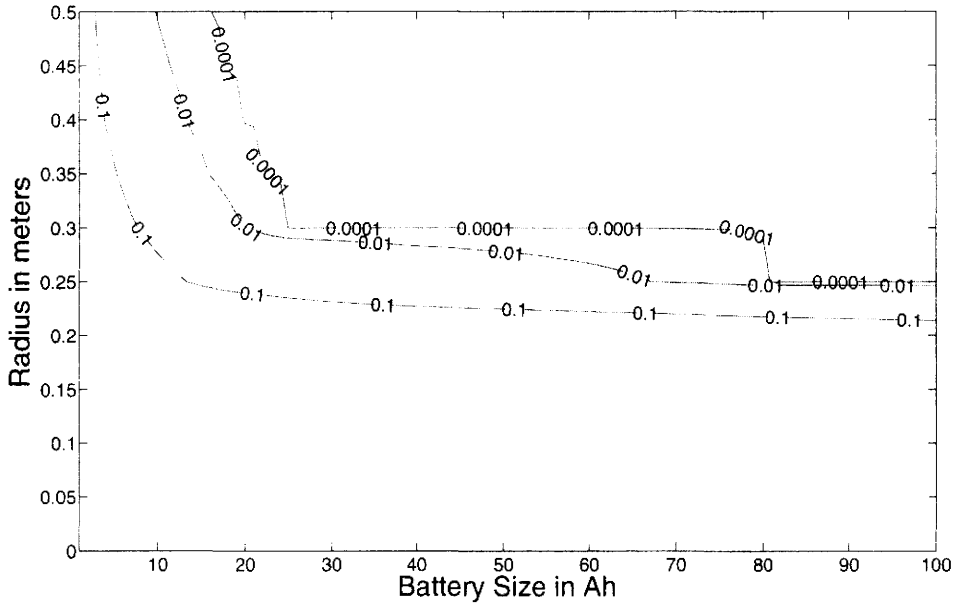

Figure 3.19: Contour Plot of P_{Out} for Different Wind Turbine and Battery Sizes for Seattle

A wind turbine cost model has been published by NREL in [1]. However, the cost model does not apply in this case because the wind turbines under consideration in the report assume wind turbines that are much larger than the ones considered here. The work by Priya et al. shows how to achieve an efficiency of 18% as opposed to 1% for small wind turbines. The new technique relies on the use of Piezoelectric conversion from mechanical to electrical energy [17]. The Hymini combines wind and solar power and costs about 50 dollars and can be used to charge ipods and other small devices. The device has a maximum claimed power of 1 watt from the turbine [3]. The work done in [62] analyzed a wind turbine having 50 cm diameter blades. The turbine was found to achieve an efficiency of 25 %. The Marlec Rutland is available commercially

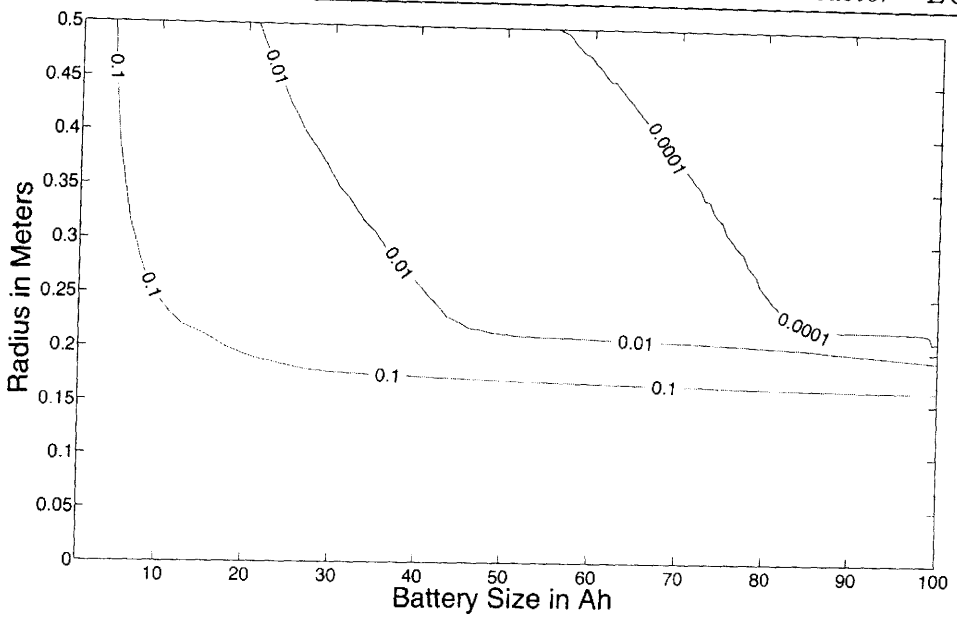

Figure 3.20: Contour Plot of P_{Out} for Different Wind Turbine and Battery Sizes for Yellowknife

in Canada and it costs 600-800 dollars. it has a maximum rating of 25 watts and has a 50 cm diameter blade. The characteristics of the turbine were shown in Figure 3.15. A wind turbine kit can be bought online at [4] for hobbyists at a price of 35 dollars. The turbine generates 1 watt at 2000 rpm. A Japanese-designed wind turbine, the NP103 is currently being sold for 9800 Yens (86 dollars) and has a wing length of 20 cm. The manufacturers claim an electrical output of 3 watts. However, it is not clear what the efficiency of this system is [5]. The Motorwind system incorporates a unique design where several wind turbines can be combined together to increase the power [6]. On the other hand, the humdinger system developed by Shawn Frayne is being touted as the world's first turbine-less wind generator. However, it is still not for sale

commercially [7]. In the following, we present our assumed cost model. The battery and solar panel costs can be found directly using extrapolation. On the other hand, we have considered both an extrapolated and parametric wind cost model due to the lack of available data.

3.5.1 Extrapolated Node Cost Model

In this section, we present the wind turbine, solar panel and battery cost model that is based on extrapolation of existing data. The Canadian Wind Energy Association (CanWea) [41] states that the cost of a small wind turbine is in the range of 5000-6400 $ CAD/KW. KW ratings are usually at 10 m/s for 300 W to 1000 W. Commercially available turbines are not very common at the ratings we are considering due to the lack of demand, and because of the use of wind technology for much higher powered applications. For this reason we mainly rely on extrapolating the costs from larger wind turbines.

Based on publicly available values, we can see that the relationship between the power output and the turbine area can be written as $1KW = 0.28Area$ $ CAD, and hence we can write that $Cost \approx 1400\pi R^2$ $ CAD where R is the turbine radius. Therefore, the cost of the wind turbine is roughly proportional to the square of the radius. For experimentation we introduce an economy-of-scale discount factor for smaller radii, η. This factor will be used to experiment with the optimal target costs for the wind turbine.

Using commercial data sheets for the solar panel, we find that the cost is roughly αP $ CAD where P is the peak panel power in watts, α is typically about 6.7. Similarly, the cost of a lead acid battery is about βB $ CAD where

B is the battery size in Ah and β is typically about 3.4.

Since the average power is also a quadratic function of the wind turbine radius, the cost per watt is constant for the turbine. In Toronto for example, it is about 10.45 $ CAD per watt and is constant for any radius. This is calculated for the average power generated by a turbine for the year 1990. On the other hand the cost per watt for the solar panel is about 41 $ CAD. This is due to the fact that the average power from a panel is low since it only produces power during the day and no power during the night. For Phoenix it is 25.27 $ CAD/W for the solar panel and 245.83 $ CAD/W for the wind turbine. For Seattle it is 46.3 for the panel and 63.51 for the wind turbine. For Yellowknife it is 40.98 for the panel and 59.95 for the wind turbine.

3.5.2 Mathematical Problem Formulation

We wish to minimize the total cost of the node while making sure that we eliminate outage events or that they never exceed a target outage probability, $P_{Outdesign}$. We also assume that the battery, solar panel and turbine have an upper and lower bound on size and that we will only optimize over discrete values of battery size B, panel size P and, wind turbine radius R. Our optimization

problem is given as

$$\min_{B,P,R} Cost \tag{3.2}$$

such that

$$Cost = Cost_P + Cost_B + Cost_R \tag{3.3}$$

$$Cost_P = \alpha P \tag{3.4}$$

$$Cost_B = \beta B \tag{3.5}$$

$$Cost_R = \eta(4400)R^2 \tag{3.6}$$

$$P_{Out} = f(B, P, R) \tag{3.7}$$

$$P_{Out} \leq P_{Outdesign} \tag{3.8}$$

$$B_{Min} \leq B \leq B_{Max} \tag{3.9}$$

$$P_{Min} \leq P \leq P_{Max} \tag{3.10}$$

$$R_{Min} \leq R \leq R_{Max}. \tag{3.11}$$

In Equation 3.2, we seek to minimize the total cost of the node. The cost function is comprised of the sum of three components as seen in Equation 3.3; namely, the costs of the battery, the solar panel and the wind turbine as seen in Equations 3.4, 3.5 and 3.6. These cost components follow the cost model that we previously discussed. In this optimization, P_{Out} is defined as the outage probability of the node. Unfortunately, for a given traffic profile, P_{Out} is a complex non-linear function of B, P and R which we define as $f(B, P, R)$ as seen in Equation 3.7. This non-linearity makes the optimization problem very difficult. In Equation 3.8 there is a constraint on P_{Out} since it must satisfy a design target, referred to as $P_{Outdesign}$. Finally, the constraints in Equations 3.9, 3.10 and 3.11 specify that there are upper and lower bounds on B, P, and R.

Parameter	Definition
α	Cost per unit solar panel power.
β	Cost per unit battery storage.
η	Economy of scale factor for the wind turbine.
P_{Out}	Outage probability.
B	Battery size in Ah.
P	Solar panel size in watts.
R	Wind turbine radius in meters.

Table 3.1: Parameter Definitions Used in the Optimization

Since discrete values of B, P and R are required, the above problem can be classified as an Integer Programming problem. The parameters defined above are listed in Table 3.1.

Due to the non-linearity of P_{Out}, we adopt an iterative approach towards solving this problem. First, we perform a discrete event simulation of different battery/panel/turbine configurations using the tool developed in [49], where we assume the increment in battery and solar panel sizes is 1 Ah and 1 W respectively and for the turbine radius we assume increments of 1 cm. The simulation will provide the associated outage probability for a given geographic location and node configuration. Once the simulation is completed, we are then able to use the results of a discrete optimizer that was written using Matlab that finds the optimal values of B, P and R for a given geographic location.

We assume the following target outage probabilities $P_{Outdesign} = [0, 0.0001, 0.001, 0.01, 0.1]$. We also assume that $\alpha = 6.7, \beta = 3.4$ (based on the cost model used in [49]) and $\eta = 1$. Finally, we have assumed that $B_{max} = 50$, $P_{max} = 50$ and $R_{max} = 0.5$. The results are shown in Tables 3.2, 3.3, 3.4 and 3.5 and apply for a 2W load for the year 1990.

As shown in Table 3.2, for Phoenix the most cost effective configurations do not include the wind turbine and hence $R = 0$ for all cases. This is not surprising based on our previous discussion of the solar and wind energy available at that location. If the required load is increased to 4 W, we can see that still the wind turbine size is zero while the total cost has increased in an almost linear fashion. If we consider Phoenix with a discount factor of $\eta = 0.25$ we still see that there is no value in using a wind powered source.

As seen in Table 3.3 for Toronto, a wind turbine of radius 0.1 m is always necessary in order to achieve optimal cost. This is due to the high cost of the battery and due to its reduced storage capacity due to cold temperatures. By comparison if we examine the no turbine case, we can see the effect of eliminating the wind turbine on the total node cost. For example for the case of $P_{Out} = 0.1$ the cost is reduced from 146.53 to 74.2 $ CAD. If we examine Toronto for higher loads of 4 W and 10 W we can see that for the 4 W case, the turbine size does not increase much. However, at the 10 W load level the turbine size increases to 23 cm for the zero outage case. As expected the cost of the node increases with the increase in loading, following an almost linear trend. If we consider a discount factor of 0.5 for a load of 2 W, the size of the wind turbine increases by 50% to 15 cm and a panel is no longer necessary.

For Seattle, as shown in Table 3.4, we see that a turbine of radius 0.11 is required for minimum cost and decreases to 0.1. In all cases, more resources need to be allocated than for Toronto. Finally, if we examine the Yellowknife location (Table 3.5), we see that a hybrid approach works well. We notice that the resources required for Yellowknife are much higher than the other locations we have considered.

If we consider the zero outage case, we can see that the total cost of the system for Yellowknife is 338.57 $ CAD, in Toronto it is $ 131.6 CAD, in Seattle it is 242.23, and finally, in Phoenix it is $ 107.2 CAD. The cost of deploying a node in Yellowknife is over three times the cost that provides the same level of service in Phoenix. By comparison, the cost in Yellowknife is almost two and a half times the cost in Toronto and finally, it is slightly less than one and a half times the cost in Seattle. We also observe that relaxing the constraints on the outage probability lead to significant cost savings, for example, in Toronto, relaxing the outage target from 0 to 0.1 leads to a reduction in cost from 131.6 $ CAD to 71.69, which is almost a factor of 2. On the other hand, in Phoenix the reduction is from 107.2 to 63.53 and in Yellowknife it is reduced from 338.75 to 175.03 $ CAD. Therefore, for Toronto, Seattle, and Yellowknife a hybrid solar/wind powered node is the optimum from a cost viewpoint. This is due to the fact that even though solar power is scarce, wind turbines are very expensive and hence a trade-off is necessary in order to minimize the cost.

Battery Size, B	Solar Panel Size, P	Wind Turbine Radius, R	P_{Out}	$P_{Outdesign}$	Cost	Comments
17	23	0	0	0	211.13	4 W Load
8	12	0	0	0	107.2	2 W Load
9	11	0.04	0	0	105.69	2 W load $\eta = 0.25$

Table 3.2: Minimum Cost Node Configuration for Phoenix in $ CAD

Battery Size, B	Solar Panel Size, P	Wind Turbine Radius, R	P_{Out}	$P_{Outdesign}$	Cost	Comments
29	26.99	0	0	0	278.59	No Turbine
14	60	0.1	0	0	131.6	2 W Load
38	13	0.1	0	0	259.87	4 W Load
50	43	0.23	0	0	689.43	10 W Load
14	0	0.15	0	0	97.10	(2 W Load) $\eta = 0.5$

Table 3.3: Minimum Cost Node Configuration for Toronto in $ CAD

3.5.3 Parametric Cost Model

The previously shown examples assumed a high efficiency, expensive wind turbine based on extrapolation of available data. This is due to the fact that currently there are very few commercially available wind turbines that can generate a few watts as needed by IEEE 802.11 Access Points. Traditionally, wind turbines have been used to power applications requiring several Kilowatts of power, if not several Megawatts. In recent years, micro wind turbines have started to receive attention, however by definition they still operate at several hundred watts. Therefore, due to the lack of available information on the turbine efficiency and the lack of an appropriate model, we introduce a parametrized cost model, that is, we will experiment with several values of the turbine efficiency and cost in order to project some scenarios.

Battery Size, B	Solar Panel Size, P	Wind Turbine Radius, R	P_{Out}	$P_{Outdesign}$	Cost
33	10	0.12	0	0	242.23
33	10	0.12	0	0.0001	242.23
32	10	0.12	0.0005	0.001	238.83
21	13	0.11	0.0098	0.01	211.31
8	11	0.10	0.0961	0.1	144.53

Table 3.4: Minimum Cost Node Configuration for Seattle (2 W Load) in $ CAD

Battery Size, B	Solar Panel Size, P	Wind Turbine Radius, R	P_{Out}	$P_{Outdesign}$	Cost
39	14	0.16	0	0	338.57
39	14	0.16	0	0.0001	338.57
37	14	0.16	0.0008	0.001	331.77
30	13	0.16	0.0095	0.01	301.31
10	10	0.13	0.0994	0.1	175.03

Table 3.5: Minimum Cost Node Configuration for Yellowknife (2 W Load) in $ CAD

We assume the following cost model:

$$Cost = F + VR \tag{3.12}$$

The model is composed of a fixed component and a variable component that depends on the rotor's radius. This approximate model has the advantage that it is simple and it is also suitable for the low size turbines assumed. Again, F and V are two cost parameters which we will experiment with. Table 3.6 shows some sample results for Toronto for a normalized cost of 2:1 for the panel and battery respectively, we assume the range of B is from 1 to 30, P from 1 to 30, and R from 0.05 to 0.25 with increments of 0.05 m.

The results indicate that the overall node configuration relies on the avail-

able wind turbine technology and the cost model. For some scenarios such as an expensive inefficient turbine, a solar approach may be better as seen in the scenario where $\eta = 0.01$, $F = 50$, and $V = 100$ clearly the turbine under consideration in this case only contributes to the overall node cost without actually capturing enough wind energy to offset this increase in cost. On the other hand, an inexpensive efficient turbine will lead to a wind only solution such as the one seen when $\eta = 0.3$, $F = 0$, and $V = 1$ in this case, the wind turbine is capturing enough energy to power the node efficiently and cost-effectively.

3.6 Discussion of Power-Saving Effects on Cost Reductions

As seen in the results, the resources allocated -and hence the costs- in hybrid WLAN mesh networks are greatly influenced by the power consumption. Hence it is imperative for the MAP/MP to go into power-saving when there is no traffic to carry since it can be shown that the power consumption is greatly reduced. Since the IEEE 802.11 standard does not provide a mechanism for placing APs into power save mode, the only available schemes are proprietary. These mechanisms were discussed in Chapter 2.

In the following discussion, we develop an analysis for connection-oriented traffic. In the following, we restrict our discussion to solar-powered nodes to simplify the analysis.

3.6.1 SMAP/SMP Power Saving in Connection Oriented Traffic

To achieve reasonable connection traffic performance, the SMAP/SMP node traffic load should not exceed certain limits, otherwise unacceptable blocking rates will occur. In this section we study the SMAP/SMP operation using VoIP as an example of connection oriented traffic. The parameters at the SMAPs are configured based on a target call blocking probability. Our objective is to show that significant cost reductions in provisioning the SMAPs can be obtained if potential power savings due to idle periods along the timeline are exploited.

Radio power consumption at the SMAP consists of coverage radio power consumption and relay radio power consumption. The relay radio protocols can be proprietary and capable of power saving. However, a significant potential for power saving is made possible by controlling the utilization of the coverage radio as well.

The analysis presented in [72] quantifies the capacity of an IEEE 802.11e HCCA access point carrying VoIP traffic. Table 3.7 summarizes the number of concurrent calls that the access point is capable of supporting using different codecs. This view of the access point capacity permits us to use the Erlang B formula to plot the call blocking probability as a function of the call arrival rate, λ. In Figure 3.21 we show the call blocking probability for different codecs as a function of the traffic arrival rate assuming an exponentially distributed holding time with a mean of 180 seconds for the 11 Mbps data rate. Throughout the following we assume the IEEE 802.11b air interface, although similar conclusions result from using IEEE 802.11a/g.

Figure 3.22 plots the utilization versus the call arrival rate. In practical telephony, designers aim at provisioning resources which result in a 1% maximum new call blocking probability. From Figure 3.21 we see that the call arrival rates corresponding to 1% blocking probability are 0.049, 0.053 and 0.062 calls per second for the G.711, G.726 and G.729, respectively. At these arrival rates, all the codecs have a similar utilization in the 55% region. This observation has strong implications on the potential for SMAP power saving. Even at unacceptably high blocking probabilities the system continues to be under-utilized, e.g., at a blocking probability of 10% the system utilization is close to 75% for the G.711 codec, affirming the feasibility of power saving as a mean of cost reduction when provisioning the system.

To give concrete examples of potential cost savings as a result of capturing system under-utilization we define a power model for the access point. We assume that an 802.11e air interface is used over relay and coverage radios. The timeline is divided between Connection Oriented (CO) traffic which spans a total superframe fraction, ρ, and Best Effort (BE) traffic which occupies the remaining time, assuming a normalized superframe time. We assume that a SMAP has a single coverage radio used for mobile station access and a single relay radio used for back-hauling traffic. The total power consumption at the node consists of 3 components. The first is the power consumed by the host processor running on the node, we refer to this as P_H. The second component is the power consumed by the coverage radio P_c and the third component is the power consumed by the relay radio P_r.

Most host processors are capable of operating in sleep mode when the net-

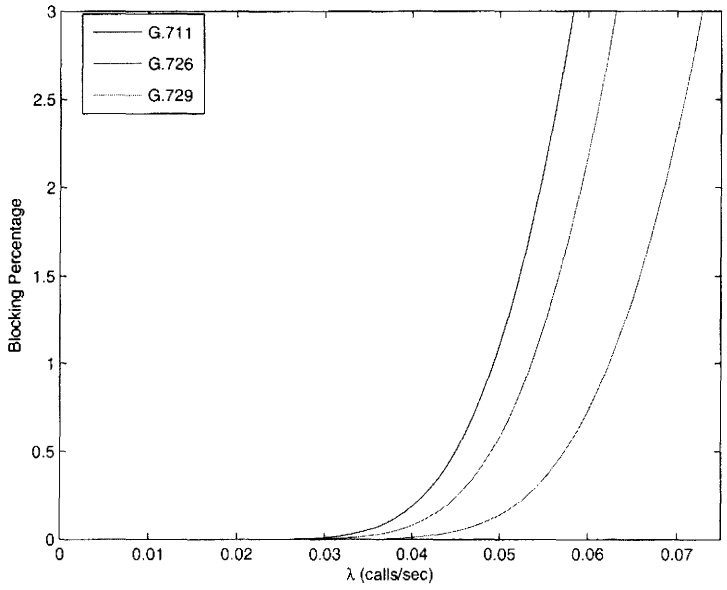

Figure 3.21: Blocking Percentage Vs. Call Arrival rate for IEEE 802.11b HCCA at 11 Mbps

work interfaces are idle. Therefore, in our power model we assume that the host processor only consumes significant power if there is traffic being processed by the coverage or relay radios. We capture this effect by

$$P_H = \max\{\min(U_c + U_r, 1)P_{Hmax}, P_{Hmin}\}, \tag{3.13}$$

where U_c and U_r represent the total utilization of the coverage and relay radios respectively. P_{Hmax} represents power consumption at the host processor when its operating at maximum capacity. P_{Hmin} represents the power consumption of the host processor when no traffic is carried. The above-mentioned relation assumes a worse-case temporal correlation between U_c and U_r.

Next we consider the power consumption of the coverage radio. As a worse-

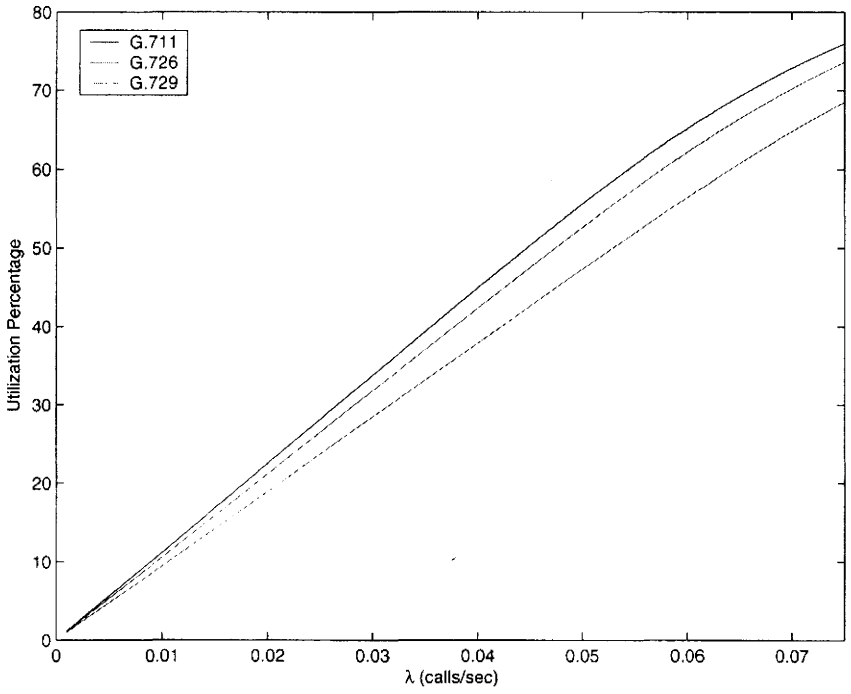

Figure 3.22: Utilization Percentage Vs. Call Arrival rate for IEEE 802.11b HCCA at 11 Mbps

case we assume that the coverage radio is fully awake during the $1-\rho$ time interval when it is servicing best effort traffic. During the remaining ρ interval the coverage radio services CO traffic. The deterministic nature of VoIP traffic allows the coverage radio to sleep during idle intervals using HCCA NAMs. The power consumption of these activities on the coverage radio's timeline is captured using

$$P_c = P_{BE} + P_{CO} \tag{3.14}$$

$$P_{BE} = (1-\rho) \times P_{Max} \tag{3.15}$$

$$P_{CO} = U_{CO} \times P_{Max} + (\rho - U_{Co}) \times P_{Sleep} \tag{3.16}$$

where P_{Max} represents the average of the maximum transmit and receive power, and P_{Sleep} represents the power dissipated when the radio is in sleep mode. The relay radios can use any proprietary power saving protocol since they do not have to interact directly with legacy MPs, and all relay traffic is regarded as connection oriented. Therefore we can describe the relay radio's power consumption as

$$P_R = U_r \times P_{Max} + (1 - U_r) \times P_{Sleep}. \tag{3.17}$$

In Table 3.8 we summarize the values of the parameters assumed in our simulations. We assume that the best effort and the VoIP signaling traffic are negligible.

For the coverage radio there are two extreme cases to consider. First is the case when the relay radio does not carry any traffic, $U_r = 0$ and $P_H = \max\{U_c \times P_{Hmax}, P_{Hmin}\}$. The power consumed by the relay radio will be P_{Sleep} which is equal to 2 mW. The coverage radio consumption will depend on U_{CO} which varies from 0 to ρ. Since we neglect any signaling or best effort traffic by assuming $U_{BE} = 0$, then $P_c = (U_{CO}) \times P_{Max} + (1 - U_{CO}) \times P_{Sleep}$. Therefore, P_c varies between 0.752 W ($U_{CO} = \rho$) and 0.002 W ($U_{CO} = 0$). P_H varies between 1 and 0.02 W respectively. Thus the total power consumed by the node varies between 0.024W and 1.752W. In the second case, the relay radio is fully utilized, $P_r = 0.75$ W, $P_H = 1$ W and P_c varies between 0.002W and 0.75W, therefore, the total power will vary between 1.752W and 2.5W.

Figure 3.23 shows P_{Total} vs U_{CO} for several different relay radio consumption scenarios varying from $U_r = 0$ to 100%. It can be seen that as the utilization of both radios increases, the power consumption also increases. When the relay

radio is fully utilized, the consumption varies between 1.752-2.5 W with a slope of 0.75 and for the case when the relay radio does not carry any traffic, the consumption varies between 0.024 to 1.752 W with a slope of 1.73. When the relay radio is under-utilized, the power consumption depends more strongly on the utilization of the CO traffic, this is clear in the variation of the slope from 0.75 to 1.73, an increase of more than 2.3 times. For example, when the relay radio utilization is 50% the power consumption increases rapidly with a slope of 1.7 up to $U_{CO} = 0.5$. After that point, the slope of the power consumption curve decreases to 0.9 which is a reduction of almost 50%. For example, when $U_{CO} = 0.5$, the power consumption is approximately 1.75 W. The reason for the change in slope is that when the sum of the utilization of both radios is less than P_{Hmax} the power consumption increases linearly, however when they exceed it, the slope of the power consumption curve remains linear but changes due to the fact that the host processor power is constant. This applies for all cases except when $U_r = 1$ or 0.

From this we can reach the conclusion that when the medium is less utilized, the power consumption is reduced rapidly and is not affected by the overheads, this is especially true when the relay radio is carrying less traffic. Therefore, there are two elements of motivation for reducing the medium utilization; satisfying the QoS guarantees as previously discussed, and the potential for power consumption reduction. If the system designer has perfect knowledge of the utilization of the relay radio, the power saving potential can be properly evaluated. For example if the node is placed in a location within the mesh network where it is relaying large amounts of traffic for other users and it has several

relay radios, then the potential for power saving is less and the designer may decide to forgo power saving protocols on the coverage radio. This will also depend on the ratio of the coverage radios to the relay radios.

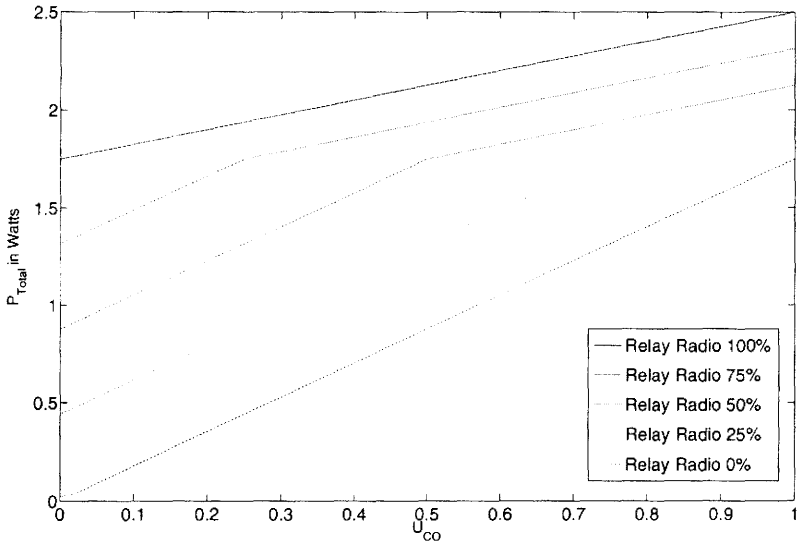

Figure 3.23: P_{Total} Vs. U_{CO}

As will be shown in Chapter 4, cost can be approximated as a linear function of power consumption for a given outage probability. Figure 3.24 shows the Cost in $ CAD vs P_{CO} for $P_{Out} = 0.0001$ for a single node. We can see that when the relay radio is off, the cost is heavily dependent on the expected value of the arrival rate. We can see that the cost varies between 35.8 to 350 $ CAD. We can also see that employing power saving at the SMAP will help significantly reduce the cost of the nodes, especially when accurate traffic forecasting is available to the designer based on traffic demands and the network topology.

We now integrate the previous results in order to estimate the potential

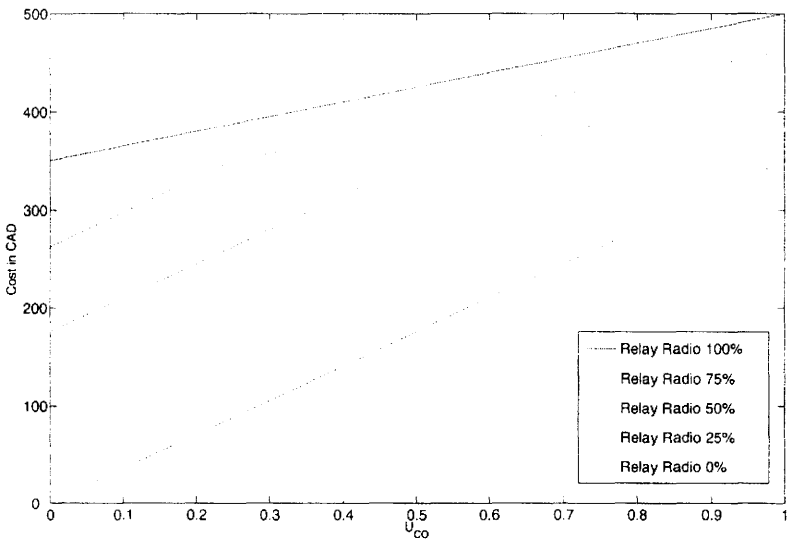

Figure 3.24: Cost Vs. U_{CO} for $P_{Outdesign} = 0.0001$

of power saving for WLAN mesh networks to facilitate the evaluation of the results. Figure 3.25 shows the power consumption versus the call arrival rate for different relay radio utilization levels. It is interesting to observe the effect of the relay radio utilization on the dependency of power consumption on the call arrival rate. We can observe this by comparing the two cases when the relay radio is on and when it is off. First, if we consider the no relay case, the power increases from approximately 0 W to 1.25 W while the arrival rate varies from 0 to 0.075 calls per second. The curve is a straight line with slope 16.67, while for the case when the relay radio is on, the power increases from 1.75 to 2.25 W again in a straight line with slope 6.7. Therefore, we notice that the slope has increased 2.5 times signifying that the dependency on the call arrival rate increases when the relay radio is sleeping or has minimal traffic.

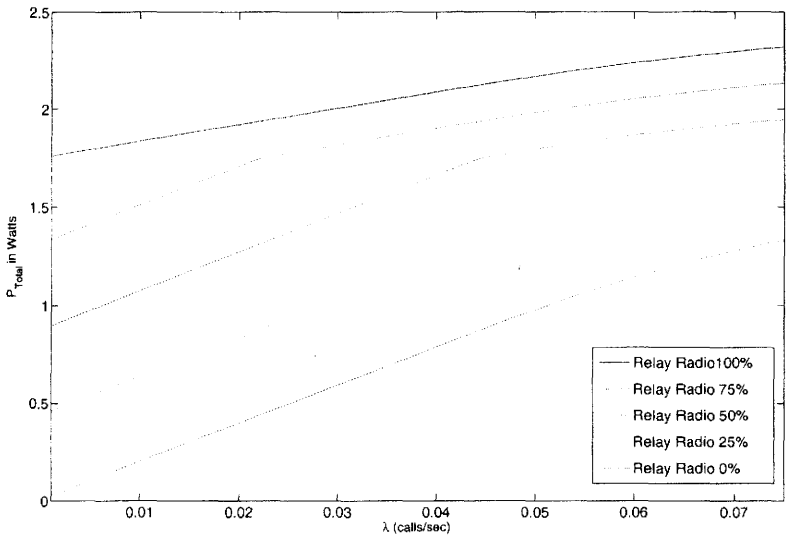

Figure 3.25: P_{Total} Vs. λ

From our discussion and from the results shown in this section, we can see that limiting the call arrival rate in order to satisfy QoS constraints also provides a significant opportunity for power saving which in turn leads to network cost savings.

3.7 Conclusions

This chapter has introduced the resource allocation problem in renewable energy powered WLAN mesh networks. The energy flow model has been presented followed by some examples showing the importance of performing long and short-term analyses of the characteristics of the energy sources being considered. This was followed by a discussion of the cost model and the ensuing

three dimensional cost optimization problem. Finally some results were presented that showed the effect of power consumption on network cost. These results have shown that in some locations, the use of an optimal mixture of energy sources presents an opportunity for enhanced network deployment cost savings. In addition, the use of power saving has been shown to greatly improve the overall network costs. In the following chapter we extend the work in this chapter to consider the case of network-wide resource allocation and routing, with emphasis on the case when the network is composed of a mixture of solar and AC powered nodes.

B	P	R	Cost	η	F	V
27	12	0.25	51.25	0.01	0	1
15	0	0.25	15.25	0.1	0	1
10	0	0.25	10.25	0.3	0	1
27	12	0.25	56	0.01	5	0
15	0	0.25	20	0.1	5	0
10	0	0.25	15	0.3	5	0
27	12	0.25	57.25	0.01	5	5
15	0	0.25	21.25	0.1	5	5
10	0	0.25	16.25	0.3	50	50
27	12	0.25	76	0.01	0	100
15	0	0.25	40	0.1	0	100
14	0	0.15	29	0.3	0	100
29	27	0	83	0.01	50	100
15	0	0.25	65	0.1	50	0
14	0	0.15	79	0.3	50	100

Table 3.6: Results for a Zero Outage 2 watt Configuration for Toronto

Codec	802.11b (11 Mbps)	802.11b (5.5 Mbps)	802.11a (54 Mbps)	802.11a (36 Mbps)	802.11a (18 Mbps)
G.711	16.1	12.7	105.6	89.3	60.9
G.726	17.8	14.8	120.7	106.1	77.9
G.729	19.3	17	135.3	123.6	98.3

Table 3.7: VoIP Capacities for IEEE 802.11e HCCA.

Parameter	Value
P_{Max}	0.75 W
P_{Sleep}	2 mW
P_{Hmax}	1 W
P_{Hmin}	20 mW
ρ	1

Table 3.8: Parameters

Chapter 4

Optimal Node Placement in Solar Powered WLAN Mesh Networks

4.1 Introduction

In this chapter we consider cost-optimal placement of energy sustainable nodes in a WLAN mesh network that includes solar and AC powered nodes. A cost model is first introduced that takes into account the solar panel and battery provisioning required to operate the nodes subject to a desired node outage criterion. A complicating factor is that the cost of renewable energy powered nodes is dependent on the amount of traffic for which a given node is provi-

sioned, and therefore the node placement and traffic routing must be considered jointly. The design problem is formulated as a Mixed Integer Quadratic Problem (MIQP) and a branch and bound approach is used to obtain node positioning solutions. This is compared with a proposed algorithm that uses optimum shortest path routes for this purpose. The proposed algorithms result in significant improvements in cost and the branch and bound approach achieves the optimum assignment for small network examples which can be computed exhaustively.

4.2 Background

To the best of our knowledge, optimum cost node assignment for hybrid sustainable-energy infrastructure deployments has not been dealt with in the context of wireless mesh networks. However, there is previous work that deals with similar problems within the context of sensor and cellular networks.

In [33], a Base Station Positioning (BSP) problem is considered for sensor networks. It is shown that the problem is NP-complete, and the paper describes results for greedy and local search algorithms. In [112] a methodology is presented for approximating the base station placement solution. The proposed technique is guaranteed to find a solution within a specified error bound. In [63] a two-tier sensor network is considered which is composed of sensors and aggregating nodes. The problem of maximizing the network lifetime of the forwarding nodes is considered by adding energy to each node or by adding relay nodes at new locations. In [64] a hybrid sensor network is considered,

containing resource-rich micro-servers and resource-impoverished sensors. An investigation of the maximum lifetime of the network and the optimal micro-server placement is performed using a tree-based anycast routing algorithm. Reference [24] describes an optimal access point placement and traffic allocation algorithm for WLANs and in [54] a base station location optimization problem is described for UMTS networks in which the demand node maps and the target base station sites are known beforehand. In [102] the cost tradeoff is considered between installing a PV system versus powering from the AC power mains for Optical Network Units (ONU). The authors show that there is a "solar cost effective distance" where the cost of using the AC mains is higher than deploying a PV system. Finally, in [93] the authors present a formulation and discussion of joint routing and gateway selection in wireless mesh networks.

In the next section, we consider the effects of varying the power loading on the system performance and the resource allocation. We also show some representative results for different North American cities where nodes are subjected to various power dissipation assumptions. The results shown here are generated using the simulator developed in [49] by implementing the energy balance shown in Equation 3.1. The simulator also incorporates the effect of battery efficiency temperature dependence.

4.3 Solar Energy Powered Provisioning Cost Model

The system is simulated accurately for different combinations of battery and panel sizes over a sufficiently large historical data set of meteorological data for the geographic location under consideration. Then, the number of times the system goes into outage are counted and the outage probability of the system P_{Out} corresponding to each battery/panel combination can be evaluated. Therefore, solar panel versus battery size contours can be generated for an assumed traffic profile and a given probability of node outage, P_{Out}. From these curves, the costs of the battery and panel can be used to compute the minimum total provisioning cost. In this thesis it is assumed that the node cost function is made up of the cost of the battery and the solar panel only, since the rest of the node consists of (typically much smaller) fixed costs. Using commercial data sheets for the solar panel, we find that the cost can be modeled as $\alpha(P_{Panel})$ $ CAD where P_{Panel} is the peak panel power in watts, α is typically about 6.7. Similarly, the cost of a lead acid battery is about $\beta(B)$ $ CAD where B is the battery size in Ah and β is typically about 3.4. We wish to minimize the total cost of the node while making sure that we eliminate outage events or that they never exceed a target outage probability, $P_{Outdesign}$. We also assume that the battery and solar panel have an upper and lower bound on size and that we will only optimize over discrete values of B, P_{Panel}. We also assume that the load profile is known in advance. Our optimization problem, which is

a special case of the one described in Equation 3.2, is given as:

$$\min_{B,P_{Panel}} Cost \tag{4.1}$$

such that

$$Cost = Cost_P + Cost_B \tag{4.2}$$

$$Cost_P = \alpha P_{Panel} \tag{4.3}$$

$$Cost_B = \beta B \tag{4.4}$$

$$P_{Out} = f(B, P_{Panel}) \tag{4.5}$$

$$P_{Out} \leq P_{Outdesign} \tag{4.6}$$

$$B_{Min} \leq B \leq B_{Max} \tag{4.7}$$

$$P_{Min} \leq P_{Panel} \leq P_{Max} \tag{4.8}$$

In Equation 4.1, we seek to minimize the total cost of the node. The cost function is comprised of the sum of two components as seen in Equation 4.2; namely, the costs of the battery and the solar panel as seen in Equations 4.3. 4.4. These cost components follow the cost model that we previously discussed. As previously mentioned, in this optimization, P_{Out} is defined as the outage probability of the node. Unfortunately, P_{Out} is a complex non-linear function of B and P_{Panel} which we define as $f(B, P_{Panel})$ as seen in Equation 4.5. This non-linearity makes the optimization problem very difficult. In Equation 4.6 there is a constraint on P_{Out} since it must satisfy a design target, referred to as $P_{Outdesign}$. Finally, the constraints in Equations 4.7 and 4.8 specify that there are upper and lower bounds on B and P_{Panel}. Since discrete values of

Parameter	Definition
α	Cost per unit solar panel power.
β	Cost per unit battery storage.
P_{Out}	Outage probability.
B	Battery size in Ah.
P_{Panel}	Solar panel size in watts.

Table 4.1: Parameter Definitions Used in the Optimization

B and P_{Panel} are required, the above problem can be classified as an Integer Programming problem. The parameters defined above are listed in Table 4.1.

If we consider a constant value of $P_{Out} = P_{Outdesign}$, this will represent the projection of the three dimensional function $f(B, P_{Panel})$ on to a constant plane of value $P_{Outdesign}$. Our experiences have shown that this projected function will be convex. Every point on the projected function will have a total cost equal to $\alpha P_{Panel} + \beta B$. the minimum value of this total cost will correspond to a unique point on the curve since it is also a convex combination of B and P_{Panel}. This point represents the optimum cost battery and panel selection and is also the unique intercept of the linear cost line with slope $-\alpha/\beta$ and the outage contour curve. An example of this is shown in Figure 4.1 which plots the superposition of the cost curves over the outage contour plots of Figure 3.3 for the city of Toronto. For this example, we show the case where $\alpha : \beta = 1.15 : 1$. More formally, this can be re-written as follows :

$$\min_{P_{Panel}} Cost = \alpha P_{Panel} + \beta\Theta(P_{Panel}, P_{Outdesign}) \tag{4.9}$$

where $\Theta\{\cdot\}$ represents the function describing the relationship between B and the outage contour curve. Taking the derivative of the cost function with respect to P_{Panel} and setting to zero allows us to obtain the global minimum due to the convexity of $\Theta\{\cdot\}$, this yields the following relation:

$$\Theta'(P_{Panel}, P_{Outdesign}) = -\frac{\alpha}{\beta} \tag{4.10}$$

This confirms that there is a unique cost minimum and that this minimum can be evaluated by finding the intersection of the convex cost curve and the line of constant slope $-\frac{\alpha}{\beta}$. This observation is in agreement with the optimality criterion for a differentiable objective function as shown in [37].

Due to the discrete nature of the values of B and P_{Panel}, we wrote a discrete optimization solver using Matlab in order to find the intersection of the cost line and the outage contours resulting in the minimum cost tuple of optimal values of B and P_{Panel} for a given geographic location. We can see from the example shown in Figure 4.1 that for the 2 watts case, the minimum cost and outage constraint will be satisfied when P_{Panel}=40 watts and B=30 Ah.

Table 4.2 shows the optimal values of B and P_{Panel} for three different locations in North America.

Now let us consider the total combined cost of the solar panel and battery. If we consider that the cost ratio of one watt of solar panel power to one Ah of battery storage is currently about 2:1. Figure 4.2 shows the total cost versus power consumption for $P_{Out} = 0$ for Toronto and Phoenix and Yellowknife.

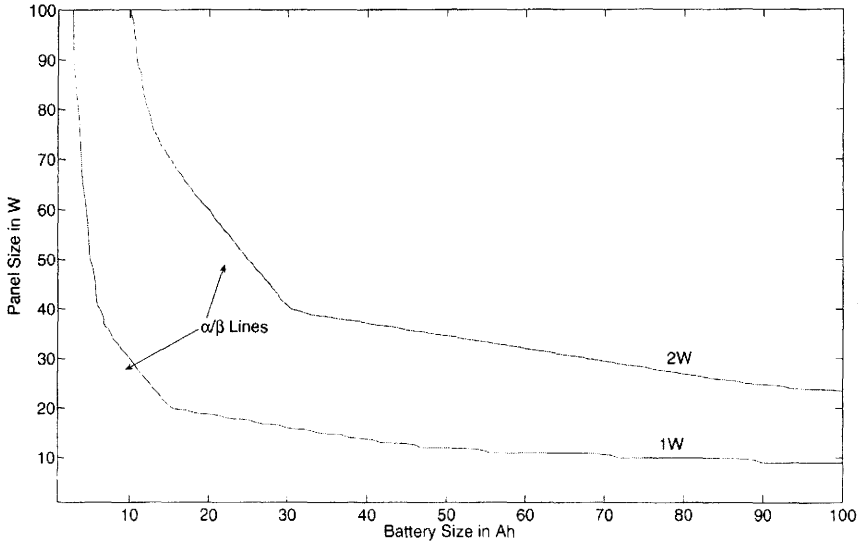

Figure 4.1: Outage Contour Plots for Toronto with Cost Model Lines Superimposed

The total cost shown here is normalized to one dollar per Ah. As seen, the total cost for each geographic location is a linear function of the power.

Many of these types of node configurations have been performed, and our simulations have confirmed that the solar node provisioning cost C_{HP} for each geographic location can be represented as a linear function of the traffic flow, L, for which the node is designed, i.e.,

$$C_{HP}(P_{Out}) \simeq K_1 L + K_2, \tag{4.11}$$

where K_1 and K_2 are dependent on P_{Out}. This is evident if one considers the total node costs in Table 4.2.

For example, in Toronto, Canada, for the case where the target outage probability P_{Out} is 0, $K_1 = 220$ and $K_2 = 1.4$. For Phoenix, USA, $K_1 = 88$

Load Power		Phoenix, AZ.	Toronto, ONT.	Yellowknife, NWT.
4W	Battery, Ah.	28.25	62.45	185.12
	Panel, W.	30	79	134
3W	Battery, Ah.	22.12	47.5	148
	Panel, W.	22	59	96
2W	Battery, Ah.	14.2	30.5	92.6
	Panel, W.	15	40	67
1W	Battery, Ah.	6.6	15.3	53.2
	Panel, W.	8	20	30
0.5W	Battery, Ah.	3.4	9.8	24
	Panel, W.	4	10	16
0.25W	Battery, Ah.	1.9	4.9	12
	Panel, W.	2	5	8

Table 4.2: Minimum Cost Solar Panel and Battery Sizes

and $K_2 = 0.47$. These values assume a normalized cost model where the panel cost to the battery cost ratio is 2:1. The load has been normalized to 4 watts.

Several cost models are available for AC powered nodes. For example, the one proposed in [102] assumes that cost is dependent on the distance to the electricity provider. In the following, we capture all these effects by assuming that the costs of deploying an AC node at each location are known beforehand.

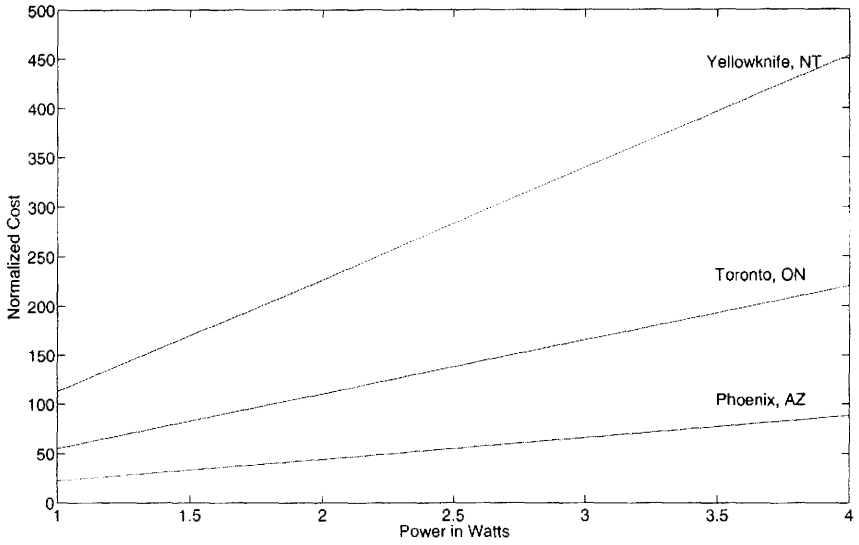

Figure 4.2: Total Minimum Cost versus Power Consumption

4.4 Problem Definition

We now focus on the problem under consideration and the classical approach towards solving this problem followed by the mathematical formulation of the problem.

We first assume that a target end-to-end traffic profile is known. Since the traffic profile is long-term, we also assume that all flows are splittable. In addition the positions of the mesh nodes have been determined in advance based on WLAN coverage considerations. The problem is to decide which nodes need to be renewable energy powered, and what the provisioning is for those nodes, so that the total cost is minimized. Since renewable powered node provisioning cost is a function of traffic flow through them, we need to flow the smallest amount of traffic through the assigned renewable nodes. Given a traffic flow matrix, and a set of N mesh node locations with associated connectivity,

we want to locate the positions of the renewable powered nodes such that the total renewable provisioning cost is minimized. We refer to this as the *Optimum Flow/Placement* (or OFP) problem.

The work in [27] discusses the interaction of the routing with the resource allocation in solar powered wireless mesh networks. The authors compared between a classical shortest path based routing algorithm and energy aware routing. Their main conclusion was that it is impossible to perform resource provisioning in a causal manner while assuming an energy aware routing algorithm in place. Based on their observations, we first present a classical design methodology. Initially, all nodes are assumed to be AC powered. The shortest path routing can then be easily found using linear programming since the network flows will be independent of cost. Once this is done, the P nodes carrying the lowest amount of traffic are assigned as renewable nodes and the total network cost is then calculated. The advantage of this approach is that the linear program is solved once followed by a simple node flow ordering. On the other hand, the main disadvantage of this approach is that it relies on the assumption that the node flow and node designs are independent, which is not true in some cases. Therefore, in the following, we present the mathematical formulation of the problem in addition to a discussion of its complexity.

4.4.1 Problem Formulation

We introduce a binary decision variable d_i which will indicate whether a location is renewable (i.e., 1) or AC mains (continuously) powered (i.e., 0). This variable is a vector with dimension $N \times 1$ where N is the number of nodes.

We have $(K = N - P)$ AC-powered nodes, and we would like to place them such that they carry as much of the traffic as possible. The problem can be formulated as the following Mixed Integer Non-linear Programming (MINLP) problem,

$$\min_{\gamma_{ij}, d_i} C \tag{4.12}$$

such that

$$\gamma_{ij} \geq 0 \quad \forall i, j \in N \tag{4.13}$$

$$\gamma_{ij} \leq 1 \quad \forall i, j \in N \tag{4.14}$$

$$C = \textstyle\sum_i (1 - d_i) C_{AC}(i) + \sum_i (d_i) CS_i \quad i \in N \tag{4.15}$$

$$C_{AC}(i) = F_i \tag{4.16}$$

$$CS_i = \Lambda(L_i, P_{Outdesign}) \tag{4.17}$$

$$L_i = \sum_{l \in N} \gamma_{il} + \sum_{h \in N} \gamma_{hi} \tag{4.18}$$

$$\sum_{l \in N} \gamma_{il} - \sum_{h \in N} \gamma_{hi} = D_i \quad \forall i \tag{4.19}$$

$$\sum_i d_i = P \tag{4.20}$$

$$d_i \in \{0, 1\}, \quad i = 1 \ldots N \tag{4.21}$$

$$P_{Outi} = \Phi(L_i, P_{Outdesign}) \quad \forall i \tag{4.22}$$

$$P_{Outi} \leq P_{Outdesign} \quad \forall i \tag{4.23}$$

As seen in Equation 4.12, the objective is to minimize the total cost over the decision variable d_i and γ_{ij}, where γ_{ij} represents the total flow on the link between nodes i and j. The constraint in Equation 4.13 ensures that the direction of flows on the link correspond to the link direction. Equation 4.14 represents the link capacity condition on the total flow through a link and

Equation 4.15 gives the total cost as the sum of the renewable and AC powered node costs. Equations 4.16 and 4.17 represent the assumed cost models for the AC nodes and the renewable nodes. F_i represents the cost of deploying an AC node at location i. In Equation 4.17 we see that $\Lambda(\cdot)$ models the functional dependency of the node cost, where L_i represent the sum of the incoming and outgoing flows for node i and $P_{Outdesign}$ is the target outage probability which is assumed to be the same for all nodes. The flow balance is shown in Equation 4.18. An additional flow balance is shown in Equation 4.19, where D_i represents the traffic demand sourced or requested by the node. This has a positive sign for sources and a negative sign for sinks, and is zero for relay nodes. The constraint in Equation 4.20 guarantees that the number of solar powered nodes is equal to P, while the condition shown in Equation 4.21 simply ensures that d_i is a binary vector. Equation 4.22 represents the non-linear dependency of the outage on L_i and $P_{Outdesign}$. Finally, Equation 4.23 shows that the outage target must not be exceeded. The constraint in Equation 4.22 can be removed by noticing that the renewable cost model guarantees that the target outage level is met exactly if the flow is equal to the design, and hence the problem

can be simplified into a Mixed Integer Quadratic Problem (MIQP).

$$\min_{\gamma_{ij},d_i} \sum_i d_i \cdot (CS_i - C_{AC}(i)) \quad i \in N \tag{4.24}$$

such that

$$\gamma_{ij} \geq 0 \quad \forall i,j \in N \tag{4.25}$$

$$\gamma_{ij} \leq 1 \quad \forall i,j \in N \tag{4.26}$$

$$CS_i = K_1 L_i + K_2 \tag{4.27}$$

$$C_{AC}(i) = F_i \tag{4.28}$$

$$\sum_l \gamma_{il} - \sum_h \gamma_{hi} = D_i \quad \forall i \tag{4.29}$$

$$\textstyle\sum_i d_i = P \tag{4.30}$$

$$d_i \in \{0,1\} \tag{4.31}$$

The objective is a quadratic combination of the variables while all of the constraints are linear. We notice that in the objective, the term containing the sum of AC costs has been dropped since it is a constant.

Our experiences with the above formulation have indicated that if the links are assumed to be bi-directional, then the objective function has to be modified in order to prevent routing loops through the AC nodes. The reason for this is that the traffic through the AC nodes does not contribute to the overall network cost and therefore the optimizer will not seek to minimize them. This can be simply solved as follows:

$$\min_{\gamma_{ij},d_i} \sum_i d_i \cdot (CS_i - C_{AC}(i)) + \sum_i \sum_j \gamma_{ij} \quad i,j \in N \tag{4.32}$$

Therefore the only change in the objective function is to add the sum of the flows. This change will cause the total flow to be minimized which will

in turn guarantee that there will be no routing loops through the AC nodes and ensure the correctness of the final results. Having formulated the problem mathematically, we can now consider the complexity of the defined problem.

4.5 Problem Complexity

Theorem 1. *The cost-optimal joint node placement and flow routing problem in hybrid powered wireless mesh networks is an NP-complete problem.* [1]

Proof. The theorem can be proven by reduction to the well-known minimum set cover problem [55]. In the set cover problem we are given a collection C of subsets of a finite set S, whose union is S. A set cover for S involves selecting a subset $C' \subseteq C$ such that every element in S belongs to at least one member of C'. The decision version of the problem can be described as follows. "Is there a set cover such that the cardinality of C', is less than or equal to K, i.e., $|C'| \leq K$?"

Assume we are given any instance of the minimum set cover problem, where $S = \{E_1, E_2, \ldots, E_{n-1}, E_n\}$. We transform this into an instance of the optimal flow/placement problem from Section 4.4 as follows. A four-stage mesh network is formed as shown in Figure 4.3. The first stage is a source node from which all traffic originates, and a unit traffic flow (chosen to be much smaller than the link capacity) is to be sent to each of the elements of the set, S. The nodes in stage 3 each represent one of the elements in S as shown. This traffic must be sent through stage 2 which consists of $|C'|$ nodes, each representing one of

[1] I would like to thank Dr. George Karakostas for his input on the NP-completeness proof.

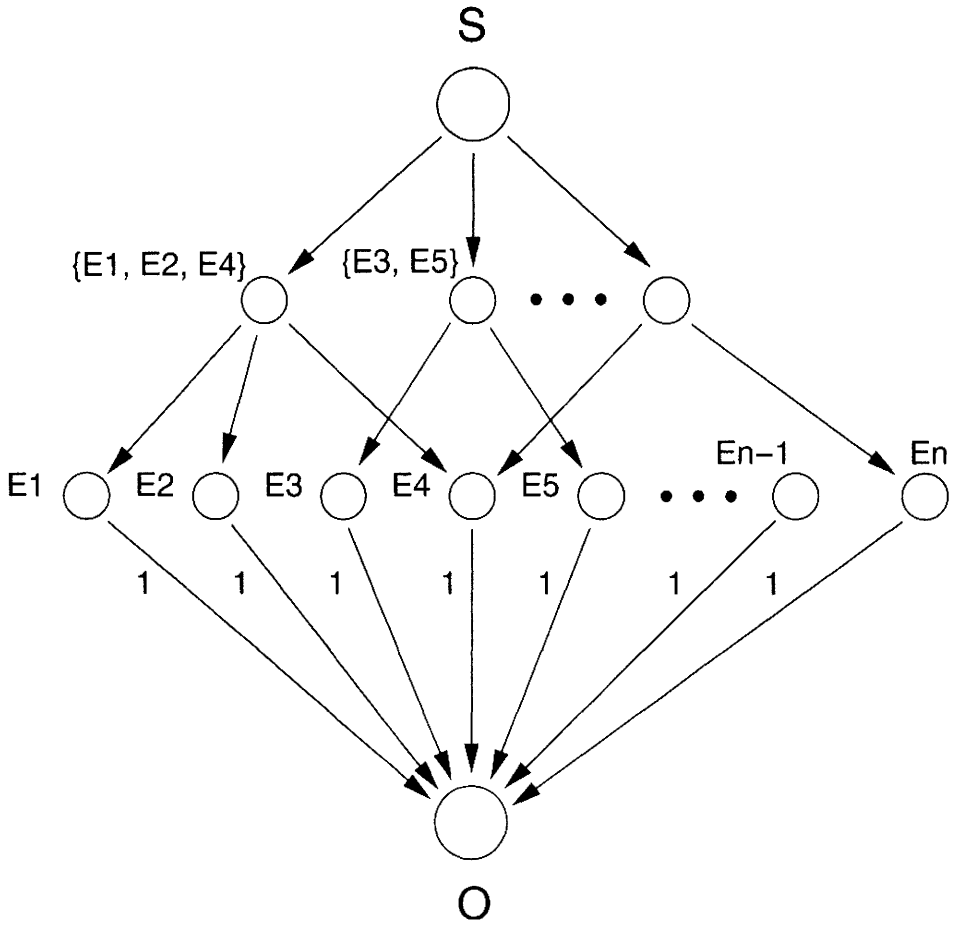

Figure 4.3: Network Construction for NP-completeness Proof

the subsets of S. The connectivity between stages 2 and 3 are defined by the entries in the provided subsets C, an example of which is shown in the figure. The traffic flow leaves the network via node O. The objective in this network is to find $K = N - P$ nodes such that all traffic flow demands are met and there is a zero renewable energy provisioning cost for the P remaining nodes. In this case K represents the number of chosen intermediate nodes for traffic routing.

Now assume that we have a polynomial time algorithm that can solve the optimum flow/placement problem from Section 4.4, and we input the network problem defined above (in Figure 4.3). The algorithm will find the best renewable node placement/provisioning cost for P renewable nodes. If this cost is zero, then the algorithm has found a subset of K second-stage nodes through which the traffic can be routed, leaving no traffic flow for the P remaining (renewable) nodes (i.e., Their panel/battery provisioning cost is zero). It can be seen that this node selection provides a set cover for the original problem. It is also easy to see that if a set cover exists for the given set of parameters, our algorithm must be able to find one, otherwise the assumed optimality of our algorithm is violated. Running this procedure for all values of K will provide an answer to the decision version of the set covering problem. It follows from this that our problem is NP-complete. □

4.6 Solution Methodology

We now present the proposed algorithm for performing the node assignment. The approach relies on solving the underlying MIQP problem using the branch and bound approach [30]. Our experiments have shown that this achieves the optimal provisioning and assignment in small networks which can be solved by exhaustive search. We also present results that compare its performance to the classical approach that uses flow routing followed by node type assignment to highlight the importance of taking into account the underlying interaction between the routing and the resource allocation.

The branch and bound approach has been shown in [52] to be appropriate

for solving MIQP problems. The numerical solver in [30] relies on removing the integer constraints and solving the relaxed version of the problem by calling the quadratic programming solver in Matlab. The solver then uses branch and bound in order to search through the binary integer subspace in order to find a solution. We used the default values of the solver since we found them to achieve the optimal value with minimal delay.

One important observation that can be made is that when the number of solar nodes is zero or equal to N, both the MIQP and classical approaches will yield exactly the same results since shifting resources from one node to the next will not change the total cost of the network. This is due to the linearity of the cost model.

4.7 Performance Results

In the following, we present a discussion of the performance results. We compare the classical approach to the branch and bound approach for different scenarios. We show deployment cost results for Toronto, Ontario. These can be easily scaled up and down depending on the geographic location since we have shown that the cost is a linear function. The cost results shown represent the normalized cost of the network meaning that the cost of one Ah of battery capacity has been normalized to one dollar. For most of the examples shown here, we show networks that are arranged in a grid topology and for ease of notation, we only show results for uni-directional links. We also distinguish between the case when the AC node costs are all equal and when they are not. We also show an example of a large-scale deployment.

4.7.1 Results for Homogeneous AC Costs

In this section we consider the case where the AC costs are all equal. In this case, the node placement will only be a factor of the traffic demand and network topology. This is due to the fact that the AC nodes will not contribute to the total cost of the network.

Our experiments have shown that the results obtained using the algorithms can significantly reduce renewable provisioning costs. In the following, we show some typical examples using a 4×4 mesh network shown in Figure 4.4. We assume the following traffic matrix for this example. Node 16 is a gateway to which all nodes are sending traffic, we assume 0.6 units of flow from node 1, 0.2 from node 5 and 0.9 from node 15.

For the case where the number of solar nodes $P = 8$, the deployments are shown in Figures 4.4 and 4.5. The shaded nodes are the renewable nodes and the unshaded nodes are the AC powered nodes. The flows are labeled on the arcs and arcs labeled with an X are not carrying traffic. We can see that the optimal routing sends as much traffic as possible through the AC nodes as opposed to the simple heuristic, as would be expected. For all values of P, the optimal placement outperforms the shortest path routing. This is shown in Figure 4.6 which plots the normalized cost of the network versus the number of renewable nodes for the shortest path heuristic versus the optimal case.

The cost results shown are for the case where $P_{Out} = 0.1$. For different outage probabilities, the costs can be easily scaled up. We can see from Figure 4.6 that when the number of renewable nodes is low, the results for the branch and bound are similar to the proposed heuristic. However, when the number

of nodes increases, the costs quickly diverge until P reaches 8.

The cost for the branch and bound solution is almost 90 dollars (normalized) while for the heuristic it is almost 175 dollars. The costs then start to converge again once the value of P approaches N. This behavior of the cost curves is related to the path diversity available for the different values of P. This effect can be interpreted as follows, when the number of solar nodes to be deployed is very low or very high compared to N the total number of feasible solutions is significantly reduced. Therefore, if the number of flows is low, the results from both approaches is expected to yield similar results especially since the AC nodes all have the same cost. As expected, this effect cannot be generalized.

We also considered the case when certain renewable nodes are pre-assigned their locations. This could occur if the nodes are deployed at locations where it is impossible to supply them with continuous power. For example, we consider the case where Nodes 10, 11, and 12 are pre-assigned in this way. The optimal deployment will try to route traffic to avoid these nodes, and the results are shown in Figure 4.8. We can see that the gap between the optimal cost and the classical approach increases. This is due to the fact that the optimal deployment must keep traffic away from these nodes. The shortest path heuristic is oblivious to the pre-assignment of the nodes and hence the cost of the network deployment increases when compared to the branch and bound solution that takes the nature of the nodes into account. This is an example of another case where the classical approach fails to perform adequately.

In the next set of results we introduce a second gateway into the network. We set Node 7 as a gateway in addition to Node 16 in addition to flows shown

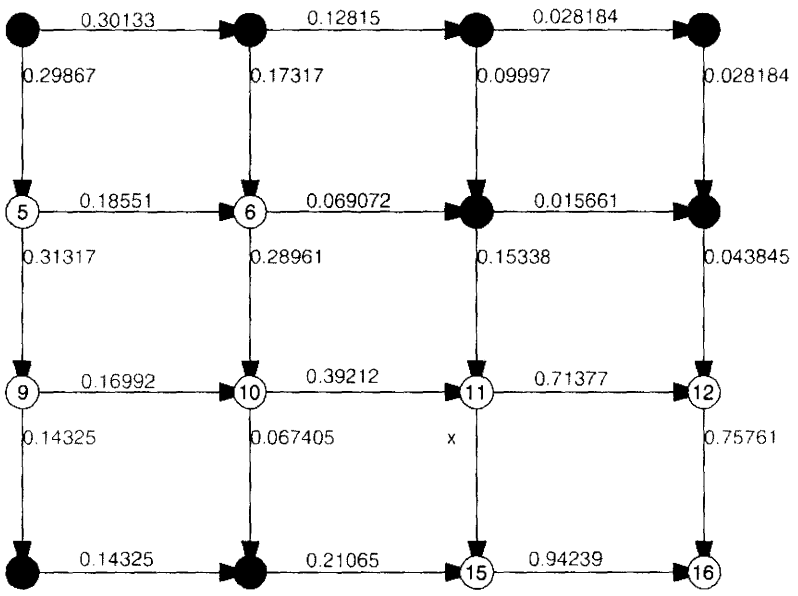

Figure 4.4: Deployment Example Using Shortest Path for a 4×4 Mesh (solar nodes are shaded in red)

in the format *node(flow)*: 1(flow=1), 2(flow=0.2), 3(flow=0.01), 4(flow=0.15) and 5(flow=0.12). The algorithm will choose node 7 as an AC node and route traffic accordingly. The results are shown in Figure 4.9. We notice that the overall cost of the network deployment has increased. We also see that the shortest path results are close to the optimal due to the congestion that was already affecting this region of the network.

We also consider the case where Nodes 9, 10, 13 and 14 are removed and the traffic matrix is 1(0.5), 4(0.3), 6 (0.6) with a destination node 16. This

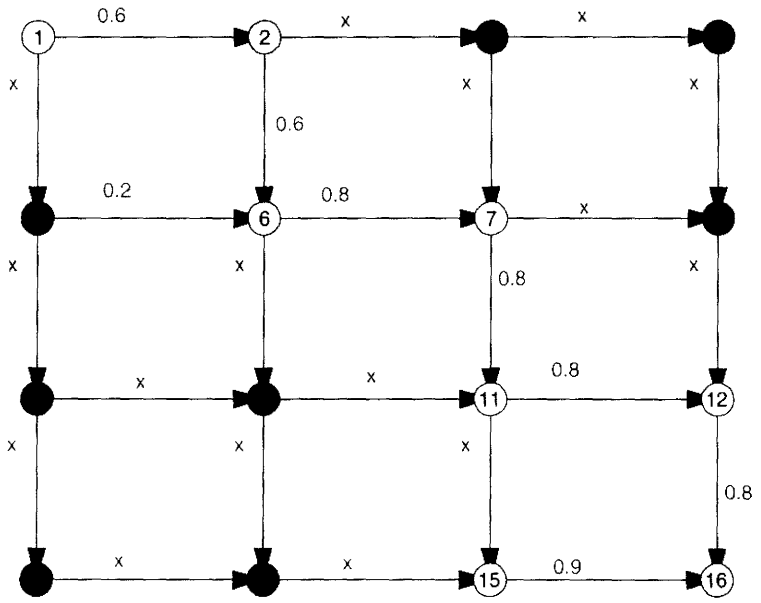

Figure 4.5: Optimal Deployment Example for a 4×4 Mesh (solar nodes are shaded in red)

corresponds to a more asymmetric case, and the normalized costs obtained are shown in Table 4.3. As before, the costs for both algorithms are very close when P is high or low (when compared to N). However, when P is close to $N/2$ the classical approach does not perform as well as the optimal solution. For example, when $P = 8$ the cost rises from 119.41 to 152.53. We can see that the divergence of the costs is not high when compared to the previous cases since the route diversity and number of nodes has decreased.

P	Optimal Cost	Shortest Path Cost
1	10.882	10.882
2	21.765	21.765
3	32.647	32.647
4	43.529	43.529
5	54.412	62.987
6	75.000	90.046
7	92.353	117.91
8	119.41	152.53
9	156.18	187.19
10	192.94	226.10
11	236.18	271.93
12	292.35	326.09
13	348.53	382.27
14	424.12	440.46
15	499.71	506.98

Table 4.3: Normalized Cost for Asymmetric Network

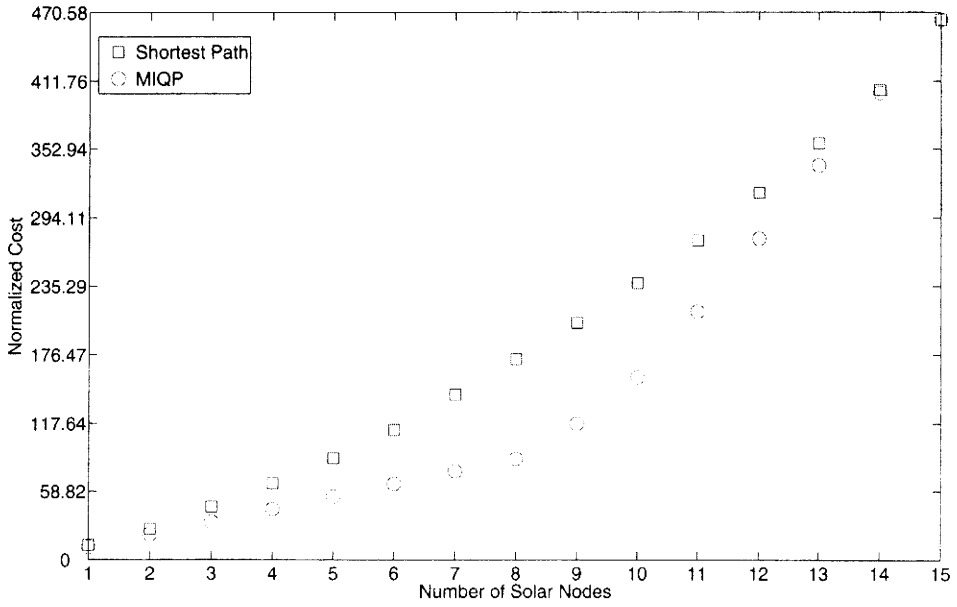

Figure 4.6: Example of Total Solar Cost Versus Number of Solar Nodes for a 4×4 Mesh

4.7.2 Larger Example

In the previous examples, we focused on a small number of flows for ease of notation. In this case we consider a case where 34 flows need to be routed through the network with different sources and destinations. Again, we found that the branch and bound approach solved the problem very rapidly. Figure 4.11 shows the routing of different flows through the network for an 8 node placement. The figure shows the net flows that are routed through each link. Figure 4.12 summarizes the cost comparison between the classical approach and the branch and bound approach assuming that the AC costs are zero. We can see that there is a clear advantage associated with using the branch and bound approach. This is due to the fact that there is a very large number of

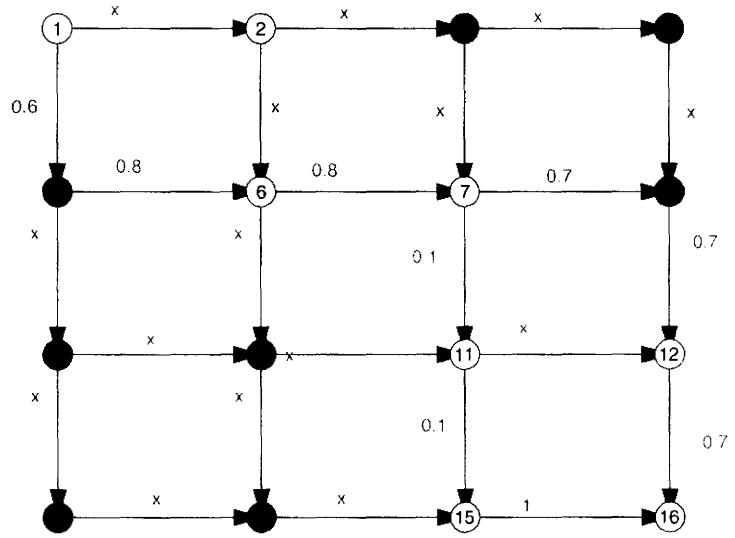

Figure 4.7: Optimal Deployment Example for a 4 by 4 Grid with Pre-assigned Solar Nodes (solar nodes are shaded in red)

flows travelling through the network while the path diversity is limited. For example, the cost of deploying 8 nodes using the classical approach costs 568 dollars while it only costs 126 dollars to perform the optimal deployment which represents an error of 350 %.

4.7.3 Results for Heterogeneous AC Costs

In this section we assume a more general case where the AC costs are not equal for all nodes. We assume the following traffic matrix: 1(0.5), 4(0.3), 6 (0.6) with a destination at Node 16. For the solar nodes, we assume that $P_{Out} = 0$,

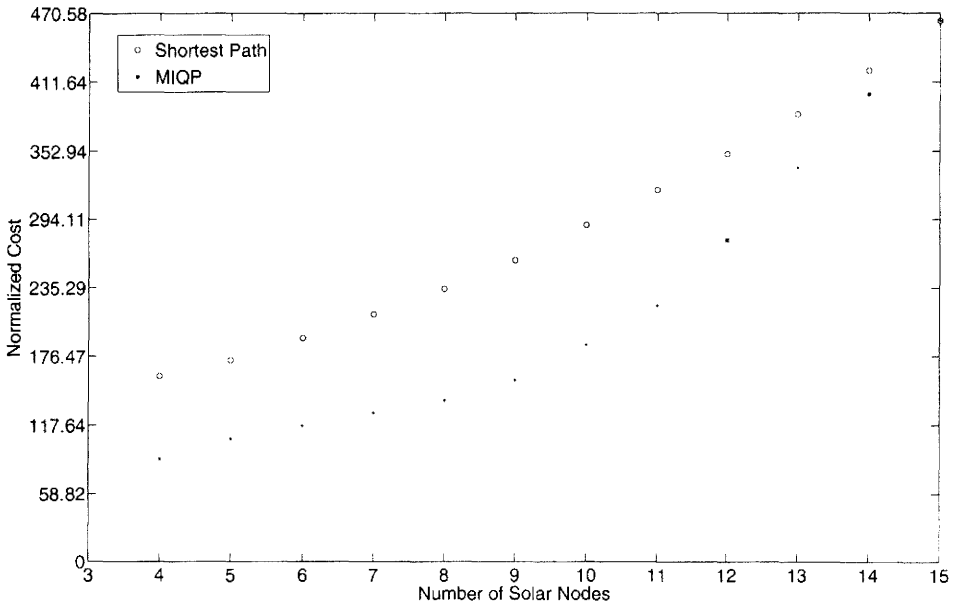

Figure 4.8: Cost of Optimal Deployment Example for a 4×4 Mesh with Pre-assigned Solar Nodes

therefore $K_1 = 220$.

In this first example, we assume a simplified distance dependence model, where the left half of the grid is cheaper and has a uniform cost of 250 while the right half has uniform cost of 1000. The results for the branch and bound and the heuristic approach are shown in Figures 4.13, 4.14 respectively for an 8 node placement. We observe that the branch and bound approach correctly placed all the AC nodes on the left side of the grid, on the other hand, the shortest path approach did not take the node costs into account. As a result, as shown in Figure 4.15, the cost diverges between both approaches especially when P is close to 8 where the branch and bound brought the network cost down to 3000 as opposed to almost 7500 for the shortest path and a 10000

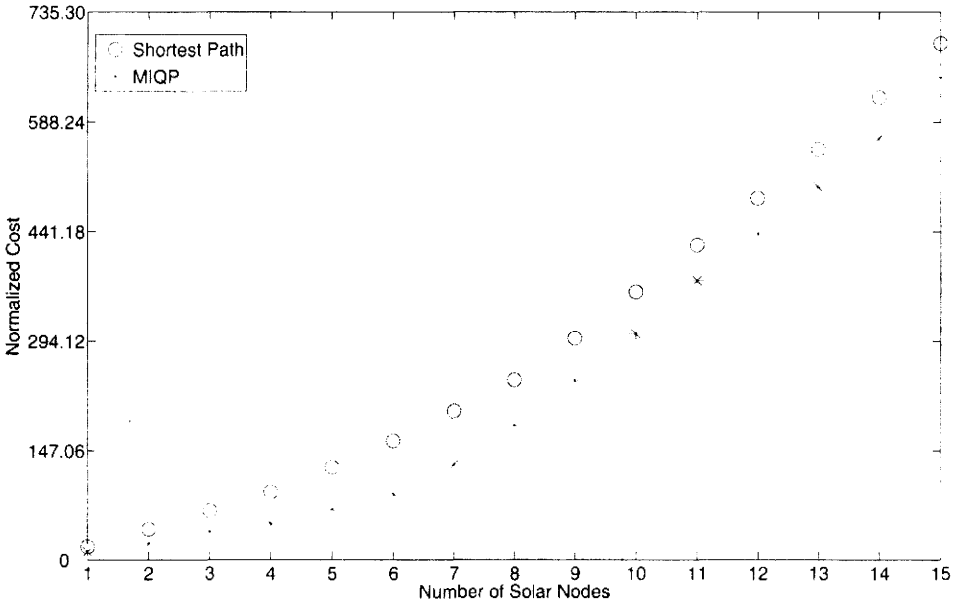

Figure 4.9: Cost of Optimal Deployment Example for a 4 × 4 Mesh with an Additional Gateway at 7

maximum for the all-AC approach.

In this second example, we show a case where the center nodes of the network are very expensive nodes, therefore we assume Nodes 6,7,10,11 are all priced at 1000 while the rest are at 250. Since Nodes 6,7,10,11 are the main transport nodes in the network, we can see that the shortest path- which will yield the same placement as that shown in Figure 4.14 will assign most of them to be AC nodes while the optimal placement as shown in Figure 4.16 will assign them all as solar nodes since it will be more cost effective. This is an example of how the AC costs in some cases could force some of the critical nodes in the network to be solar-powered. A cost comparison is shown in Table 4.4, we can see the significant cost savings achievable especially when $P = 8$. We notice

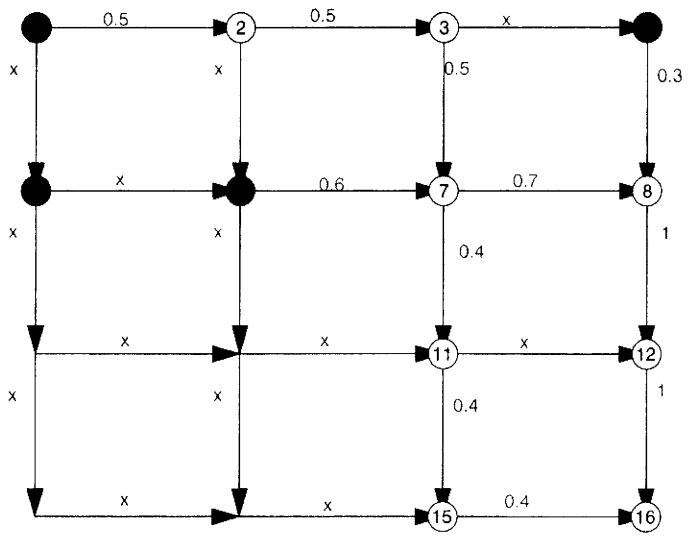

Figure 4.10: Example of Optimal Deployment for Asymmetric Network (solar nodes are shaded in red)

that again an all-AC approach is not recommended even though the solar nodes being deployed are expensive since they have such a low outage requirement.

4.7.4 Results for a Tree Topology Example

Throughout the previous discussion, we assumed that the routing and node placement were variable. In this section we show an example where the routing is no longer a factor. In this case, the only deciding factor is the individual AC node cost. We present our discussion in the form of an example. We consider a mesh network that is arranged into a tree topology. Figure 4.17

P	Optimal	Shortest Path	Maximum
1	6000.0	6819.1	7000.0
2	5000.0	6638.3	7000.0
3	4132.0	6466.4	7000.0
4	3396.0	6317.0	7000.0
5	3146.0	6177.0	7000.0
6	2896.0	6042.9	7000.0
7	2712.0	5912.4	7000.0
8	2572.0	5070.3	7000.0
9	2542.0	4981.0	7000.0
10	2512.0	4929.3	7000.0
11	2482.0	4135.2	7000.0
12	2408.0	3341.0	7000.0
13	2334.0	2598.0	7000.0
14	2392.0	2646.6	7000.0
15	2582.0	2704.6	7000.0

Table 4.4: Normalized Cost for Network with Expensive Center Nodes

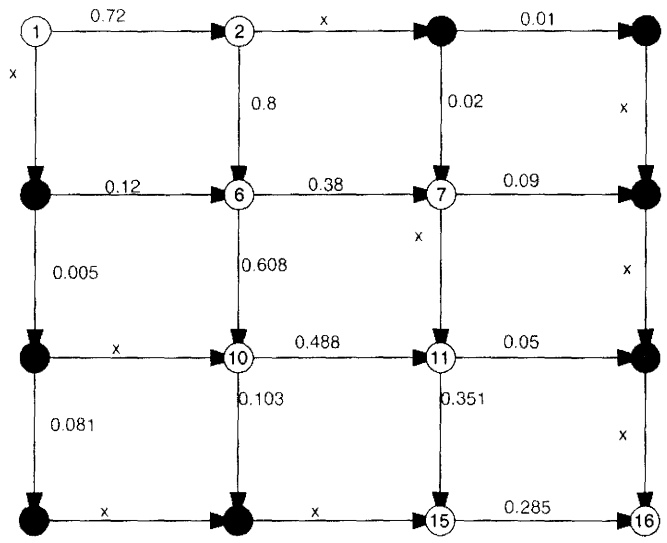

Figure 4.11: Solving a Larger Example (solar nodes are shaded in red)

shows an example of nodes sending traffic to the gateway destination (node 1) the amount of traffic being sent is shown in between brackets. In this case, the routing is unique. The figure also shows the deployment results for $P = 7$ assuming homogeneous AC costs. As expected, both the classical approach and the branch and bound approaches will yield the same results. In our example, the optimal solution is to deploy the leaf nodes as solar nodes since they are the nodes carrying the minimum traffic.

We now consider the case where the AC costs are heterogeneous. Node 3 and all the nodes below it move further away and their AC cost is now more expensive. We assume all nodes have zero AC cost except for those that are

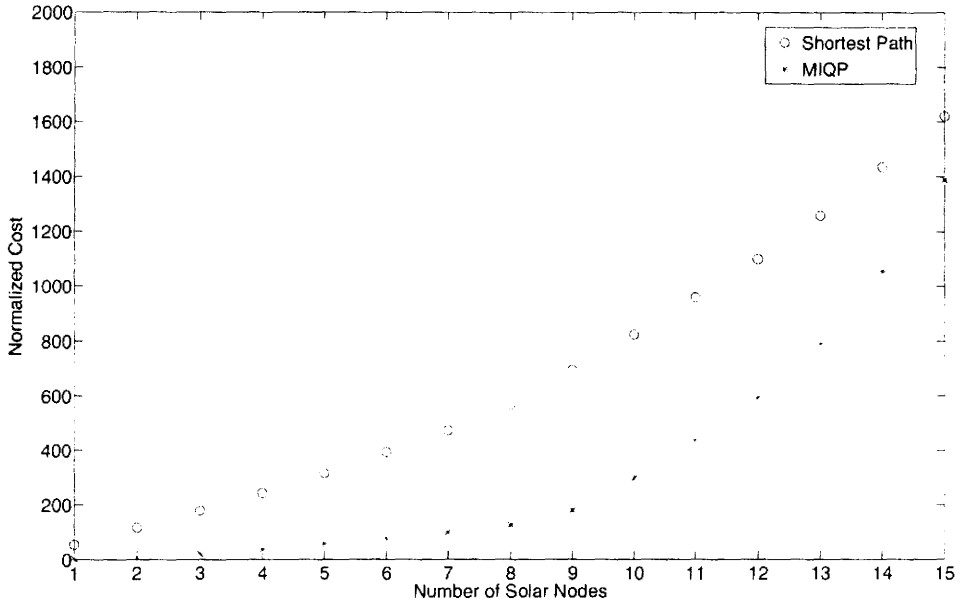

Figure 4.12: Cost Comparison for a Larger Example

deployed further away which have a cost of 1000. The results can be seen in Figure 4.18, the link between node 1 and node 3 is highlighted to show that the distance is higher. When $P = 7$, the solar assignment will be for all the 7 nodes attached to node 3. Node 3 will be an AC node since it is the cheapest alternative because it is aggregating all the traffic of the other nodes. If P had been equal to 8, then node 3 would also have been a solar node. On the other hand, the classical approach would still have only factored in the traffic and performed a leaf node solar deployment. A comparison between the total network costs is shown in Figure 4.19. The maximum cost in this case is 8000 dollars based on the assumed AC costs, we can observe that both approaches will yield results that are far below the maximum especially when the number of solar nodes increases. We observe that the curves almost follow the same

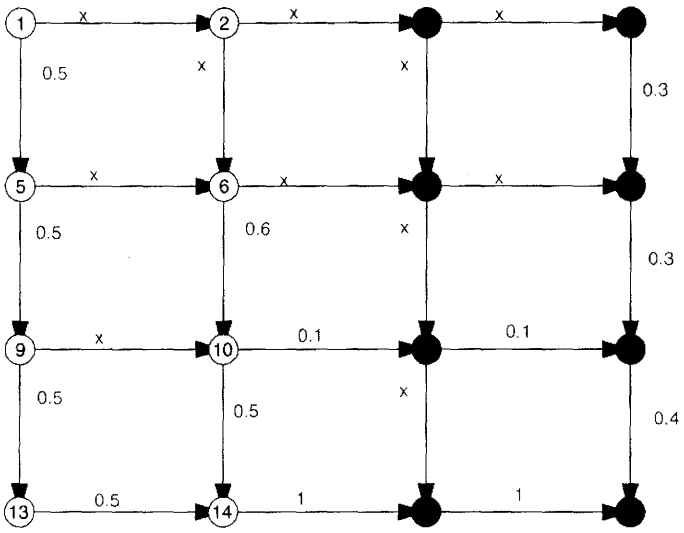

Figure 4.13: Optimal Deployment Example for a 4×4 Mesh with Distance Dependence (solar nodes are shaded in red)

trend for most values of P and the results are close because of the lack of route diversity since the routing is fixed and because the AC nodes that are closer to the gateway are assumed to have a cost of zero. The only exception to this is when P is between 6 and 9. In this case, the impact of taking the solar costs into account makes an appreciable difference. For example, when $P = 8$, the total network cost achieved varies between 600 for the branch and bound approach to 2200 dollars achieved using the classical approach.

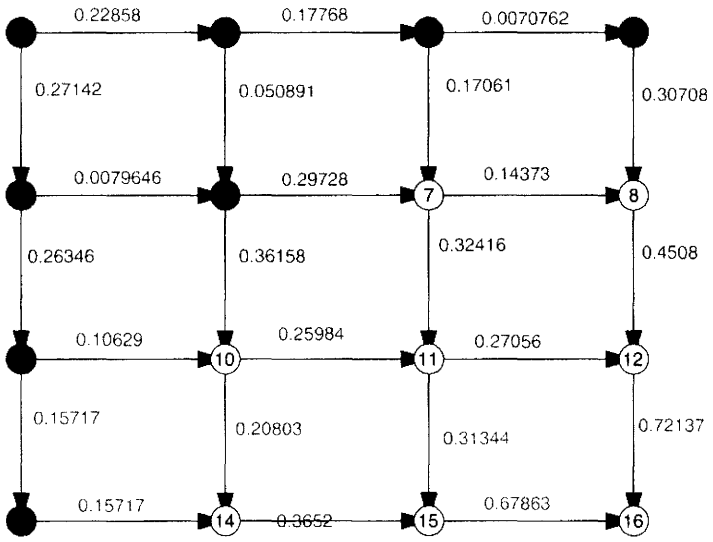

Figure 4.14: Shortest Path Deployment Example for a 4×4 Mesh with Distance Dependence (solar nodes are shaded in red)

4.8 Conclusions

In this chapter we considered the problem of cost-optimal renewable powered node assignment in hybrid WLAN mesh networks. The problem formulation is a binary mixed-integer non-linear problem that can be simplified into a binary mixed-integer quadratic problem. It has been shown that the problem is NP-hard in the most general case, and deployment results were shown using a branch and bound and shortest path heuristic. Our results show that there is a significant improvement in cost that can be obtained using the proposed algorithms, and that the branch and bound approach achieves the optimum

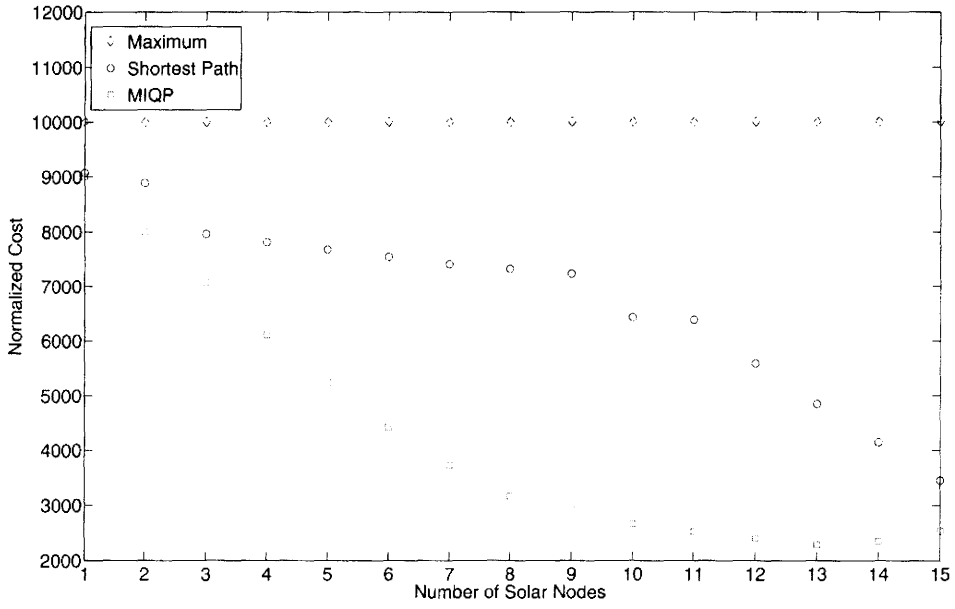

Figure 4.15: Cost Comparison for a 4×4 Mesh with Distance Dependence

assignment for small network examples. In the following chapter, we present an in-depth analysis of the energy management problem in these networks.

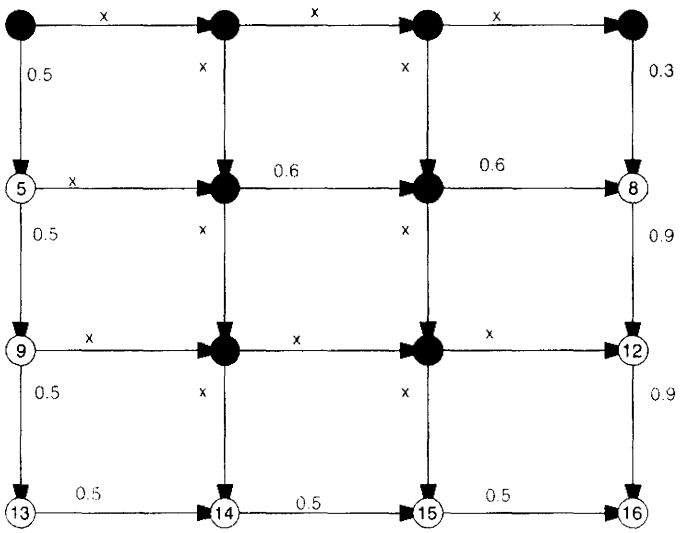

Figure 4.16: Optimal Deployment Example for Expensive Center Nodes for a 4×4 Mesh (solar nodes are shaded in red)

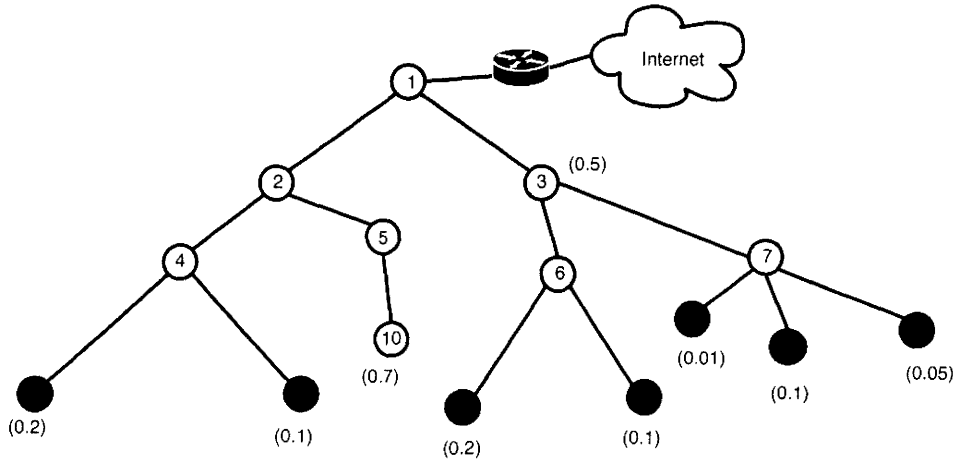

Figure 4.17: Optimal Deployment Example a Tree Topology with Homogeneous AC Node Costs (solar nodes are shaded in red)

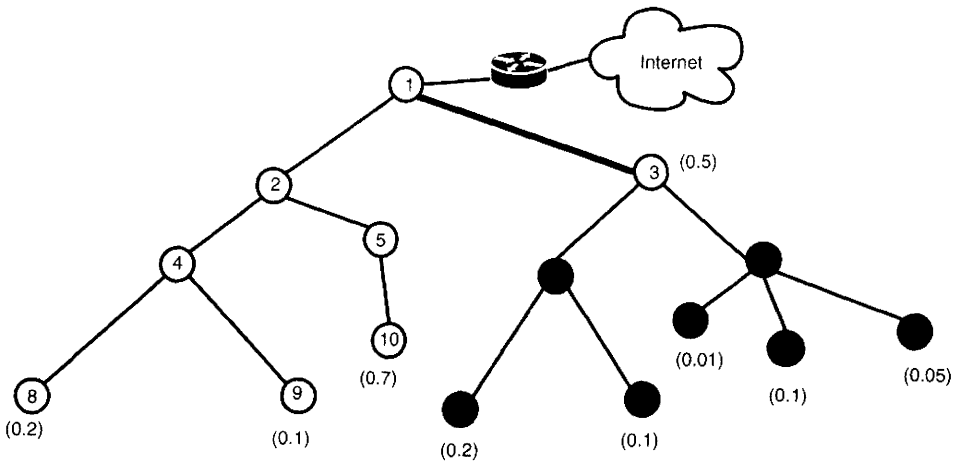

Figure 4.18: Optimal Deployment Example a Tree Topology with Heterogeneous AC Node Costs (solar nodes are shaded in red)

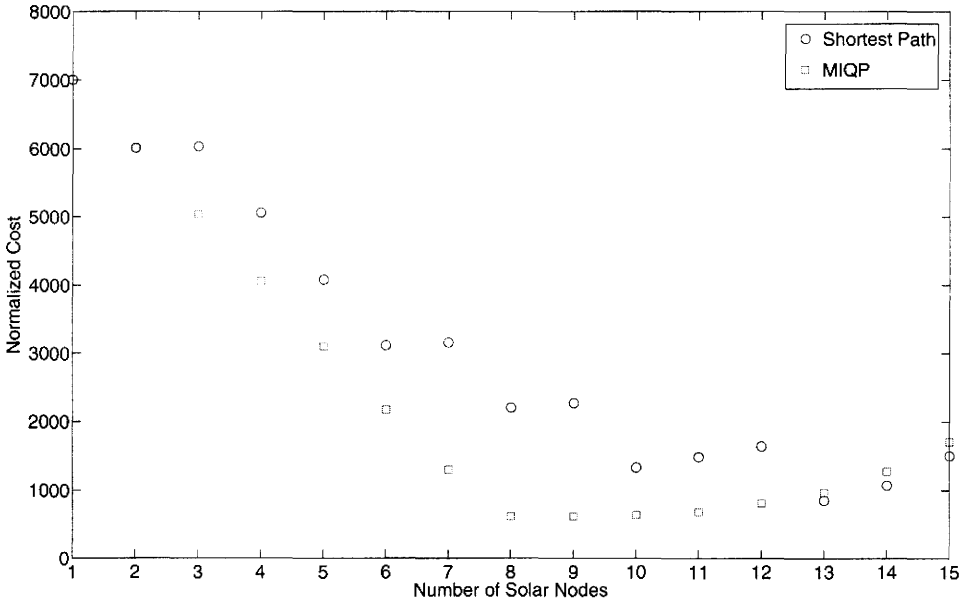

Figure 4.19: Cost Comparison for a Tree Topology With Heterogeneous AC Costs

Chapter 5

Fair Energy Management and Outage Control in Sustainable Solar Powered WLAN Mesh Networks

5.1 Introduction

In this chapter we consider the problem of energy management in solar powered WLAN mesh networks. The traffic control issue is first formulated as a non-linear optimal control problem. A Linear Programming (LP) approximation is then given and solved based on an offline optimization where future solar insolation is known. This result gives a bound on the performance of any real energy management algorithm. We show that the LP solution is accurate in

that it achieves results which are very close to a known no-control capacity deficit lower bound. In addition, the LP approximation is capable of finding out whether traffic admission schemes exist that can reduce node outage events if not eliminate them. Based on this approximation, we then formulate a two-fold optimization problem that ensures fairness in the max-min sense while minimizing the overall energy capacity deficit. We then propose an energy management scheme based on the two-fold optimization that relies on the node having access to meteorological forecasts for the node's geographical location in conjunction with an energy management algorithm running on the node.

This chapter is organized as follows: we present an extensive survey of previous works related to the different problems under consideration. We follow this by a description of the proposed system architecture and related assumptions. We follow this by a formulation of the optimization problem and LP approximation including numerical results. In the subsequent section, we present the proposed energy management algorithm. We then present some strategies for performing prediction. Finally, we perform an in-depth analysis of the algorithm's performance.

5.2 Background

A lot of previously related work deals with energy-aware protocol design and routing [23] [26] [42] [73] [78] [111]. However, there is much less that deals with energy awareness in networks which use renewable-energy. When a long-term traffic stream is admitted, it will require the node to expend energy, and thus it is important for the traffic admission decision to be energy aware in order to

allow the node to stay on-line and meet its outage design target.

In [49] the design of solar-powered WLAN mesh networks was considered from a resource allocation and outage control point of view. A solar panel/battery configuration methodology was introduced based on a proposed AP power-aware version of IEEE 802.11 and public meteorological data was used to provision each node based on an averaged offered capacity profile. In [80] a power-aware routing algorithm is presented for wireless networks with renewable energy sources. The proposed algorithm is shown to be asymptotically optimal when compared to the full knowledge case (competitive analysis). No information is assumed regarding the arrival process and it is assumed that the node has full knowledge of the energy it will receive until the next renewal point by looking at previous data. The proposed routing algorithm uses a composite cost metric that includes power for transmission and reception, replenishment rate, and residual energy. The work also includes non-uniform energy replenishment rates and introduces a battery energy threshold scheme to decrease overhead.

Reference [70] presents an analysis of environmentally powered sensor networks. A model is provided for characterizing energy sources and includes a harvesting theory that governs storage and power consumption requirements. The results are developed for constant and variable power operation. A communication protocol is described for sustainable performance of a network of sensors. The authors then expanded this work in [69] to develop a characterization model for energy sources and traffic loads in a sensor network. The authors also develop the optimization problem of duty cycle adjustment and present

a low-complexity algorithm to solve it. The algorithm uses an Exponentially Weighted Moving Average (EWMA) approach to predict the energy received at a given location. The problem of optimal energy allocation and admission control for solar powered communications satellites has been studied in [53]. The case is considered where each admitted request has an associated reward that is unknown a-priori but has a known pdf. The objective is to maximize the expected value of the reward while not exceeding the energy constraints. A dynamic programming approach was used to establish the optimal policy and was found to be characterized in terms of thresholds. Two heuristic approaches were provided (certainty equivalency, unlimited demand) to speed up the processing time.

In [92] solar powered OFDM wireless mesh networks with sleep management and connection admission control were described. An analytic queuing model was formulated to evaluate the performance at the mesh nodes. Based on this model, the authors present an optimization problem formulation to determine the optimal sleep and wakeup parameters or the CAC threshold in order to meet the desired QoS constraints.

In [119] improved communication energy efficiency is considered for networks powered by renewable energy sources. The work analyzes the energy consumption in the one transmitter, multiple receiver, case. Optimal scheduling algorithms are presented for data transmission at different rates such that the throughput is maximized under given time limits and energy constraints.

On the other hand, previous works have proposed the use of energy management in conjunction with both prediction and regular controllers. For example,

the work in [117] has shown how target state prediction can be used in order to dynamically manage the energy consumption in a sensor network. The energy consumption was optimized in a distributed manner using genetic algorithms and simulated annealing. In [59] a modified form of the previously proposed LPDP algorithm is presented in order to optimize the operation of a stand-alone PV/diesel operated power system. The algorithm uses a combination of linear programming and dynamic programming . The work presented in [86] presents an integrated scheme where neural networks are used to predict the solar insolation and genetic algorithms are used to optimize the power generation of the PV system when it supplies power to a distribution system with random load. In [101] a control strategy for a solar-powered domestic hot water system is presented. The authors adopt a predictive control strategy that involves solving an optimization problem and the implementation of a state estimator. The proposed controller makes use of available online weather forecasts by the Swiss Meteorological Institute (SMI) in addition to predictions of the users' needs via an extended Kalman filter. In [61] the authors present an adaptive optimal control strategy for a grid-independent photovoltaic system. the control algorithm is based on Q-learning. the authors assume that there are two types of loads being serviced; critical and non-critical loads. Finally, in [118] two optimal control strategies are presented for a grid-independent photovoltaic system. The algorithms are based on ADHDP and a fuzzy logic control scheme respectively. Again, similar to [61] the authors assume there is a critical base load that must be supplied at all times.

There are also some biological models for energy management such as those

presented in [100] where a study of energy management for small birds in winter with emphasis on survivability is presented. This was achieved by modelling the experimental data as a dynamic program. The data collected measured the storage of energy in the birds' bodies as fat or externally in caches, the study also measured the variation of the energy stored with changes in temperature and length of nights and predictability of food sources.

There exists a wealth of previous work that deals with statistical prediction of cyclostationary signals and meteorological processes. The following is a brief survey. The work in [110] includes a complete bibliography of more than 1500 papers written on the analysis of cyclostationary signals organized by topic and applications. In [56] the authors survey all the current efforts for short-term wind prediction including reference schemes and error metrics. This document was generated as part of the ANEMOS (EU R&D) project. The work in [74] shows how Empirical Orthogonal Functions (EOFs) can be generalized for statistical prediction of cyclostationary processes.
Finally, in [104] the authors compare the performance of four measure-correlate-predict algorithms for predicting wind speed at a given location. Measure-correlate-predict techniques rely on collecting data locally over a period of time and comparing it to a reference site in order to build a model. Once the model is built, the long-term data at the reference site can be used to model the long-term statistics of the target site.

The following papers represent a collection of the most pertinent research articles written on load forecasting and analysis in WLAN networks. In [94] the authors analyze WLAN traffic collected at the University of North

Carolina. They show the diurnal and weekly periodicity of the traffic by analyzing the power spectrum of the traffic at heavily-loaded APs. They then propose prediction algorithms based on the collected data. In [32], Kotz studied the Verizon Wi-Fi hot-spot network in Manhattan, USA for over 5 weeks. Several traffic statistics were gathered in this study including the hourly traffic load. Their work in [44] presents how the authors gathered WLAN traces from a national restaurant chain in order to provide insight into the required provisioning of WLANs. They developed a throughput prediction model based on their analysis.

The energy management algorithm presented in this paper relies on the use of receding horizon control. In the following is a brief presentation of some of the work that has influenced this study the most. In [103] the author presents an introduction to Model Predictive Control (MPC) and receding horizon control. In [76] the authors present offline and online techniques for energy management in hybrid electric vehicles. Finally, in [47] the author discusses the horizon in predictive energy storage control and how to eliminate the reduction in performance due to finite prediction horizons.

In the following section we present the proposed system architecture.

5.3 Proposed System Architecture

In this section we present the proposed system architecture. The architecture assumes that the energy management algorithm takes into account forecasts of meteorological data. There are several ways of setting up the system depending

on the forecasting technique being used and the processing power of the AP. There are two major calculations that must be performed in order for the traffic admission control algorithm to operate properly. The first one is to generate forecasts of the meteorological data, while the second step is to calculate the maximum admissible load. More details of this second step will be presented in the following section. To conserve power and other mesh node resources, the forecasting could be offloaded to an external server. In this case the mesh node would periodically report the required parameters being collected locally to the server. In this case, the server would also perform the calculations needed in order to evaluate the maximum allowable power dissipation and report back directly to the mesh node the admissible load. Figure 5.1 shows the proposed system architecture. The prediction and energy management calculations are performed on an external prediction server that is accessible by the APs through the Internet.

In the following section we introduce the energy management optimization problem along with a detailed discussion of generating performance bounds on the system operation using offline data.

5.4 Optimization Problem Formulation

Traffic admission control can be formulated as a stochastic control problem. We define $\mathcal{L}(k)$ to be the energy loading of the AP during the time interval $[(k-1)\Delta, k\Delta]$. We then define the *actual* energy loading delivered to the AP during $[(k-1)\Delta, k\Delta]$ to be $\mathcal{E}_a(k)$. In the absence of any control and outage, $\mathcal{E}_a(k) = \mathcal{L}(k)$, but when a control mechanism is in place, the activity level of

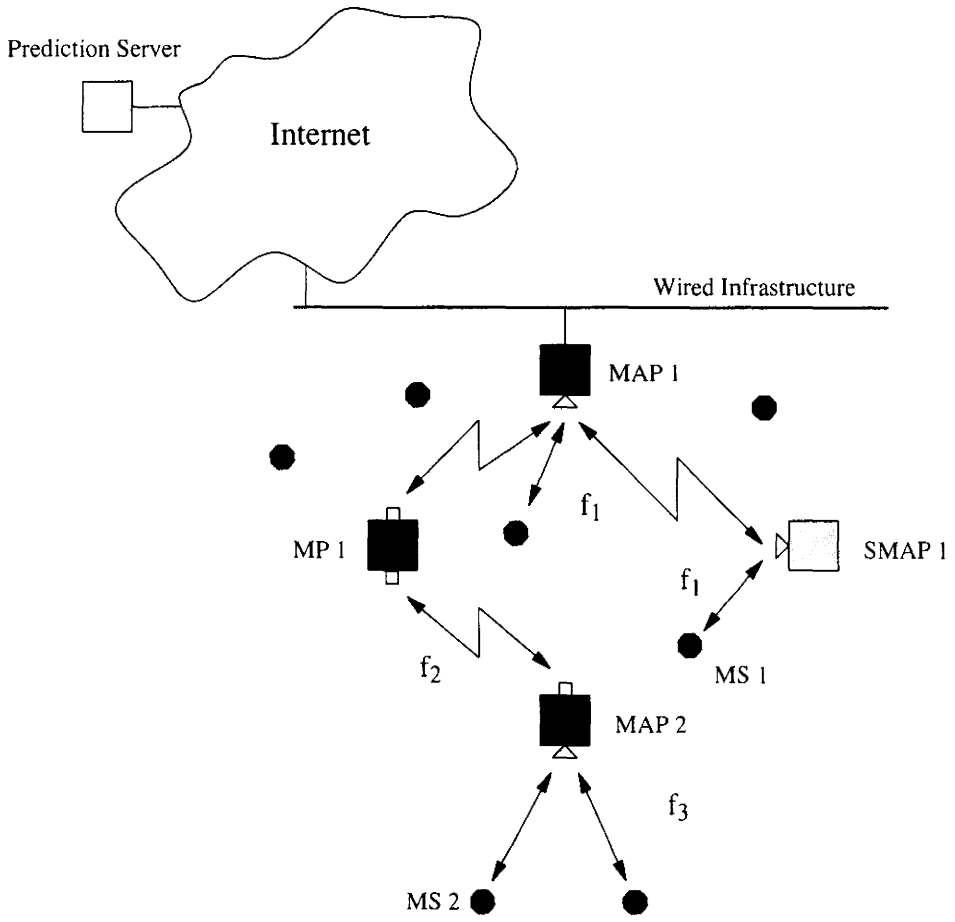

Figure 5.1: Proposed System Architecture

the AP may sometimes be artificially reduced to save power, i.e.,

$$\mathcal{E}_a(k) = \min(\mathcal{L}(k), \mathcal{E}_{max}(k)), \tag{5.1}$$

where $\mathcal{E}_{max}(k)$ is a control variable that specifies the maximum energy consumption in the next interval. The actions of the control variable lead to an energy deficit, $\mathcal{E}_{def}(k)$, defined by

$$\mathcal{E}_{def}(k) = \mathcal{L}(k) - \mathcal{E}_a(k). \tag{5.2}$$

The outage probability P_{Out} for the node is defined as the fraction of time that the battery level drops below $\mathbf{B}_{outage}$. Throughout this chapter, we assume that the node is targeting a zero outage probability.

In addition to an outage requirement, we assume that the normalized level of offered AP capacity should never drop below some acceptable design value, $\mathbf{U}_{min}$, otherwise the operation of the AP would be too impaired. This is similar to the assumption in [61] and [118] that there is a minimum critical base load that the system must be able to supply. In wireless mesh networks this critical base load could represent emergency calls or network management traffic. For example the work in [113] represents an example where a critical base load is needed. The authors parametrized and analyzed the traffic being carried by a wireless public safety network in Southwestern British Columbia. In other cases, the AP may be required to offer premium services to certain traffic types such as real-time traffic. In this case, these traffic types could also be considered critical base loads. Therefore, $\mathbf{U}_{min}$ can be viewed as a control parameter that is set by the network designer depending on the applications running on the network.

Based on this assumption, we must constrain $\mathcal{E}_a(k)$ so that it does not drop below the value needed to provide $\mathbf{U}_{min}$ AP activity level, i.e., $\mathcal{E}_a(k) \geq \mathcal{F}(\mathbf{U}_{min})$. The function $\mathcal{F}[\cdot]$ translates the average activity of the AP into an average energy consumption over $[(k-1)\Delta, k\Delta]$.

The first objective of the control scheme is to satisfy the target outage rate while reducing the capacity deficit as much as possible. For a given loading condition, the optimum control scheme is to select $\mathcal{E}_{max}(k)$ for all k, such that

the energy deficit over all time is minimized, i.e.,

$$\min_{\{\mathcal{E}_{max}(k)\}} \sum_{k=0}^{K_{max}} \mathcal{E}_{def}(k), \tag{5.3}$$

such that

$$\mathcal{E}_a(k) = \min(\mathcal{L}(k), \mathcal{E}_{max}(k)), \tag{5.4}$$

$$\mathcal{E}_{def}(k) = \mathcal{L}(k) - \mathcal{E}_a(k). \tag{5.5}$$

$$\mathcal{B}(k) = \min\{\max[\mathcal{B}(k-1) + \mathcal{E}_{panel}(k) - \mathcal{E}_a(k), \mathbf{B}_{outage}], \mathbf{B}_{max}\}, \tag{5.6}$$

$$P_{Out} = 0, \tag{5.7}$$

and

$$\mathcal{E}_a(k) \geq \mathcal{F}(\mathbf{U}_{min}). \tag{5.8}$$

Equation 5.6 is the energy flow equation for the system, Equation 5.7 is the outage requirement and Equation 5.8 is the constraint on minimum AP activity. As previously mentioned, normally the AP will be designed for a zero outage probability target and in this case Equation 5.7 is equivalent to the requirement that $\mathcal{B}(k) > \mathbf{B}_{outage}$ for all k. Unfortunately Equation 5.3 describes an extraordinarily hard optimal control problem. In the following, we formulate the offline version of this optimization problem, this will serve as a bound for the performance of all energy management algorithms. In addition, we present an LP approximation to increase the computational speed.

We also define the total normalized Capacity Deficit (CD) as

$$CD = 1 - \frac{\sum_{k=1}^{K_{max}} \mathcal{E}_a(k)}{\sum_{k=1}^{K_{max}} \mathcal{L}(k)}. \tag{5.9}$$

The CD for the case where no control is applied was proven mathematically in [49] and [53] to be a lower bound on capacity deficit for any algorithm when the reward associated with a requested load is time invariant. This is referred to as the No Control Lower Bound (NCLB). In the case when there is no control, the system expends energy (and admits traffic) at the earliest possible time. This metric was used in [49] as one of the criteria for measuring the performance of the proposed algorithms, more details will be shown in Section 5.7. In the following we present the optimal offline formulation of the problem along with an efficient LP approximation.

5.4.1 Optimal Offline Formulation and LP Approximation

In this section we show a simplified formulation of the offline version of the traffic admission control problem and an LP approximation in order to solve large-scale system runs. This formulation assumes that outages are eliminated completely. We assume that we have full knowledge of the future solar insolation and load, which will result in a bound on performance for any realizable algorithm.

Let us first assume that $\mathcal{E}_a(k)$ is the control variable to be optimized. We introduce a new variable, $S(k)$ which serves a dual purpose; it can be used to represent the surplus amount of energy received by the system that cannot be stored by the battery or it can take a negative value when the battery charge is found to be negative. Let us define $EB(k)$ as the right-hand side of the energy balance equation at time k i.e., $EB(k) = \mathcal{B}(k-1) + \mathcal{E}_{panel}(k) - \mathcal{E}_a(k)$. We can

write $S(k)$ as follows:

$$S(k) = \begin{cases} 0 & , \ \mathbf{B}_{outage} \leq EB(k) \leq \mathbf{B}_{max} \\ EB(k) - \mathbf{B}_{outage} & , \ EB(k) < \mathbf{B}_{outage} \\ EB(k) - \mathbf{B}_{max} & , \ EB(k) > \mathbf{B}_{max}. \end{cases} \tag{5.10}$$

The problem can be re-written as

$$\min_{\{\mathcal{E}_a(k)\}} \sum_{k=0}^{K_{max}} \mathcal{E}_{def}(k) \tag{5.11}$$

such that

$$\mathcal{E}_{def}(k) = \mathcal{L}(k) - \mathcal{E}_a(k) \tag{5.12}$$

$$\mathcal{F}(\mathbf{U}_{min}) \leq \mathcal{E}_a(k) \leq \mathcal{L}(k) \tag{5.13}$$

$$S(k) + \mathcal{B}(k) = \mathcal{B}(k-1) + \mathcal{E}_{panel}(k) - \mathcal{E}_a(k) \tag{5.14}$$

$$\mathbf{B}_{outage} < \mathcal{B}(k) \leq \mathbf{B}_{max} \tag{5.15}$$

We notice that all the constraints and the objective are linear except for the definition of $S(k)$ that was previously shown.

The above formulation can be used to find the offline solution to the problem. It can also be used to establish a performance benchmark and to establish the conditions necessary for the optimization to exist. The optimizer will be able to find an optimal system run (if one exists) that leads to the minimum capacity deficit. The disadvantage of the off-line optimization is that although it can determine the existence of an optimal solution, and it provides the full-knowledge solution, no insight is given as to how to develop an algorithm to find an optimal causal run.

Since non-linear optimization problems are difficult to solve for large scale problems, an approach is to approximate it by an LP or a convex problem for which there are several efficient large scale solvers [37]. We notice that $S(k)$ is obtained via a non-linear expression, however, by careful examination we notice that we want to minimize its absolute value for all cases with the exception of the case when the non-linear constraint is active. Therefore, the problem can be re-formulated as the following LP problem [1]:

$$\max_{\{\mathcal{E}_a(k),B(k),S(k)\}} \sum_{k=0}^{K_{max}} \mathcal{E}_a(k) - \lambda t(k) \tag{5.16}$$

such that

$$\mathcal{F}(\mathbf{U}_{min}) \leq \mathcal{E}_a(k) \leq \mathcal{L}(k) \tag{5.17}$$

$$\mathcal{B}(k) + S(k) = \mathcal{B}(k-1) + \mathcal{E}_{panel}(k) - \mathcal{E}_a(k) \tag{5.18}$$

$$\mathbf{B}_{outage} < \mathcal{B}(k) \leq \mathbf{B}_{max} \tag{5.19}$$

$$-t(k) \leq S(k) \leq t(k), \tag{5.20}$$

where λ is a control factor that is set so as to not interfere with the operation of the original objective and $t(k)$ is a dummy variable used to linearize the absolute value operation of $S(k)$.

In the previous formulation, the controller will aim to reduce the overall capacity deficit. However, since the objective of the optimization is to reduce the total capacity deficit for the entire timeline of the system run, this optimization will not guarantee that there are no abrupt changes in offered capacity from one time period to the next. Thus, temporal fairness is not guaranteed. This

[1] I would like to thank Prof. Tim Davidson for his assistance with the formulation of the LP approximation problem.

means that the offered load could vary dramatically from one hour to the next, for example, the offered load in the final hour of the night and during the first hour of daylight may vary significantly due to the abrupt change in received solar insolation.

In order for the controller to maintain fairness then the minimization in the objective function can be converted into a max-min operation. However, the max-min optimization may increase the overall total capacity deficit, hence the optimization has to be solved as a two-fold optimization problem. In the first one, the minimum value of the total capacity deficit $\mathcal{E}_{defmin}$ is found using the previous optimization formulation and the second one can be written as follows:

$$\max_{\{\mathcal{E}_a(k),B(k),S(k)\}} (\min_k(\mathcal{E}_a(k)) - \sum_{k=0}^{K_{max}} \lambda t(k)) \tag{5.21}$$

such that

$$\textstyle\sum_{k=0}^{K_{max}} \mathcal{E}_{def}(k) = \mathcal{E}_{defmin} \tag{5.22}$$

$$\mathcal{F}(\mathbf{U}_{min}) \leq \mathcal{E}_a(k) \leq \mathcal{L}(k) \tag{5.23}$$

$$\mathcal{B}(k) + S(k) = \mathcal{B}(k-1) + \mathcal{E}_{panel}(k) - \mathcal{E}_a(k) \tag{5.24}$$

$$\mathbf{B}_{outage} < \mathcal{B}(k) \leq \mathbf{B}_{max} \tag{5.25}$$

$$-t(k) \leq S(k) \leq t(k), \tag{5.26}$$

This two-fold optimization formulation guarantees that the resultant solution enforces temporal max-min fairness while still achieving the lower bound on energy deficit.

Any proposed causal energy management algorithm must primarily eliminate or reduce outages while minimizing capacity deficit. However, the algo-

rithm should strive to provide comparable service for traffic requests arriving within a short period of time of each other. In the following section we propose our energy management algorithm that relies on forecasted meteorological data in order to minimize and redistribute the capacity deficit incurred while eliminating outages from the solar-powered WLAN mesh node. We first discuss the previously proposed On/Off controller followed by motivation for the newly proposed algorithm.

5.5 Energy Management Algorithms

The On/Off controller was first presented in [49], in it the authors proposed this algorithm as a simple control scheme that tries to mimic the no control action that results in the NCLB bound on CD. The algorithm is presented in Algorithm 1. The algorithm is quite simple; as long as the battery level is above the optimal battery threshold $\mathbf{L}_{thonoff}$, then the load that the system accepts $L(k)$ is identical to the requested load $\mathcal{L}(k)$. On the other hand, if the charge dips below the threshold, then $L(k)$ is immediately set equal to $\mathbf{U}_{min}$. Hence, the controller is inactive until the battery charge at time k dips below the given optimal threshold that is calculated offline using historical weather data for a given geographic location.

As an illustration, Figure 5.2 shows an example of the results obtained for the offline optimizer in addition to a comparison to the On/Off case. We assume a battery size of 20 Ah and a panel size of 31.6 watts, $\mathcal{F}(\mathbf{U}_{min}) = 1$ watt and we found $\mathbf{L}_{thonoff}$ to be 0.18 (for 10 years of data) using the methodology outlined in [49]. The offline optimizer results are achieved by running the two-

Algorithm 1 On/Off Control Algorithm

$L(0) = \mathcal{L}(0)$, $\mathcal{B}(0) = \mathcal{B}_0$
for $k = 1$ to K_{Max} **do**
  $\mathcal{B}(k) = \min\{\max[\mathcal{B}(k-1) + \mathcal{E}_{panel}(k-1) - L(k-1), \mathbf{B}_{outage}], \mathbf{B}_{max}\}$
  if $\mathcal{B}(k) < \mathbf{L}_{thonoff}$ **then**
    $L(k) = \mathcal{F}(\mathbf{U}_{min})$
  else
    $L(k) = \mathcal{L}(k)$
  end if
end for

fold optimization over the solar insolation data assuming that is is known in advance.

The figure is divided into three figures that show the battery charge, admitted load, and the received solar insolation as they evolve over time for both the Optimal Offline Controller (OOC) and On/Off cases. The first figure shows the battery charge for both cases and we notice that the charge for the OOC case is higher. The second figure shows the offered load and we notice that the OOC case is less abrupt. Finally, the third figure shows the total received solar power. We notice that the battery charge never dips below $\mathbf{B}_{outage}$ and the admitted load never dips below $\mathcal{F}(\mathbf{U}_{min})$, as required.

We can also see that the admitted load is evenly distributed as opposed to the On/Off case, which simply turns the system on and off. This is due to the max-min objective formulation. For example, we see that between the 1st hour and the 100th hour, the offline optimizer withheld energy from the load by only suppling 2.7 W instead of 4 W. On the other hand, the On/Off algorithm provided the complete load but it started with a half full battery and ended with an empty battery. If we examine the hours between 80-120, we notice

that the solar insolation dips down to zero and the On/Off case is incapable of satisfying requests while the offline optimizer has accumulated enough energy in the battery so that it can supply slightly more than 2.7 W over the no insolation period.

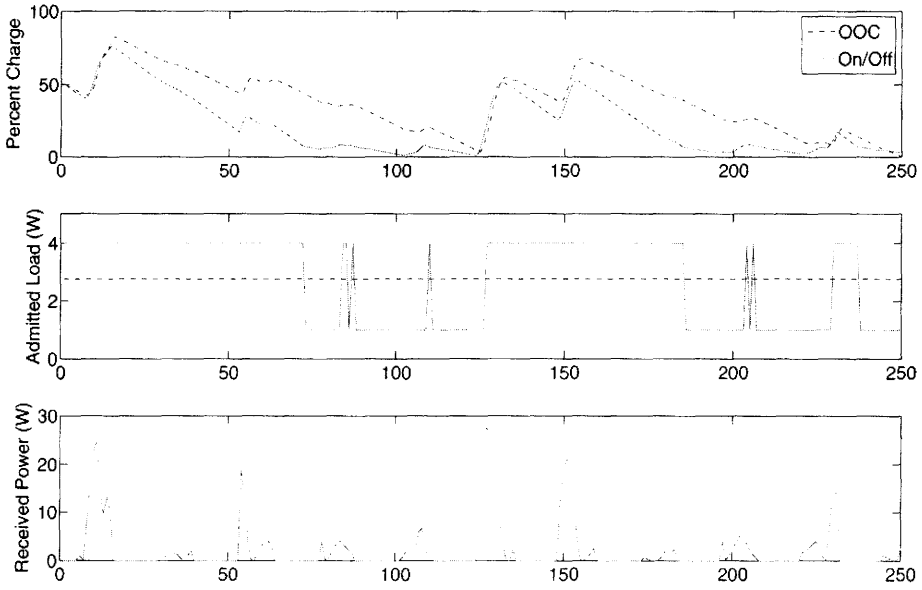

Figure 5.2: Sample Run of OOC versus On/Off Controller

This example suggests the need for a measure in addition to the max/min criterion for comparing the energy fairness of different algorithms. Accordingly, we define the *Average Conditional CD* as the average of the CD over the times when the capacity deficit is non-zero. More formally, if we define the time instances when the controller is active as a set, $K_{CD} \subset \{0, 1, \ldots, K_{max}\}$, then the average conditional CD is defined as

$$\text{Avg.Cond.CD} = \frac{\sum_{k \in K_{CD}} CD(k)}{|K_{CD}|}, \tag{5.27}$$

where $|K_{CD}|$ is the cardinality of K_{CD}. In the above example, the average conditional CD is about 30% in the OOC case while it is 75% for the on/off controller. This is due to the fact that the OOC will activate the controller more frequently, and at a reduced level of capacity deficit when compared to the abrupt on/off control action. However, it should be noted that both controllers come very close to achieving the same minimum total capacity deficit. More results and discussion will be presented in Section 5.7.

This qualitative example also suggests that having access to weather predictions improves the fairness of the energy management algorithm in use. Therefore, we now present the proposed energy management algorithm, which we refer to as the Prediction Based Energy Management Controller (PBEMC) throughout this chapter.

5.5.1 Prediction Based Energy Management Controller

The proposed algorithm is motivated by the non-causal controller action of the offline optimal two-fold optimizer. The operation of the proposed prediction controller can be summarized as follows. It makes use of the available forecasted meteorological data in addition to the current battery charge in order to assess the maximum admissible load in the following hour. Once the maximum admissible load is calculated, the traffic admission control can be performed.

The two-fold optimization is performed W Δ time periods into the future where W is a judiciously chosen window size. The procedure is repeated at discrete time periods, which would typically be equal to one hour (i.e., $\Delta = 1$).

The optimizer will return a specific optimal loading sequence having W entries, the first value of this sequence is then used as the value of the maximum admissible load for the next Δ. This approach is referred to in the literature as Model Predictive Control (MPC) or receding horizon control [103], [76], [47]. As previously discussed, the weather data used for the finite window optimization will typically either be online weather forecasts if they are available, or predicted weather forecasts using the online server architecture that was previously introduced. Since decisions are based on such long intervals, any enforced power saving can easily be applied to both best effort traffic and connection oriented traffic admission.

Due to the finite window size used in the optimization and the expected errors in meteorological data prediction, the controller must set a target on the battery charge $\mathbf{L}_{th}(k)$. This was previously discussed in [76]. If there was no endpoint for the battery charge, the battery would be constantly be depleted by the controller action since the optimization is performed over a finite window without taking into account the impact of the control action on the system in subsequent time windows. The choice of $\mathbf{L}_{th}(k)$ will be discussed in Section 5.7 in further detail.

The constraints in the two-fold optimization must be modified as follows:

$$\mathcal{B}(k) > 0 \tag{5.28}$$

$$\mathcal{B}(k+W-1) \geq \mathbf{L}_{th}(k+W-1) \tag{5.29}$$

Equation 5.28 implies that the battery charge must always exceed zero for any k. This is to guarantee that there are no outages. On the other hand, Equation 5.29 implies that the target battery charge value $\mathbf{L}_{th}(k)$ must always

Algorithm 2 Energy Management Algorithm (PBEMC)

k = Current time
W = Window Size
$R(k-1)$= Requested Load
$\mathbf{L}_{th}(k+W-1)$= Target
$\mathcal{B}(k)$= Current Battery Charge
$L_{max}(1 \ldots W)$=$\Gamma(\mathbf{L}_{th}(k+W-1), \mathcal{B}(k), \mathcal{F}(\mathbf{U}_{min}), R(k-1), \mathcal{E}^*_{panel})$
if $R(k-1) > L_{max}(1)$ **then**
  $L(k) = L_{max}(1)$
else
  $L(k) = R(k-1)$
end if

be met or exceeded in order to guarantee that the algorithm does not run into outage over the entire timeline.

The proposed algorithm is summarized in Algorithm 2. The algorithm seeks to find the admissible load at time $k\Delta$ which is referred to in the algorithm as $L(k)$. At each decision point, $k\Delta$, the algorithm finds the maximum admissible energy that satisfies the max-min fairness objective during the next $W\Delta$ time increments, $[(k)\Delta, (k+1)\Delta \ldots (k+W-1)\Delta]$ while still maintaining the battery charge above the target level $\mathcal{L}(k)$. This step is performed independently of the requested load. For ease of notation, we denote the two-fold optimizer action as $\Gamma(\cdot)$. Using the predicted meteorological data $\mathcal{E}^*_{panel}$, the two-fold optimizer ($\Gamma(.)$) is run over the subsequent W time increments (i.e., hours) into the future. The result of this run yields a sequence of W admissible loads into the future $L_{max}(1 \ldots W)$. The maximum admissible load at time $k\Delta$ will be the first value of the admissible load sequence $L_{max}(1)$ in the algorithm. $L_{max}(1)$ is guaranteed to be always above $\mathcal{F}(\mathbf{U}_{min})$ since this is embedded into the optimizer action. Once the maximum admissible load is found, it can be

compared to the requested load $R(k-1)$, if the requested load is less than the maximum admissible load, then it is admitted. In this case, the admitted load is equal to the requested load $L(k) = R(k-1)$ otherwise, it is reduced using power saving until $L(k) = L_{max}(1)$. In this case, there will be capacity deficit incurred by the requested load. Therefore, the PBEMC algorithm's action can be seen as accepting the current hour of day $k\Delta$ and the window of prediction W and the load that is being considered for admission $R(k-1)$. It then yields $L(k)$ which is the admissible load.

Theorem 2. *The proposed energy management algorithm is optimal when the window size W is equal to the simulation run length and when the prediction error goes to zero.*

Proof. When the window size is equal to the simulation run, this implies that we are directly solving the optimal offline two-fold optimization and that the optimality achieved is solely bounded by the prediction error. When the prediction error tends to zero, the optimal solution will be realized. □

With respect to generating meteorological forecasts, the simplest scheme is when the AP accesses online weather forecasts directly from available online databases, in this case, the AP would access them using the infrastructure directly without performing any processing for the forecasting. If the AP does not have access to online databases, then there are several ways of performing the forecasting, the AP could perform the forecasting in a stand-alone fashion without accessing any external data. In this case it could rely on prediction coefficients that are pre-programmed or generated on-the-fly. The pre-programmed coefficients could be generated from historical data available. The dynamically

updated coefficients are generated based on the localized weather data being collected by the AP over a statistically sufficient period of time preceding the prediction period. The coefficients could also be generated by combining the pre-programmed coefficients and the dynamically updated ones hence making use of the historical and current data at the same time. Therefore, the hybrid method would combine publicly available forecasted data with locally measured data from the mesh node. In this case the forecasted data would represent the long term trends and averages while the AP would provide adaptive refinement based on actual conditions at its spatial location. In the following section, we present our proposed solar insolation forecasting algorithm, this algorithm will be shown in subsequent sections to provide sufficiently accurate results for the PBEMC controller.

5.6 Solar Insolation Forecasting Model (SIFM)

Motivated by our previous discussion, it is clear that there is a need for accurate weather predictions in order to improve the performance of the energy management algorithms. For most geographic locations, there is a wealth of available historical data. This data can be used in conjunction with local measurements by the AP in order to generate forecasts that are accurate enough for the system to achieve excellent performance in terms of CD and outage performance. In this section we discuss our proposed prediction algorithm that achieves this goal. The proposed algorithm is based on a Minimum Mean Square Error

(MMSE) criterion. [2]

These techniques are only applied to the hours when there is expected solar insolation, since the night hours are known deterministically based on astronomical calculations. Therefore, we aim to predict the "non-dark" hours. As mentioned in [69] the solar insolation will exhibit diurnal and seasonal periodicity and hence we need to make use of the available literature that deals with predicting cyclostationary signals. In the following section, we show how we made use of the work in [51] in order to calculate the offline initial coefficients.

As explained in [51] there is a need to have a prediction coefficient for every hour of the day, in our case we also need a different set of coefficients for every day of the year due to the diurnal and seasonal periodicity of the solar insolation data. If the solar insolation to be predicted at hour m is $x(m+1)$ with a window of prediction L, by assuming a linear predictor we can write that

$$\hat{x}(m+1) = \sum_{i=m-L+1}^{m} \alpha_i x(i) \tag{5.30}$$

where $\hat{x}(m+1)$ is the predicted signal. Therefore, the error between the predicted signal and the real one will be:

$$E(m+1) = x(m+1) - \sum_{i=m-L+1}^{m} \alpha_i x(i) \tag{5.31}$$

Assuming that we wish to minimize the mean of the square of the error and thus taking the partial derivative with respect to α and equating to zero, we

[2] I would like to thank Dr. Ramy Gohary for his assistance with the formulation of the prediction equations.

get the following expression:

$$\alpha = (E\{XX^T\})^{-1}E\{x(m+1)X\} \tag{5.32}$$

where:

$$\alpha = \{\alpha_1, \alpha_2, \ldots \alpha_m\} \tag{5.33}$$

$$X = \{x_1, x_2, \ldots x_m\} \tag{5.34}$$

We notice that these equations represent the predictive version of the Wiener-Hopf filter equations. This formulation requires that the value of $x[m+1]$ should be known in advance, therefore we can only make use of the above equations to generate the values of α for every hour of the year knowing that the yearly stationarity from year to year can be used in order to predict the hours in the year in question.

Now, the $E\{\cdot\}$ operation shown in the above equations is transformed into an ensemble operation. This ensemble will be done over the historical data available if it spans several years back. On the other hand, if this is not available, then the AP can make use of the locally collected weather data for the corresponding hours over the past days on record. After conducting many experiments, our simulations have shown that using time or historical averaging for the calculation of the coefficients yields almost identical results in terms of error performance. [3]

[3]It is important to note that the number of data samples used must be at least equal to the window size L in order to regulate the rank of the matrix. In order to increase the smoothness of the data, we can also consider data from the days surrounding the day in question since the daily variations are expected to be minimal.

While there are several criteria for the error performance such as those shown in [56], we chose the simple mean error criterion since it was found to generate the most significant results for our application. We also notice that this is the error in non-dark hours, and that the night hours will have zero error since they are perfectly predictable. Using smaller window sizes will improve the accuracy of the predictions due to high correlations, however they will make the job of predicting the $m + k^{th}$ sample harder.

In order to predict multiple hours in advance, the methodology we adopt is as follows. We assume that we only need to predict the next non-dark hours only since the dark hours are known beforehand. Our technique relies on extending the approach presented by using the Wiener Hopf Equations for predictions beyond the one step such as $X(m+2)\ldots$ etc., each hour will be predicted separately to avoid error accumulations.

In the following section, we present a discussion of the mathematical performance bounds in addition to an evaluation of the performance of the proposed algorithm.

5.7 Results

In this section we present our performance analysis results in addition to a discussion of the results. We begin by presenting a discussion of the offline bound to verify the accuracy of the proposed linear approximations. This is followed by an in depth analysis of the different characteristics of the PBEMC algorithm in conjunction with the SIFM model for insolation prediction. Finally we conclude this section by comparing the performance of the On/Off

P_{Out}	$\mathbf{B}_{max}$	S_{pn}
10^{-2}	20.0	31.6
10^{-3}	30.1	38.0
10^{-4}	40.6	38.0

Table 5.1: Example Optimum Price Panel/Battery Configurations for Different Load Profiles, Toronto, Canada.

controller to the PBEMC algorithm.

5.7.1 Offline Bound

For the off-line optimization problem, the cvx [57] and the Matlab linprog toolboxes were used to generate the following results. Both tools were found to achieve the same results. In the following, we first show a sample comparison of the output of the offline optimization (OOC) with that of the No Control Lower Bound (NCLB) on capacity deficit. The case when no control action is applied to the system (No Control case) has been shown independently by the work in [49], and [53] to be a lower bound on CD. The only condition for this bound to hold is that the reward for accepting requests for all time instances is the same. The presented results are typical of what we have found in that the computed version achieves CD values very close to the lower bound.

We assume that the battery and panel have been designed for a nominal 2 watt power consumption load with an outage probability $P_{Out} = 10^{-2}$ as shown in Table 5.1. We then subject the node to a constant load power that is higher

than its design value by a factor of C_{Excess}, with $\mathbf{B}_{outage} = 0.1067$, $\mathcal{F}(\mathbf{U}_{min}) = 0.1$ watts. The system was then simulated for 3000 hours using meteorological data for the city of Toronto. Figure 5.3 shows a sample comparison of the offline optimizer (OOC) results to the lower bound. We can see that the CD results are indistinguishable for the two cases. For example, the maximum deviation of the bound for the $P_{Out} = 10^{-2}$ case is about 1.9%. Since the OOC output has generated a zero outage solution and CD is so close to the theoretical lower bound, it is clear that it is very close to an optimal traffic control. However, although the result is near optimal, it is not necessarily causal since it is based on an offline optimization. However this result is significant in that it can be used as a bound for any proposed practical algorithm. In the next section we propose a traffic control approach that makes use of historical weather data and/or predicted weather data over a finite time horizon.

Throughout the remainder of this section we assume the following default parameters that are shown in Table 5.2.

In the folllowing we provide a discussion of the selection of the battery threshold value $\mathcal{L}_{th}(k)$.

5.7.2 Optimizing the Value of $\mathcal{L}_{th}(k)$

In this section, we present a discussion of the selection of the battery threshold used by the PBEMC algorithm.

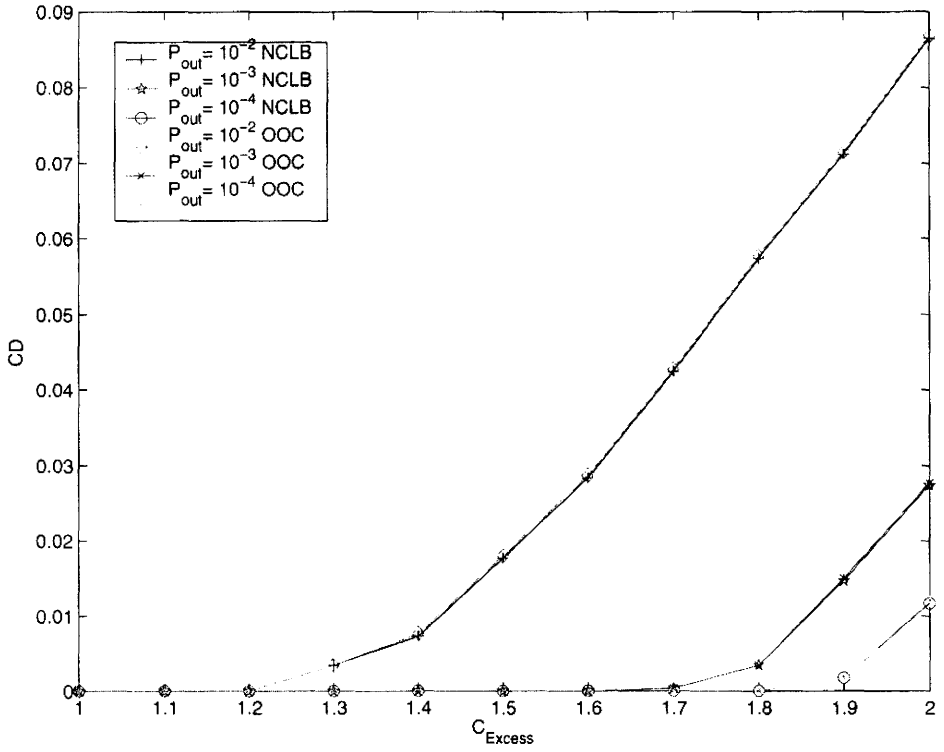

Figure 5.3: OOC versus NCLB

Optimizing the Value of $\mathcal{L}_{th}$ Theoretically

Since the proposed energy management algorithm relies on the battery threshold sequence $\mathbf{L}_{th}(k)$, in this section we discuss how to obtain the optimal value of this threshold which acts as a *target* of the control action. Any proposed algorithm seeks to minimize the P_{Out} and to distribute the CD fairly when compared to the off-line bounds. Therefore, the optimal value for $\mathbf{L}_{th}(k)$ needs to be found by solving the following optimization problem which assumes full knowledge of the load and the solar insolation beforehand. This can be written as follows.

Parameter	Value
Simulation Run	250 hours
City	Toronto
Year	1990
P_{Out}	0
Battery	20 Ah
Panel	31.6 W
$\mathcal{F}(\mathbf{U}_{min})$	1 watt
Nominal Power	2.76 watts

Table 5.2: Parameters Used in Generating Results

$$\min_{\mathbf{L}_{th}(k)} \sum_{k=0}^{K_{max}} \mathcal{E}_{def}(k) - \mathcal{E}_{defmin}, \tag{5.35}$$

such that

$$\mathcal{E}_{def}(k) = \mathcal{L}(k) - \mathcal{E}_a(k), \tag{5.36}$$

$$\mathcal{B}(k) = \min\{\max[\mathcal{B}(k-1) + \mathcal{E}_{panel}(k) - \mathcal{E}_a(k), \mathbf{B}_{outage}], \mathbf{B}_{max}\}, \tag{5.37}$$

$$Pr\{\bigcap_k (\mathcal{B}(k) > \mathbf{B}_{outage})\} \geq 1 - P_{Out}, \tag{5.38}$$

and

$$\mathcal{E}_a(k) = \Omega(L_{th}, \mathbf{U}_{min}, \ldots) \tag{5.39}$$

$$\mathcal{E}_a(k) \geq \mathcal{F}(\mathbf{U}_{min}). \tag{5.40}$$

here $\Omega(\cdot)$ represents the control action used by the algorithm to avoid outages and minimize the CD. In addition, $\mathcal{E}_{defmin}$ is the minimum achievable CD. Due

to the difficulty involved with solving the above optimization problem because of the non-linear nature of the controller action, we propose a simulation-based approach in order to obtain the optimal values. The algorithm is summarized in Algorithm 3.

Assuming a given year of historical data i and starting from a given time k, the system is accurately simulated by implementing Equation 3.1. The simulation is performed using historical data for a given year i for a load equal to the critical base load $\mathcal{F}(\mathbf{U}_{min})$ till the end of the simulation run K_{Max}. Initially, $\mathbf{L}_{th}(k,i)$ is chosen to be zero and the initial battery charge for each simulation is always chosen to be the current $\mathbf{L}_{th}(k,i)$, if the system goes into outage meaning that $B(\cdot,i) < \mathbf{B}_{outage}$, then $\mathbf{L}_{th}(k,i)$ is increased by an arbitrary value ϵ. This is repeated until the lowest value of $\mathbf{L}_{th}(k,i)$ is found that guarantees no outage.

This algorithm is repeated for different years on record. Therefore, this will result in an array of values of $\mathbf{L}_{th}(k,i)$ whose size will be equal to the number of years on record i. The value of $\mathbf{L}_{th}(k)$ can then be chosen by averaging it over the array or by choosing the maximum value as a conservative approach. The value of $\mathbf{L}_{th}(k)$ must be chosen carefully, since too high of a value will lead to increased capacity deficits. It is also worth noting that increasing $\mathbf{U}_{min}$ will lead to an increase in $\mathbf{L}_{th}(k)$.

This procedure is performed offline once over the historical data, and our experiences have found that the execution time is very reasonable and depends on the number of years under consideration and the total time window being examined. For example, if we assume that the procedure will be performed

Algorithm 3 Algorithm to Evaluate $\mathbf{L}_{th}(k,i)$

$i = Year$ $\mathbf{L}_{th}(k,i) = 0$
while $B(\cdot,i) < \mathbf{B}_{outage}$ **do**
  $B(k,i) = \mathbf{L}_{th}(k,i)$
  for $j = k+1$ to K_{Max} **do**
    $\mathcal{B}(j,i) = \min\{\max[\mathcal{B}(j-1,i) + \mathcal{E}_{panel}(j-1,i) - \mathcal{F}(\mathbf{U}_{min}), \mathbf{B}_{outage}], \mathbf{B}_{max}\}$
  end for
  $\mathbf{L}_{th}(k,i) = \mathbf{L}_{th}(k,i) + \epsilon$
end while

for a window length of 250, then the procedure is repeated 250 times for every year of historical data. It is worth noting that some adjustments to the above procedure are necessary due to the finite window under consideration, meaning that in practice the simulation should be performed over a longer time window.

Evaluation of Different $\mathbf{L}_{th}(k)$ Selection Strategies

We now evaluate the use of different strategies for choosing $\mathbf{L}_{th}$. We assume a window size of 24, and three different strategies for evaluating $\mathbf{L}_{th}$. The first assumes the mean of $\mathbf{L}_{th}(k)$ for historical data, a fixed $\mathbf{L}_{th}$ that is calculated in the same way as the On/Off control threshold and finally, using a maximum value approach for historical data.

Figure 5.4 shows a comparison of the total CD for all three strategies. Clearly, the mean approach gives the best results since it is adaptive as opposed to the fixed approach, and it is less conservative than the maximum value approach.

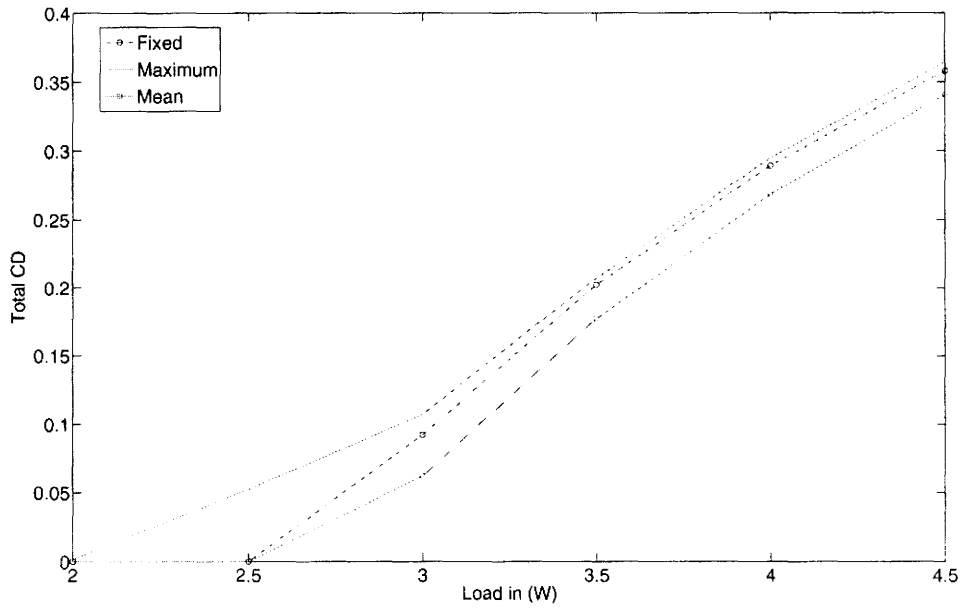

Figure 5.4: Comparison of Total CD for Different Values of L_{th}

5.7.3 Performance Analysis of PBEMC Algorithm

In this section we evaluate the performance of the proposed algorithm. We evaluate its performance for two sets of meteorological data, the first set is a non-causal data set (i.e., assuming zero prediction error) that will be used to establish bounds on performance. We refer to this as *bound* data within the results. The second one is the causal data set that uses predicted meteorological data in order to establish the algorithm performance practically and to show that it is only bounded by the error in prediction and not by the effect of using a finite window W. We refer to these as *Predict* data sets. We evaluate the results for window sizes of 6, 12, 24, and 36. To simplify the analysis of the results, throughout the following we assume a constant load for the duration of the timeline under consideration. The PBEMC algorithm as described in

section 5.5 does not take into account the requested load while performing the admissible load calculations. Therefore, the results shown here also apply for time-varying traffic requests.

We show results for different $\mathcal{F}(\mathbf{U}_{min})$ values, however the results for different values cannot be compared directly to each other since the value of CD is directly dependent on $\mathbf{U}_{min}$. We also assume that the value of $\mathbf{U}_{min}$ has already been mapped on to a power consumption value in watts. Throughout the following we show results only for the cases when outages have been eliminated.

Total CD

Table 5.3 shows the effect of overloading the system beyond its nominal value of operation on the values of the total CD for different window sizes. We show the results for the non-causal data sets. The no control bound values are also shown. We can see that the results are in agreement although there is a slight increase in total CD when the window size is increased. For example, the value of the total CD goes up from 0.33122 to 0.34092 when the window size increases from 6 to 36 hours. When compared to the offline control bound of 0.32566 this represents a maximum difference of 4.62 % which shows that the use of finite window sizes does not significantly affect the overall CD. Next, we analyze the effect of using the SIFM forecasting algorithm on the value of the total CD.

Figure 5.5 plots the increase in total CD that occurs when the system is subjected to different load powers that greatly exceed the nominal design value (2.76 W) and will lead to outage if no control is applied. The figure

$Load(W)$	$NCLB$	$CD_{W=6}(bound)$	$CD_{W=12}(bound)$	$CD_{W=24}(bound)$	$CD_{W=36}(bound)$
2	0.0000	0.0000	0.0000	0.0000	0.0000
2.5	0.0000	0.0000	0.0000	0.0024	0.0000
3	0.0184	0.0274	0.0378	0.04545	0.0491
3.5	0.1501	0.1573	0.1650	0.1695	0.1709
4	0.2488	0.2551	0.2616	0.2654	0.2665
4.5	0.3256	0.3312	0.3369	0.3401	0.3409

Table 5.3: Comparison of Total CD for Different Window Sizes for the PBEMC Controller

also compares the performance of the algorithm when the solar insolation data is forecasted using the SIFM algorithm presented in the previous section for window sizes of 6 and 24 and the results are compared to the non-causal bounds. As seen, the error in total CD is nearly zero when the window size is small ($W = 6$). This is due to the fact that the error in prediction for the SIFM is reduced for smaller window sizes. For example, at 5 watts the results using both data sets are identical and equal to 0.2551. When the window sizes increases, the error in prediction begins to slightly influence the results, this is especially true at low load values. However, at higher overload levels the total CD is similar meaning that the quality of the predictions is less relevant since the system is severely overloaded and is being constantly depleted. For example, at 3.5 watts load the CD for the $W = 24$ case increases from 0.1695 to 0.1772 (4.5 %) due to the prediction error, however at 4 watts it only increases from 0.2654 to 0.2684 (1.13 %).

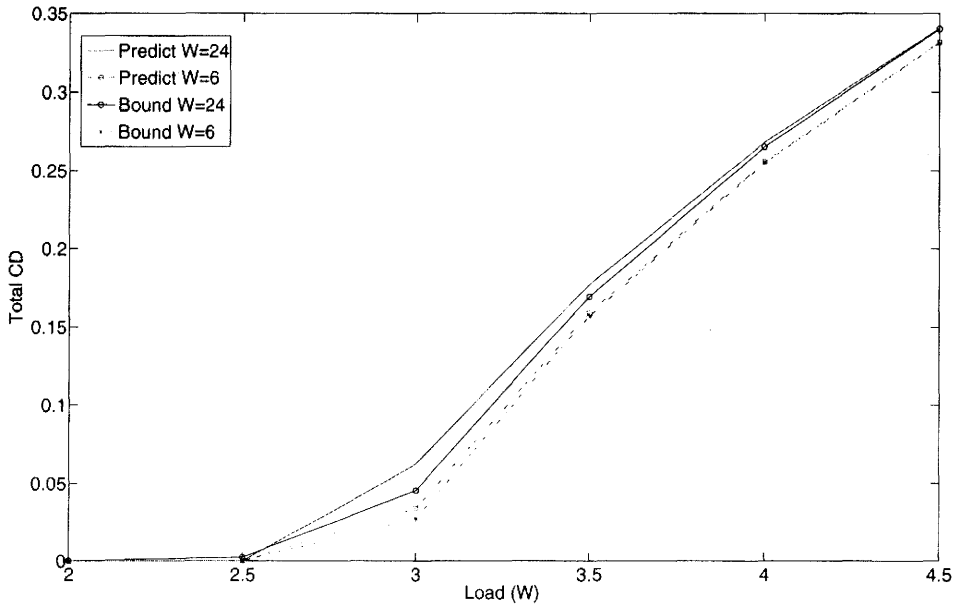

Figure 5.5: Total CD for Different Window Sizes

Table 5.4 shows a comparison of the total CD for window sizes of 24 and 12 when compared to the NCLB for a value of $\mathcal{F}(\mathbf{U}_{min}) = 1.5$ watts. We can make similar conclusions as those made for the $\mathcal{F}(\mathbf{U}_{min}) = 1$ watt case. The values of the total CD are identical for smaller window sizes and diverge slightly for larger window sizes although at higher load levels, the performance is almost identical.

To confirm our observations, we also show results in Table 5.5 for $\mathcal{F}(\mathbf{U}_{min}) = 0.5$ watts and $W = 6$ and $W = 24$. The same observations can be made again, we observe that the error is reduced when compared to higher values of $\mathcal{F}(\mathbf{U}_{min})$ since there are less constraints on the minimum system energy expenditure.

$Load(W)$	$NCLB$	$CD_{W=12}(bound)$	$CD_{W=12}$	$CD_{W=24}(bound)$	$CD_{W=24}$
2	0.0000	0.0000	0.0000	0.0000	0.0000
2.5	0.0000	0.0072	0.0115	0.0030	0.0248
3	0.0185	0.0519	0.0679	0.0641	0.0856
3.5	0.1501	0.1720	0.1746	0.1824	0.1905
4	0.2489	0.2677	0.2679	0.2761	0.2768
4.5	0.3257	0.3423	0.3411	0.3496	0.3454

Table 5.4: Comparison of Total CD for Different Window Sizes for the PBEMC Controller ($\mathcal{F}(\mathbf{U}_{min}) = 1.5$ watts)

$Load(W)$	$NCLB$	$CD_{W=6}(bound)$	$CD_{W=6}$	$CD_{W=24}(bound)$	$CD_{W=24}$
2	0.0000	0.0000	0.0000	0.0000	0.0000
2.5	0.0000	0.0000	0.0000	0.0000	0.0000
3	0.0185	0.0185	0.0185	0.0350	0.0466
3.5	0.1501	0.1501	0.1501	0.1591	0.1644
4	0.2489	0.2489	0.2489	0.2602	0.2596
4.5	0.3257	0.3257	0.3257	0.3326	0.3349

Table 5.5: Comparison of Total CD for Different Window Sizes for the PBEMC Controller ($\mathcal{F}(\mathbf{U}_{min}) = 0.5$ watts)

Conditional Average CD

Figure 5.6 shows the conditional average value of the CD for different values of load power and different window sizes. The optimal offline controller (OOC) will have the lowest possible value since it will distribute the capacity deficit in an optimal manner over the entire timeline. The larger window sizes will also have better values of average CD especially when the quality of the prediction increases. On the other hand, the NCLB has a much higher average CD since there is no control action and hence the capacity deficit temporal distribution is more abrupt. For example, the maximum value of the average CD is more than 0.8 for the NCLB while it is at 0.38 and 0.5 for the OOC and PBEMC $W = 24$ (bound) respectively. This represents a significant improvement in the average conditional CD. We also notice that none of the algorithms introduced CD when the system was capable of sustaining a load, such as in the case of the 2 watts load.

Table 5.6 shows the conditional average of the CD for $\mathcal{F}(\mathbf{U}_{min}) = 1.5$ watts. We again notice that there is a relative error between the predicted and bound values. Therefore, we can conclude that the error in prediction slightly reduces the smoothness of the controller action. The smaller window size results in higher values of average conditional CD which is an indication of the abruptness of the algorithm performance in this case.

Table 5.7 shows the conditional average of the CD for $\mathcal{F}(\mathbf{U}_{min}) = 0.5$ watts. We notice that the conditional average CD is higher in this case because the value of $\mathbf{U}_{min}$ has decreased meaning that the maximum permissible CD has also been increased. For example, for $W = 24$ the average CD increases from

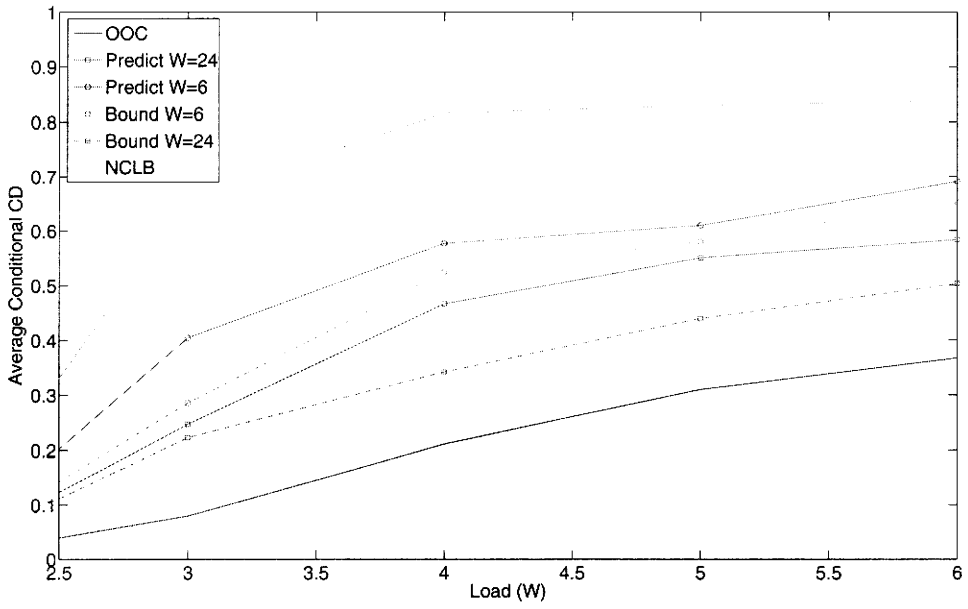

Figure 5.6: Conditional Average CD for Different Window Sizes

0.5330 to 0.5814 when $\mathcal{F}(\mathbf{U}_{min})$ drops from 1.5 to 0.5 watts when the load on the system is 4.5 watts.

One point that we must draw attention to is that if the total value of the resultant CD is significantly different between two algorithms, then comparing the average conditional CD values directly could lead to false results since they are conditioned on a different total observed CD. Therefore, significant conclusions about the relative performance of any two algorithms can only be made when the total CD is comparable. This effect has been taken into account while comparing different algorithms in this thesis and is justified by the very small error in total CD. We also note that the only exception to the above statement is if both controllers are active for a comparable number of times. In that case, if the one with the higher total CD still achieves a lower average

$Load(W)$	$CD_{W=12}(bound)$	$CD_{W=12}$	$CD_{W=24}(bound)$	$CD_{W=24}$
2	0.0000	0.0000	0.0000	0.0000
2.5	0.1628	0.2051	0.0672	0.2216
3	0.4474	0.4041	0.3641	0.3450
3.5	0.3773	0.4280	0.3378	0.4215
4	0.4921	0.5274	0.4133	0.5242
4.5	0.5063	0.5610	0.4751	0.5330

Table 5.6: Comparison of Conditional Average of CD for Different Window Sizes for the PBEMC Controller ($\mathcal{F}(\mathbf{U}_{min}) = 1.5$ watts)

$Load(W)$	$CD_{W=6}(bound)$	$CD_{W=6}$	$CD_{W=24}(bound)$	$CD_{W=24}$
2	0.0000	0.0000	0.0000	0.0000
2.5	0.0000	0.0000	0.0000	0.0000
3	0.3302	0.2890	0.2731	0.2709
3.5	0.5005	0.5213	0.3520	0.4194
4	0.5982	0.6285	0.4581	0.5277
4.5	0.6729	0.6900	0.5165	0.5814

Table 5.7: Comparison of Conditional Average of CD for Different Window Sizes for the PBEMC Controller ($\mathcal{F}(\mathbf{U}_{min}) = 0.5$ watts)

CD, then it still outperforms the one with the lower CD, since the temporal distribution in this case will be fairer. Conversely, one can argue that if two algorithms have the same total CD, then the one which activates its controller more frequently can be considered fairer.

Maximum CD

Figure 5.7 shows the maximum capacity deficit level throughout the simulation run. The OOC has the minimum value while NCLB has the highest value. This is an indication of how well the max-min objective is being achieved. We notice that at high levels of overloading, the maximum value achieved by the PBEMC algorithm is bounded by $\mathbf{U}_{min}$ since there will be times when the system is so overloaded it will only be able to admit $\mathcal{F}(\mathbf{U}_{min})$ load.

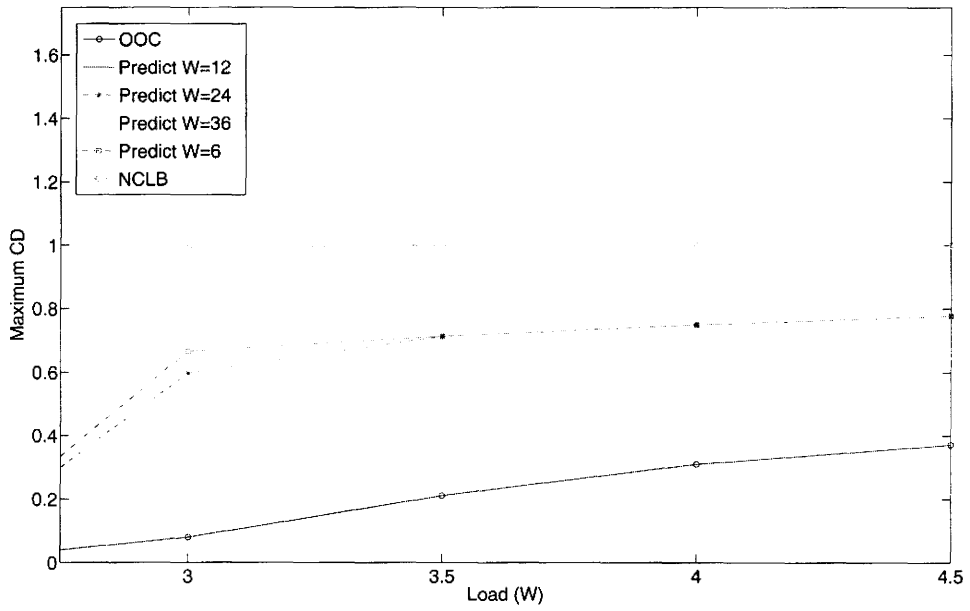

Figure 5.7: Maximum CD for Different Window Sizes

$Load(W)$	$CD_{W=12}(bound)$	$CD_{W=12}$	$CD_{W=24}(bound)$	$CD_{W=24}$
2	0.0000	0.0000	0.0000	0.0000
2.5	0.3033	0.4000	0.1245	0.4000
3	0.5000	0.5000	0.5000	0.5000
3.5	0.5714	0.5714	0.5714	0.5714
4	0.6250	0.6250	0.6250	0.6250
4.5	0.6667	0.6667	0.6667	0.6667

Table 5.8: Comparison of Maximum Value of CD for $\mathcal{F}(\mathbf{U}_{min}) = 1.5$ watts

Table 5.8 shows the results for maximum CD case for $\mathcal{F}(\mathbf{U}_{min}) = 1.5$ watts. We notice that at high load values, the maximum CD will be the same since the system must provide a minimum value of $\mathbf{U}_{min}$. Table 5.9 shows the results for maximum CD for $\mathcal{F}(\mathbf{U}_{min}) = 0.5$ watts which yield similar values.

Conditional Standard Deviation of CD

Table 5.10 shows the conditional standard deviation for different window sizes for $\mathcal{F}(\mathbf{U}_{min}) = 1$ watt. The OOC has a standard deviation of zero since it will always offer the same load over the entire timeline. We can see that the increase in window size leads to an increase in conditional standard deviation for the predicted data sets when compared to the bound. This means that there is an increase in the coefficient of variation caused by the error in prediction.

$Load(W)$	$CD_{W=6}(bound)$	$CD_{W=6}$	$CD_{W=24}(bound)$	$CD_{W=24}$
2	0.0000	0.0000	0.0000	0.0000
2.5	0.0000	0.0000	0.0000	0.0000
3	0.9460	0.8073	0.4687	0.5876
3.5	0.8571	0.8571	0.7581	0.8160
4	0.8750	0.8750	0.8750	0.8750
4.5	0.8889	0.8889	0.8889	0.8889

Table 5.9: Comparison of Maximum Value of CD for $\mathcal{F}(\mathbf{U}_{min}) = 0.5$ watts

$Load(W)$	OOC	$CD_{W=24}(bound)$	$CD_{W=24}$	$CD_{W=6}(bound)$	$CD_{W=6}$
2	0.0000	0.0000	0.0000	0.0000	0.0000
2.5	0.0000	0.0000	0.0000	0.0000	0.0000
3	0.0000	0.1607	0.1546	0.1777	0.2614
3.5	0.0000	0.1866	0.1801	0.22214	0.2284
4	0.0000	0.1686	0.2238	0.1750	0.1665
4.5	0.0011	0.1810	0.2410	0.1940	0.1708

Table 5.10: Comparison of Conditional Standard Deviation of CD for Different Window Sizes for the PBEMC Controller

5.7.4 Comparison to On/Off Controller

The results in [49] have shown that the On/Off controller can eliminate outage by judiciously choosing $\mathbf{L}_{thonoff}$ while achieving the bound on total CD. However, as the authors noted, their results have shown that there is an abrupt change in the offered service, in this section we compare the proposed algorithm to the On/Off controller in terms of the temporal smoothness of the offered load.

Table 5.11, shows the conditional average of the capacity deficit versus the load power as previously explained. The conditional average of the On/Off controller can be calculated analytically for fixed load requests, since it only depends on the load requested and the value of $\mathcal{F}(\mathbf{U}_{min})$. The value of the average conditional CD is high in the case of the On/Off controller and is very close to the NCLB case. This is especially true for lower load values since the PBEMC algorithm will have some flexibility in terms of redistributing the total CD. For example, at a load of 3 watts which is only slightly above the nominal design load, the value for the On/Off case is 0.66667 while it is only 0.2228 and 0.2467 for the PBEMC using $W = 24$ for the bound and the predicted data respectively. This represents an increase of almost 180 % in average CD. Tables 5.12, and 5.13 also show the maximum deviation and conditional standard deviation respectively. From the results we can conclude that the proposed algorithm improves the temporal smoothness substantially and reduces the abruptness when compared to the On/Off controller. We see that the average CD of the On/Off control is very close to the NCLB. We also notice that the maximum value of the CD is higher than the PBEMC algorithm

$Load(W)$	$NCLB$	On/Off	$CD_{W=24}(Bound)$	$CD_{W=24}$	OOC
2	0.0000	0.0000	0.0000	0.0000	0.0000
2.5	0.0000	0.0000	0.0000	0.0000	0.0000
3	0.6605	0.6667	0.2228	0.24667	0.0795
3.5	0.8159	0.7143	0.3418	0.4663	0.2109
4	0.8296	0.7500	0.4394	0.5499	0.3096
4.5	0.8393	0.7778	0.5031	0.5834	0.3671

Table 5.11: Comparison of Conditional Average of CD for On/Off Controller

until the overloading factor increases substantially. Finally, we notice that the coefficient of variation of the On/Off controller is zero since it only offers one value of load when it is active.

5.7.5 Time Varying Example

In this section, we show results for a time-varying load sequence that varies on an hourly basis. We assume the same traffic sequence as that shown in [32]. We assume that the peak of the sequence is normalized to one watt and that the sequence has an average value of 0.5311 watts over the time run under consideration. We also assume $\mathcal{F}(\mathbf{U}_{min}) = 0.5$ watt and $W = 24$. In the following we show the results generated when overloading the system uniformly. This is achieved by multiplying the hourly value of the load time sequence by a constant load factor.

Table 5.14 shows a comparison of the total CD for the PBEMC algorithm for bound and causal data to the NCLB and the On/Off controller. We observe

$Load(W)$	OOC	$NCLB$	On/Off	$CD_{W=36}$
2	0.0000	0.0000	0.0000	0.0000
2.5	0.0000	0.0000	0.0000	0.0000
3	0.0795	0.99121	0.6667	0.6667
3.5	0.2109	1.0000	0.7143	0.7143
4	0.3096	1.0000	0.7500	0.7500
4.5	0.3710	1.0000	0.7778	0.7778

Table 5.12: Comparison of Maximum Deviation of CD for On/Off Controller

$Load(W)$	OOC	$NCLB$	On/Off	$CD_{W=36}$
2	0.0000	0.0000	0.0000	0.0000
2.5	0.0000	0.0000	0.0000	0.0201
3	0.0000	0.3214	0.0000	0.1797
3.5	0.0000	0.3025	0.0000	0.1886
4	0.0000	0.2877	0.0000	0.2226
4.5	0.0011	0.2676	0.0000	0.2503

Table 5.13: Comparison of Standard Deviation of CD for On/Off Controller

$LoadFactor$	$NCLB$	On/Off	$CD_{W=24}(bound)$	$CD_{W=24}$
1	0.0000	0.0000	0.0000	0.0000
2	0.0000	0.0000	0.0000	0.0000
3	0.0000	0.0000	0.0000	0.0000
4	0.0000	0.0000	0.0000	0.0000
5	0.0000	0.0000	0.0034	0.0029
6	0.0718	0.1219	0.0834	0.0942
7	0.1957	0.2383	0.2042	0.2094
8	0.2887	0.3258	0.2961	0.2989
9	0.3609	0.3927	0.3675	0.3697

Table 5.14: Comparison of Total CD for the PBEMC Controller for Time-Varying Traffic

that the total CD for the On/Off controller is much higher than the bound (8.78 % for a load factor of 9). Again we see that the results for the PBEMC algorithm are in agreement with our previous observations. The difference between the bound and causal data is minimal (0.6 % for a load factor of 9) and both approach the NCLB.

Table 5.15 shows the average conditional CD. We compare the NCLB, OOC, On/Off and PBEMC with bound and causal data. As expected, the OOC again achieves the lowest value while the NCLB and On/Off controller will have significantly higher values. We notice that both the causal and bound data results are very close (9 % difference for a load factor of 9). In addition, we notice that both approach the value of the OOC limit while not achieving

$LoadFactor$	$NCLB$	On/Off	OOC	$CD_{W=24}(bound)$	$CD_{W=24}$
1	0.0000	0.0000	0.0000	0.0000	0.0000
2	0.0000	0.0000	0.0000	0.0000	0.0000
3	0.0000	0.0000	0.0000	0.0000	0.0000
4	0.0000	0.0000	0.0000	0.0000	0.0000
5	0.0000	0.0000	0.0000	0.0000	0.1952
6	0.7531	0.8196	0.1471	0.2931	0.3309
7	0.8510	0.8469	0.2835	0.3754	0.4631
8	0.8581	0.8648	0.3856	0.4528	0.5424
9	0.8381	0.8815	0.4650	0.5041	0.5550

Table 5.15: Comparison of Conditional Average CD for the PBEMC Controller for Time-Varying Traffic

it.

5.8 Conclusions

This chapter considered the use of traffic admission control for outage prevention in solar powered WLAN mesh nodes. We first formulated the traffic control objective as a non-linear control problem. An accurate Linear Programming (LP) approximation was then defined and solved based on an offline optimization where future solar insolation is known. This gives a bound on the performance of any real algorithm which was used to compare with a proposed traffic control scheme.

A traffic control algorithm was proposed whose operation uses dynamic access to publicly available meteorological data. We showed that the proposed algorithm eliminates node outage events completely in the case when the system is heavily overloaded beyond its nominal design value. The outage elimination came at the expense of an increase in the capacity deficit. However, the scheme's capacity deficit performed favorably when compared to the formulated offline and no-control bounds. The algorithm was also found to distribute the capacity deficit in a fair way that avoided abrupt changes in offered capacity. This demonstrates the effectiveness of traffic admission control as a tool for reducing outage for solar powered IEEE 802.11 WLAN mesh networks. In the following chapter we conclude this thesis.

Chapter 6

Conclusions

This thesis has focused on the resource allocation and design of energy sustainable wireless mesh networks.

In Chapter 3 we presented geographic provisioning results for solar and wind powered WLAN mesh nodes. A cost model was introduced which was used to optimize the hybrid provisioning of solar and wind powered WLAN mesh nodes. The model suggests that in certain geographic locations a hybrid wind/solar powered WLAN mesh node is the optimum cost configuration. The presented results compared various design alternatives including infrastructure power saving and non-power saving options.

As an example, for the city of Toronto our results suggest that the cost increases greatly with the load power. This example showed the importance of power-saving on the node cost. Our results also showed that for Toronto a hybrid solution is much more cost effective than a solar-only powered approach especially for high efficiency wind turbines. Our results have also seen that not all geographic locations will be able to make use of a hybrid mix of energy

sources. For example, locations such as Phoenix, AZ cannot make use of wind power to reduce cost due to the abundance of solar insolation. We have also shown that the temporal distribution of the power sources is of utmost importance when the node is being sized. Our results suggest that the short-term statistics are not sufficient in order to assess the optimal ratio of solar to wind power used in the system. The long-term and yearly statistics are much more important.

Our results and examples also showed that mesh AP power saving is highly beneficial since it reduces the allocated resources and hence the node cost. This is based on the observation that total cost is almost linearly proportional to the node load power consumption which may be greatly reduced by using power saving.

In Chapter 4 we considered the problem of cost-optimal solar powered node assignment in hybrid WLAN mesh networks. The problem formulation was found to be a binary mixed-integer non-linear problem that can be simplified into a binary mixed-integer quadratic problem. It was also shown that the problem is NP-hard in the most general case, and deployment results were shown using a branch and bound and shortest path heuristic. Our results show that there is a significant improvement in cost that can be obtained using the proposed algorithms, and that the branch and bound approach achieves the optimum assignment for several network examples that we considered.

Finally, in Chapter 5 we considered the use of traffic admission control for outage prevention in solar powered WLAN mesh nodes. We first formulated the traffic control objective as a non-linear control problem. An accurate Linear

Programming (LP) approximation was then defined and solved based on an offline optimization where future solar insolation is known. This gives a bound on the performance of any real algorithm which was used to compare with a proposed traffic control scheme.

A traffic control algorithm was then proposed whose operation uses dynamic access to publicly available meteorological data. We showed that the proposed algorithm eliminates node outage events completely in the case when the system is heavily overloaded beyond its nominal design value. The outage elimination came at the expense of an increase in the capacity deficit. However, the scheme's capacity deficit performed favorably when compared to the formulated offline and no-control bounds. The algorithm was also found to distribute the capacity deficit in a fair way that avoided abrupt changes in offered capacity. The work in this chapter demonstrated the value of traffic admission control as a tool for reducing outage for solar powered IEEE 802.11 WLAN mesh networks.

This work has a few limitations that can be addressed in future work. For example, in Chapter 3, the wind turbine cost models used can be further developed to include realistic values once wind turbines operating at this lower power level are developed. The assumptions in Chapter 4 can be modified in order to consider other practical problems, for example, the assumption of splittable flows could be modified to consider the case of unsplittable flows. In Chapter 5, the energy management formulation could be expanded to include other fairness definitions, and new fairness metrics can be developed.

This work can also be extended in several ways. A direct extension of this work would be to consider the node placement problem for cases when the objective is to select the optimum subset of solar-powered node deployments when a large number of candidate locations exists. Another interesting problem would be to examine the effect of using different routing algorithms on the initial resource allocation of a node. Energy-aware routing is expected to be able to reduce the initial resource allocation. However, analyzing this problem would not be straightforward since there is mutual dependency between the resource allocation and the routing in this case. In addition, the energy management algorithm proposed in this thesis assumes that each node in the network sheds load independently. Finally, this work can also be extended so that the energy management is performed in a distributed manner in order to enhance fairness.

Bibliography

[1] "Wind Turbine Design Cost and Scaling Model," *Technical Report NREL/TP-500-40566*, December 2006.

[2] http://www.itfacts.biz, 2008.

[3] http://www.hymini.com/, 2008.

[4] http://www.windlabjunior.com/wljrpurchase.html, 2008.

[5] http://web-japan.org/nipponia/nipponia28/en/feature/feature07.html, 2008.

[6] http://www.motorwavegroup.com/new/motorwind/index.html, 2008.

[7] http://www.humdingerwind.com/, 2008.

[8] "BOSCO." http://www.bosco-uganda.org/, 2008.

[9] "Drop Zone Networks." http://www.ezoresystems.com/, 2008.

[10] "Green WiFi." http://www.green-wifi.org/, 2008.

[11] "Intel Background on IEEE 802.11 Standard." http://www.intel.com/standards/case/case_802_11.htm, 2008.

[12] "Intelligraphics Background on IEEE 802.11 Standard." http://www.intelligraphics.com/articles/80211_article.html, 2008.

[13] "Inveneo." http://www.inveneo.org/, 2008.

[14] "IR Data Corporation." http://www.irdatacorp.com/, 2008.

[15] "Lumin Innovation Products Inc.." http://www.luminip.com/, 2008.

[16] "Meraki." http://www.meraki.com/, 2008.

[17] "Mini Windmills Power Wireless Networks." http://www.nature.com/news/2005/051108/full/news051107-5.html, 2008.

[18] "ParkWiFi Project." http://www.parkwifi.com/, 2008.

[19] "Wikipedia Article on IEEE 802.11 WLANs." http://en.wikipedia.org/wiki/IEEE_802.11, 2008.

[20] "Wikipedia Article on WMNs." http://en.wikipedia.org/wiki/Wireless_mesh_network, 2008.

[21] M. A. Abdelrahman and M. A. Elhadidy, "Comparison of Calculated and Measured Values of Total Radiation on Tilted Surfaces in Dhahran, Saudi Arabia," *Solar Energy*, vol. 37, pp. 239–243, 1986.

[22] I. Abouzahr and R. Ramakumar, "Loss of Power Supply Probability of Stand-Alone Photovoltaic Systems: A Closed Form Solution Approach," *Energy Conversion, IEEE Transactions on*, vol. 6, no. 1, pp. 1–11, 1991.

[23] K. Akkaya and M. Younis, "A Survey of Routing Protocols in Wireless Sensor Networks," *Elsevier Ad Hoc Network Journal, Vol. 3/3 pp. 325-349*, 2005.

[24] R. Akl and S. Park, "Optimal Access Point Selection and Traffic Allocation in IEEE 802.11 Networks," vol. 8, pp. 75–79, July 2005.

[25] I. Akyildiz and X. Wang, "A Survey on Wireless Mesh Networks," in *IEEE Communications Magazine*, vol. 43, pp. 23–30, September 2005.

[26] J. N. Al-Karaki and A. Kamal, "Routing Techniques in Wireless Sensor Networks: A Survey," *Wireless Communications, IEEE Volume: 11, Issue: 6, pp. 6- 28*, December 2004.

[27] G. Badawy, A. Sayegh, and T. Todd, "Solar Powered WLAN Mesh Network Provisioning for Temporary Deployments," *IEEE Wireless Communications and Networking Conference (WCNC)*, pp. 2271–2276, April 2008.

[28] A. Bagul, Z. Salameh, and B. Borowy, "Sizing of a Stand-Alone Hybrid Wind-Photovoltaic System Using a Three-Event Probability Density Approximation," *Solar Energy*, vol. 56, no. 4, pp. 323–335(13), April 1996.

[29] P. Baikie, M. Gillibrand, and K. Peters, "The Effect of Temperature and Current Density on the Capacity of Lead-Acid Battery Plates," *Electrochimica Acta*, vol. 17, pp. 839–844, 1972.

[30] A. Bemporad, "Hybrid Toolbox - User's Guide," 2004. http://www.dii.unisi.it/hybrid/toolbox.

[31] B. Bing, "Emerging Technologies in Wireless LANs: Theory, Design, Deployment," *Tutorial Presented at IEEE WCNC*, April 2008.

[32] D. Blinn, T. Henderson, and D. Kotz, "Analysis of a Wi-Fi Hotspot Network," *Proceedings of the International Workshop on Wireless Traffic Measurements and Modeling (WiTMeMo '05)*, June 2005.

[33] A. Bogdanov, E. Maneva, and S. Riesenfeld, "Power-Aware Base Station Positioning for Sensor Networks.," 2004.

[34] J. Boland, L. Scott, and M. Luther, "Modelling the Diffuse Fraction of Global Solar Radiation on a Horizontal Surface," *Environmetrics*, vol. 12, pp. 103–116, 2001.

[35] B. S. Borowy and Z. M. Salameh, "Optimum Photovoltaic Array Size for a Hybrid Wind/PV System," *Energy Conversion, IEEE Transactions on*, vol. 9, no. 3, pp. 482–488, 1994.

[36] M. Bouzguenda and S. Rahman, "Energy Management Onboard the Space Station-a Rule-Based Approach," *Aerospace and Electronic Systems, IEEE Transactions on*, vol. 27, no. 2, pp. 302–310, 1991.

[37] S. Boyd and L. Vandenberghe, *Convex Optimization*. New York, NY, USA: Cambridge University Press, 2004.

[38] L. L. Bucciarelli, "Estimating Loss-of Power Probabilities of Stand-Alone Photovoltaic Solar Energy Systems," *Solar Energy*, vol. 32, no. 2, pp. 205–209, 1984.

[39] L. L. Bucciarelli, "The Effect of Day-to-Day Correlation in Solar Radiation on the Probability of Loss of Power in a Stand-Alone Photovoltaic Energy System," *Solar Energy*, vol. 36, no. 1, pp. 11–14, 1986.

[40] J. R. C. Williams, " Evaluation of Photovoltaic Panels at the South Pole Station," *US Army Cold Regions Research and Engineering Laboratory Technical report ERDC/CRREL TR-00-4*, 2000.

[41] Canadian Wind Energy Association (CanWEA), "Cost Comparison for Small Wind Turbine Sizes ," *http://www.smallwindenergy.ca/en/Overview/Costs/CostComparison.html.*

[42] J. Chang and L. Tassiulas, "Energy Conserving Routing in Wireless Ad-hoc Networks," *INFOCOM 2000*, pp. 22–31, 2000.

[43] J. Chen, K. M. Sivalingam, P. Agrawal, and S. Kishore, "A Comparison of MAC Protocols for Wireless Local Networks based on Battery Power Consumption," in *Proceedings of IEEE INFOCOM'98*, vol. 1, pp. 150–157, 1998.

[44] N. Chen, J. Chen, and T. Rappaport, "Measured Traffic Statistics and Throughput of IEEE 802.11b Public WLAN Hotspots with Three Different Applications," *IEEE Transactions on Wireless Communications*, vol. 5, pp. 3296–3305, November 2006.

[45] Cisco Systems, "802.11n: The Next Generation of Wireless Performance," 2008.

[46] W. B. D. King, J. Kratochvil, "Temperature Coefficients for PV Modules and Arrays: Measurement Methods, Difficulties, and Results," *26th IEEE Photovolataic Specialists Conference*, September 1997.

[47] B. de Jager, "The Horizon in Predictive Energy Storage Control," *Proceedings of the 2004 American Control Conference*, vol. 1, pp. 662–676 vol.1, 2004.

[48] C. de Morais Cordeiro, S. Abhyankar, and D. P. Agrawal, "Reducing Power Consumption and Enhancing Performance by Direct Slave-to-Slave and Group Communication in Bluetooth WPANs," *Computer Networks*, vol. 45, no. 2, pp. 119–141, 2004.

[49] A. Farbod, "Design and Resource Allocation for Solar-Powered ESS Mesh Networks," Master's thesis, McMaster University, 1280 Main St. West, Hamilton, Ontario, Canada L8S 4K1, August 2005.

[50] S. Fashandi and T. D. Todd, "Real-Time Handoff in Solar/Battery Powered ESS Mesh Networks," in *16th International Symposium on Personal Indoor and Mobile Radio Communications (PIMRC'2005)*, August 2005.

[51] E. R. Ferrara and B. Widrow, "The Time-Sequenced Adaptive Filter," *IEEE Transactions on Acoustics, Speech, and Signal Processing*, June 1981.

[52] R. Fletcher and S. Leyffer, "Numerical Experience with Lower Bounds for MIQP Branch-And-Bound," *SIAM J. on Optimization*, vol. 8, no. 2, pp. 604–616, 1998.

[53] A. Fu, E. Modiano, and J. Tsitsiklis, "Optimal Energy Allocation and Admission Control for Communications Satellites," *IEEE/ACM Trans. Netw.*, vol. 11, no. 3, pp. 488–500, 2003.

[54] M. Galota, C. Glaßer, S. Reith, and H. Vollmer, "A Polynomial-Time Approximation Scheme for Base Station Positioning in UMTS Networks," pp. 52–59, 2001.

[55] M. Garey and D. Johnson, *Computers and Intractability; A Guide to the Theory of NP-Completeness*. New York, NY, USA: W. H. Freeman & Co., 1990.

[56] G. Giebel, "The State-Of-The-Art in Short Term Prediction of Wind Power: A Literature Overview," *ANEMOS Project*, 2003.

[57] M. Grant, S. Boyd, and Y. Ye, "CVX: Matlab Software for Disciplined Convex Programming," *http://www.stanford.edu/ boyd/cvx/*, June 2006.

[58] U. Grasselli, "Probabilistic Design of High Quality Power Supply Photovoltaic Systems," in *Industrial and Commercial Power Systems Technical Conference, 1993. Conference Record, Papers Presented at the 1993 Annual Meeting*, 1993.

[59] M. Hancock, H. Outhred, and R. Kaye, " A New Method for Optimising the Operation of Stand-Alone PV Hybrid Power Systems," vol. 1, pp. 1188–1191, 1994.

[60] D. Heinemann, "Energy Meteorology: Lecture Notes," *Postgraduate Programme Renewable Eenergy Carl von Ossietzky University*, 2002.

[61] G. Henze and R. Dodier, "Adaptive Optimal Control of a Grid-Independent Photovoltaic System," in *Journal of Solar Energy Engineering, ASME*, vol. 125, pp. 34–42, February 2003.

[62] H. Hirahara, M. Z. Hossain, M. Kawahashi, and Y. Nonomura, "Testing Basic Performance of a Very Small Wind Turbine Designed for Multi-Purposes," in *Renewable Energy*, vol. 30, pp. 1279–1297, July 2005.

[63] Y. T. Hou, Y. Shi, H. D. Sherali, and S. F. Midkiff, "On Energy Provisioning and Relay Node Placement for Wireless Sensor Networks ," *IEEE Transactions on Wireless Communications*, vol. 4, no. 5, September 2005.

[64] W. Hu, C. Chou, and S. Jha, "Deploying Long-Lived and Cost-Effective Hybrid Sensor Networks," 2004.

[65] IEEE Standards Department, *Wireless LAN Medium Access Control (MAC) And Physical Layer Specifications.* IEEE Press, 1997.

[66] IEEE Standards Department, "IEEE 802.11s ESS Mesh Networking working group," 2004.

[67] IEEE Standards Department, *Part 11: Wireless Medium Access Control (MAC) and Physical Laye r (PHY) specifications: Medium Access Control (MAC) Quality of Service (QoS) Enh ancements.* IEEE Press, 2005.

[68] IEEE Standards Department, *Part 11: Wireless LAN Medium Access Control (MAC) and Physical Layer (PHY) specifications: Amendment 4: Enhancements for Higher Throughput. IEEE P802.11n/D3.00.* IEEE Press, 2007.

[69] A. Kansal, J. Hsu, S. Zahedi, and M. B. Srivastava, " Power Management in Energy Harvesting Sensor Networks," vol. 1, 2006.

[70] A. Kansal, D. Potter, and M. Srivastava, "Performance Aware Tasking for Environmentally Powered Sensor Networks," *SIGMETRICS Perform. Eval. Rev.*, vol. 32, no. 1, pp. 223–234, 2004.

[71] W. Kellogg, M. Nehrir, G. Venkataramanan, and V. Gerez, "Generation Unit Sizing and Cost Analysis for Stand-Alone Wind, Photovoltaic, and Hybrid Wind/PV Systems," *IEEE Transactions on Energy Conversion*, vol. 13, no. 1, pp. 70–75, March 1998.

[72] A. Kholaif and T. Todd, "WLAN VoIP Capacity Allocation Using an Adaptive Voice Packetization Server," *Computer Communications*, vol. 30, no. 13, pp. 2661–2675, 2007.

[73] D. Kim, J. Garcia-Luna-Aceves, K. Obraczka, J. C. Cano, and P. Manzoni, "Routing Mechanisms for Mobile Ad Hoc Networks based on the Energy Drain Rate," *IEEE Transactions on Mobile Computing, Vol. 2, No. 2,pp. 161-173*, April-June 2003.

[74] K. Kim, "On Statistical Prediction of Cyclostationary Processes," *Journal of Climate*, vol. 13, pp. 1098–1115, 2000.

[75] S. A. Klein, "Calculation of Monthly Average Insolation on Tilted Surfaces," *Solar Energy*, vol. 19, pp. 325–329, 1977.

[76] M. Koot, J.T.B.A.Kessels, A. de Jager, W. Heemels, P. van den Bosch, and M. Steinbuch, "Energy Management Strategies for Vehicular Electric Power Systems." *IEEE Trans. on Vehicular Technology*, vol. 54, pp. 771–782, 2005.

[77] C. Leclerc and C. Masson, "Abnormally High Power Output of Wind Turbine in Cold Weather: A Preliminary Study," *International Journal of Rotating Machinery*, vol. 9, no. 1, pp. 23–33, 2003.

[78] I. Ledvich and A. Segall, "Threshold-Related Throughput A New Criterion for Evaluation of Sensor Network Performance," *CCIT Report 552, Technion - Department of Electrical Engineering*, August 2005.

[79] Y. Li, T. D. Todd, and D. Zhao, "Access Point Power Saving in Solar/Battery Powered IEEE 802.11 ESS Mesh Networks," in *The Second International Conference on Quality of Service in Heterogeneous Wired/Wireless Networks (QShine)*, August 2005.

[80] L. Lin, N. Shroff, and R. Srikant, "Asymptotically Optimal Power-Aware Routing for Multihop Wireless Networks with Renewable Energy Sources," *INFOCOM 2005. 24th Annual Joint Conference of the IEEE Computer and Communications Societies. Proceedings IEEE , vol.2, no.pp. 1262- 1272 vol. 2*, March 2005.

[81] A. F. M. Davis and B. Dougherty, "Measured Versus Predicted Performance of Building Integrated Photovoltaics," *ASME Journal of Solar Energy Engineering*, vol. 125, no. 1, pp. 21–27, February 2003.

[82] M. S. M. Marwali and M. Daneshdoost, "Probabilistic Production Costing for Photovoltaic-Utility Systems with Battery Storage," *IEEE Transactions on Energy Conversion*, vol. 12, no. 2, pp. 175–180, June 1997.

[83] D. Macomber, "Optimizing Residential Photovoltaic System Size Using Approximate Reasoning," in *Proceedings., First International Symposium on Uncertainty Modeling and Analysis,*, pp. 558–563, 1990.

[84] H. A. M. Maghraby, M. H. Shwehdi, and G. K. Al-Bassam, "Probabilistic Assessment of Photovoltaic (PV) Generation System," *IEEE Transactions on Power Systems*, vol. 17, no. 1, pp. 205–208, 2002.

[85] Marlec Engineering Co. Ltd., "Rutland 503 Wind Charger Data Sheet," *http://www.marlec.co.uk/products/prods/rut503.htm.*

[86] Y. E.-P. F. Momoh, J.A.; Wang, "Optimal Power Dispatch of Photovoltaic System with Random Load," in *IEEE Power Engineering Society General Meeting*, vol. 2, pp. 1939–1945, June 2004.

[87] T. Muneer, M. S. Gul, and J. Kubie, "Models for Estimating Solar Radiation and Illuminance From Meteorological Parameters," *ASME Journal of Solar Energy Engineering*, vol. 122, no. 3, pp. 146–153, August 2000.

[88] D.-H. Nam and H.-K. Min, "An Energy-Efficient Clustering Using a Round-Robin Method in a Wireless Sensor Network," *Proceedings of the 5th ACIS International Conference on Software Engineering Research, Management and Applications (SERA 2007)*, vol. 0, pp. 54–60, 2007.

[89] L. Narvarte and E. Lorenzo, "On the Usefulness of Stand-Alone PV Sizing Methods," *Progress in Photovoltaics: Research and Applications, Prog.Photovolt: Res.Appl.*, vol. 8, pp. 391–409, 2000.

[90] National Climate Data and Information Archive, "http://www.climate.weatheroffice.ec.gc.ca/." The Meteorological Service of Canada, Canada., 2008.

[91] National Solar Radiation Data Base, "http://rredc.nrel.gov/solar/." National Renewable Energy Laboratory (NREL), U.S. Department of Energy, 2008.

[92] D. Niyato, E. Hossain, and A. Fallahi, "Solar-Powered OFDM Wireless Mesh Networks with Sleep Management and Connection Admission Control," pp. 653–658, 2006.

[93] K. Papadaki and V. Friderikos, "Joint Routing and Gateway Selection in Wireless Mesh Networks," *IEEE Wireless Communications and Networking Conference (WCNC)*, pp. 2325 – 2330, April 2008.

[94] M. Papadopouli, H. Shen, E. Raftopoulos, M. Ploumidis, and F. Hernandez-Campos, "Short-Term Traffic Forecasting in a Campus-Wide Wireless Network," *Proceedings of the IEEE 16th International Symposium on Personal, Indoor and Mobile Radio Communications, 2005. PIMRC 2005.*, vol. 3, pp. 1446– 1452, 2005.

[95] R. Perez, P. Ineichen, R. Seals, J. Michalsky, and R. Stewart, "Modeling Daylight Availability and Irradiance Components from Direct and Global Irradiance," *Solar Energy*, vol. 44, pp. 271–289, 1990.

[96] R. Perez, R. Seals, P. Ineichen, R. Stewart, and D. Menicucci, "A New Simplified Version of the Perez Diffuse Irradiance Model for Tilted Surfaces," *Solar Energy*, vol. 39, pp. 221–232, 1989.

[97] R. Perez and R. Stewart, "Solar Irradiance Conversion Models," *Solar Cells*, vol. 18, pp. 213–222, 1986.

[98] X. Perez-Costa and D. Camps-Mur, "AU-APSD: Adaptive IEEE 802.11e Unscheduled Automatic Power Save Delivery," in *Proceedings of IEEE International Conference on Communications (ICC)*, vol. 5, pp. 2020–2027, June 2006.

[99] A. Pesaran and V. Johnson, "Battery Thermal Models for Hybrid Vehicle Simulations," *Journal of Power Sources*, vol. 110, pp. 377–382, 2002.

[100] V. Pravosudov and J. Lucas, "A Dynamic Model of Short-Term Energy Management in Small Food-Caching and Non-Caching Birds," *Behavioral Ecology*, vol. 12, pp. 207–218, 2001.

[101] T. Prud'homme and D. Gillet, "Advanced Control Strategy of a Solar Domestic Hot Water System With a Segmented Auxiliary Heater," in *Energy and Buildings*, vol. 33, pp. 463–475, Elsevier, May 2001.

[102] C. Quinones, M. Vazqvez, A. del Prado, E. de la Cruz, and A. Garrido, "Technical and Economical Comparison of PhotoVoltaic Solar System and AC Mains Powering for Advanced Optical Network Units at Remote Sites," pp. 790–796, October 1998.

[103] J. Rawlings, "Tutorial: Model Predictive Control Technology," *Proceedings of the 1999 American Control Conference*, vol. 1, pp. 662–676, 1999.

[104] L. Rogers, J. Rogers, and J. Manwell, "Comparison of the Performance of Four Measure-Correlate-Predict Algorithms," *Journal of Wind Engineering and Industrial Aerodynamics*, vol. 93, pp. 243–264, March 2005.

[105] S. Saengthong and S. Premrudeepreechacham, "A Simple Method in Sizing Related to the Reliability Supply of Stand-Alone Photovoltaic Systems," in *Photovoltaic Specialists Conference, 2000. Conference Record of the Twenty-Eighth IEEE*, pp. 1630–1633, 2000.

[106] F. Safie, "Probabilistic Modeling of Solar Power Systems," in *Reliability and Maintainability Symposium, 1989. Proceedings.*, pp. 425–430, 1989.

[107] A. Safwat and H. Hassanein, "Infrastructure-based Routing in Wireless Mobile Ad Hoc Networks," *Computer Communications*, vol. 25, no. 3, pp. 210–224, 2002.

[108] A. Safwat, H. Hassanein, and H. Mouftah, "Power-aware Virtual Base Stations for Wireless Mobile Ad Hoc Communications," *Computer Networks*, vol. 41, no. 3, pp. 331–346, 2003.

[109] Z. Salameh, M. Casacca, and W. Lynch, "A Mathematical Model for Lead-Acid Batteries," *Energy Conversion, IEEE Transactions on*, vol. 7, no. 1, pp. 93–98, 1992.

[110] E. Serpedin, F. Panduru, I. Sari, and G. B. Giannakis, "Bibliography on Cyclostationarity," *Signal Process.*, vol. 85, no. 12, pp. 2233–2303, 2005.

[111] R. Shah and J. Rabaey, "Energy Aware Routing for Low Energy Ad-hoc Sensor Networks," *In Proc. IEEE Wireless Communications and Networking Conference (WCNC), Orlando, FL.*

[112] Y. Shi, Y. Hou, and A. Efrat, "Design of Low-Complexity Approximation Algorithms for Base Station Placement Problems in Sensor Networks," *Technical Report- Bradley Dept. of ECE Virginia Tech*, July 2005.

[113] J. Song and L. Trajkovic, "Modeling and Performance Analysis of Public Safety Wireless Networks," *Proc. 24th IEEE Int. Performance, Computing, and Communications Conference*, pp. 567–572, April 2005.

[114] The SolarMESH Network, "http://owl.eng.mcmaster.ca/ todd/SolarMESH//." McMaster University. Hamilton, Ontario, Canada., 2008.

[115] Y. C. Tseng, C. S. Hsu, and T. Y. Hsieh, "Power-saving Protocols for IEEE 802.11-based Multi-hop Ad Hoc Networks," *Computer Networks*, vol. 43, no. 3, pp. 317–337, 2003.

[116] H. Velayos and G. Karlsson, "Techniques to Reduce the IEEE 802.11b Handoff Time," in *IEEE International Conference on Communications, 2004*, pp. 3844- 3848 Vol.7, 2004.

[117] X. Wang, J. Ma, S. Wang, and D. Bi, "Prediction-based Dynamic Energy Management in Wireless Sensor Networks," *Sensors*, vol. 7, pp. 251–266, March 2007.

[118] R. Welch and G. Venayagamoorthy, "Comparison of Two Optimal Control Strategies for a Grid Independent Photovoltaic System," in *Conference Record of the IEEE Industry Applications Conference 41st IAS Annual Meeting*, vol. 3, pp. 1120–1127, October 2006.

[119] F. Zhang and S. Chanson, "Improving Communication Energy Efficiency in Wireless Networks Powered by Renewable Energy Sources," vol. 54, pp. 2125–2136, November 2005.

[120] F. Zhang, T. D. Todd, D. Zhao, and V. Kezys, "Power Saving Access Points for IEEE 802.11 Wireless Network Infrastructure," in *IEEE Wireless Communications and Networking Conference 2004, WCNC'2004*, March 2004.